

WRDC-TR-90-2001

AD-A220 371



REACTIONS OF SILANE IN ACTIVE NITROGEN

Charles A. DeJoseph, Jr.
Power Components Branch
Aerospace Power Division

January 1990

Final Report for the Period September 1984 - January 1990

Approved for Public Release, Distribution Unlimited

AERO PROPULSION AND POWER LABORATORY
WRIGHT RESEARCH AND DEVELOPEMENT CENTER
AIR FORCE SYSTEM COMMAND
WRIGHT-PATTERSON AIR FORCE BASE, OHIO 45433-6563

CR

NOTICE

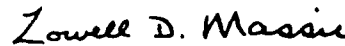
WHEN GOVERNMENT DRAWINGS, SPECIFICATIONS, OR OTHER DATA ARE USED FOR ANY PURPOSE OTHER THAN IN CONNECTION WITH A DEFINITELY GOVERNMENT-RELATED PROCUREMENT, THE UNITED STATES GOVERNMENT INCURS NO RESPONSIBILITY OR ANY OBLIGATION WHATSOEVER. THE FACT THAT THE GOVERNMENT MAY HAVE FORMULATED OR IN ANY WAY SUPPLIED THE SAID DRAWINGS, SPECIFICATIONS, OR OTHER DATA, IS NOT TO BE REGARDED BY IMPLICATION, OR OTHERWISE IN ANY MANNER CONSTRUED, AS LICENSING THE HOLDER, OR ANY OTHER PERSON OR CORPORATION; OR AS CONVEYING ANY RIGHTS OR PERMISSION TO MANUFACTURE, USE, OR SELL ANY PATENTED INVENTION THAT MAY IN ANY WAY BE RELATED THERETO.

THIS REPORT HAS BEEN REVIEWED BY THE OFFICE OF PUBLIC AFFAIRS (ASD/PA) AND IS RELEASABLE TO THE NATIONAL TECHNICAL INFORMATION SERVICE (NTIS). AT NTIS IT WILL BE AVAILABLE TO THE GENERAL PUBLIC INCLUDING FOREIGN NATIONS.

THIS TECHNICAL REPORT HAS BEEN REVIEWED AND IS APPROVED FOR PUBLICATION.



CHARLES A. DEJOSEPH JR.
Aerospace Power Division
Aero Propulsion and Power Laboratory



LOWELL D. MASSIE, Branch Chief
Power Components Branch
Aerospace Power Division
Aero Propulsion and Power Laboratory

FOR THE COMMANDER



MICHAEL D. BRAYDICH, Maj, USAF
Deputy Director
Aerospace Power Division
Aero Propulsion & Power Laboratory

IF YOUR ADDRESS HAS CHANGED, IF YOU WISH TO BE REMOVED FROM OUR MAILING LIST, OR IF THE ADDRESSEE IS NO LONGER EMPLOYED BY YOUR ORGANIZATION PLEASE NOTIFY WRDC/POOC-3, WRIGHT-PATTERSON AFB, OH 45433-6563 TO HELP MAINTAIN A CURRENT MAILING LIST.

COPIES OF THIS REPORT SHOULD NOT BE RETURNED UNLESS RETURN IS REQUIRED BY SECURITY CONSIDERATIONS, CONTRACTUAL OBLIGATIONS, OR NOTICE ON A SPECIFIC DOCUMENT.

UNCLASSIFIED

SECURITY CLASSIFICATION OF THIS PAGE

REPORT DOCUMENTATION PAGE				Form Approved OMB No. 0704-0188	
1a. REPORT SECURITY CLASSIFICATION UNCLASSIFIED			1b. RESTRICTIVE MARKINGS N/A		
2a. SECURITY CLASSIFICATION AUTHORITY N/A			3. DISTRIBUTION / AVAILABILITY OF REPORT		
2b. DECLASSIFICATION / DOWNGRADING SCHEDULE N/A			Approved for Public Release, Distribution Unlimited		
4. PERFORMING ORGANIZATION REPORT NUMBER(S) WRDC-TR-90-2001			5. MONITORING ORGANIZATION REPORT NUMBER(S)		
6a. NAME OF PERFORMING ORGANIZATION Aero Propulsion and Power Lab Aerospace Power Division		6b. OFFICE SYMBOL (If applicable) WRDC/POOC-3	7a. NAME OF MONITORING ORGANIZATION		
6c. ADDRESS (City, State, and ZIP Code) Wright-Patterson AFB, OH 45433-6563			7b. ADDRESS (City, State, and ZIP Code)		
8a. NAME OF FUNDING / SPONSORING ORGANIZATION AFOSR		8b. OFFICE SYMBOL (If applicable) NP	9. PROCUREMENT INSTRUMENT IDENTIFICATION NUMBER N/A		
8c. ADDRESS (City, State, and ZIP Code) Bolling AFB, DC 20332			10. SOURCE OF FUNDING NUMBERS		
PROGRAM ELEMENT NO. 61102F		PROJECT NO. 2301	TASK NO. S2	WORK UNIT ACCESSION NO. 06	
11. TITLE (Include Security Classification) Reactions of Silane in Active Nitrogen					
12. PERSONAL AUTHOR(S) Charles A. DeJoseph, Jr.					
13a. TYPE OF REPORT Final		13b. TIME COVERED FROM 9/84 TO 6/90		14. DATE OF REPORT (Year, Month, Day) 1990 January 29	
15. PAGE COUNT 130					
16. SUPPLEMENTARY NOTATION The material is based on the author's dissertation submitted in partial fulfillment of the requirements for the degree of Doctor of Philosophy at the University of Oklahoma, Norman, Oklahoma.					
17. COSATI CODES			18. SUBJECT TERMS (Continue on reverse if necessary and identify by block number)		
FIELD	GROUP	SUB-GROUP			
20	05		Silanes, SiH ₄ , Silicon Nitride, Nitrogen Afterglow		
20	06		Active Nitrogen, Silicon Nitride, Nitrogen Afterglow		
19. ABSTRACT (Continue on reverse if necessary and identify by block number) Silane is used in the production of amorphous silicon and thin films of silicon nitride. In the production of the latter, silane is mixed with either ammonia or nitrogen in a low pressure electric discharge, and a thin film of silicon nitride is formed at the boundaries of the discharge. Besides the chemical reactions which are driven directly by electrons in the discharge, a number of reactions are believed to occur among chemically reactive, neutral species. These reactions can have a significant effect on the silane dissociation which occurs in these discharges. To study this neutral chemistry, an experimental program along with a coupled rate equation modeling effort was undertaken of the reactions of silane in discharge-produced 'active nitrogen'. Measurements of silane dissociation produced by 'active nitrogen', spectra of the chemiluminescence produced in the reaction, and a rate equation model developed to described the results are presented.					
20. DISTRIBUTION / AVAILABILITY OF ABSTRACT <input checked="" type="checkbox"/> UNCLASSIFIED/UNLIMITED <input type="checkbox"/> SAME AS RPT <input type="checkbox"/> DTIC USERS			21. ABSTRACT SECURITY CLASSIFICATION UNCLASSIFIED		
22a. NAME OF RESPONSIBLE INDIVIDUAL CHARLES A. DeJOSEPH, Jr.			22b. TELEPHONE (Include Area Code) (513) 255-2923		22c. OFFICE SYMBOL WRDC/POOC-3

DD Form 1473, JUN 86

Previous editions are obsolete.

SECURITY CLASSIFICATION OF THIS PAGE

UNCLASSIFIED

cont.
BLK 18-

Keywords: Images, Detectors, Microelectronic Devices,

PECVD, Plasma Enhanced Chemical Vapor

→ Deposition, Ammonia, Dissociation, Emission

→ Spectra

↑↑
(JB)

FOREWORD

The material reported herein is based on the author's dissertation submitted in partial fulfillment of the requirements for the degree of Doctor of Philosophy at the University of Oklahoma, Norman, Oklahoma. The work was performed under Project 2301, Task S2, and Work Unit 06, while the author was employed in the Advanced Plasma Research Group, Aero Propulsion and Power Laboratory of the Wright Research and Development Center at Wright Patterson Air Force Base, Ohio.

Accession For	
100-100000	<input checked="checked" type="checkbox"/>
100-100000	<input type="checkbox"/>
100-100000	<input type="checkbox"/>
A-1	



TABLE OF CONTENTS

FOREWARD	iii
LIST OF FIGURES	vii
LIST OF TABLES	ix
Chapter I: Introduction	1
Purpose and Objective of This Study	1
Overview of the Contents and Results	2
Background and Motivation for this Work	6
Silane Dissociation	7
Previous Work	11
Chapter II: Description of the Experiment	15
Description of the Experiment- Flowing Afterglow System	15
Tunable Diode Laser (TDL) System	19
Calibration of the TDL System	21
Visible and U.V. Spectrometer	27
Relative Calibration of the Spectrometer	28
Fourier Transform Spectrometer/Long Path Cell	29
Chapter III: Experimental Results	32
General Observations of the Reaction	32
Reaction Flame Emission Spectra	33
Pressure Effects on the Emission	39
SiN B-State Vibrational Populations	45
Silane Dissociation Measurements	48
FT-IR Absorption Measurements	52
Disilane Production by Silane Reaction with Nitrogen Metas- tables	55
Chapter IV: Development of the Reaction Model	59
General Rate Equation Approach	59
General Characteristics of the Reaction Scheme	61
Initial Silane Dissociation in the Afterglow	63
Reactions of N-atoms with Silane Radicals	67
The Si and SiN Chemiluminescence	69

Species Generated to Dissociate Silane	72
Summary of the Proposed Reaction Scheme	76
Chapter V: The Reaction Model	79
Early Models	79
The Afterglow Model	80
Vibrationally Excited $N_2(X^1\Sigma)$	81
The Silane Reactions	87
General Behavior of the Model	90
Comparison with the Data of Reference 30	94
Behavior of the Vibrational Distribution	97
Final Products, Higher Nitrides	100
Chapter VI: Summary, Conclusions, and Recommendations	101
Recommendations for Further Work	104
References	105
Appendix A : Heat of Formation of SiN	113
Appendix B: Heats of Formation Used in this Work	115
Appendix C: Function $P(T)$ in Equation 5-10	116

LIST OF FIGURES

<u>Figure</u>	<u>Page Number</u>
Figure 2-1: Schematic of the Experiment.....	16
Figure 2-2: Tunable Diode Laser System.....	20
Figure 2-3: Silane Absorption Near 900 cm^{-1} (1 cm^{-1} Resolution).....	22
Figure 2-4: Silane Absorption Near 900 cm^{-1} (0.06 cm^{-1} Resolution) ...	24
Figure 2-5: Tunable Diode Laser Scan of Silane Lines Near 910 cm^{-1} ...	25
Figure 2-6: FT-IR/Long-Path Absorption Cell System.....	30
Figure 3-1: Emission Spectrum of Reaction Flame at 2 torr.....	34
Figure 3-2: Most Intense Silicon Lines Seen in Flame.....	35
Figure 3-3: Detail of SiN Emission Seen in Flame.....	37
Figure 3-4: Emission Spectrum of Reaction Flame at 0.5 torr.....	40
Figure 3-5: Emission Spectrum of Reaction Flame at 1 torr.....	41
Figure 3-6: Emission Spectrum of Reaction Flame at 4 torr.....	42
Figure 3-7: Emission Spectrum of Reaction Flame at 8 torr.....	43
Figure 3-8: Emission Spectrum of Nitrogen Afterglow at 2 torr.....	44
Figure 3-9: Morse Potentials for SiN.....	46
Figure 3-10: Measured Relative SiN B-State Vibrational Populations... ..	47
Figure 3-11: Helium/Silane Mass Flow vs. Downstream Silane Density .	50
Figure 3-12: Dissociated Silane vs. First Positive Emission Intensity..	51

Figure 3-13: Long-Path Absorption of Downstream Reaction Products (residual silane present)	53
Figure 3-14: Long-Path Absorption of Downstream Reaction Products (reduced silane flow)	54
Figure 3-15: Schematic of Argon Metastable Transfer Experiment.....	56
Figure 3-16: Disilane Absorption After Substraction of Residual Silane Absorption.	58
Figure 4-1: Morse Potentials for Nitrogen (simplified)	65
Figure 4-2: Reproduction of Figure 4 of Reference 30	74
Figure 4-3: Schematic of the Proposed Reaction Scheme.....	78
Figure 5-1: Selected V-T and V-V Rates for Nitrogen at 300°K.	86
Figure 5-2: Calculated Fractional Vibrational Populations of N ₂ in the Afterglow.	88
Figure 5-3: Calculated Time Dependence of SiN Excited State Density as a Function of Pressure	91
Figure 5-4: Calculated Time Dependence of SiN Excited State Density as a Function of SiH ₄ Density	93
Figure 5-5: Comparison of Model Results with Measurements of Reference 30	96
Figure 5-6: Calculated Time Dependence of Fractional Vibrational Populations in Nitrogen.....	98
Figure 5-7: Calculated Time Dependence of Fractional Vibrational Population Available for SiH ₄ Dissociation	99

LIST OF TABLES

Table 1-1: Rate Coefficients for Various Nitrogen Species with Silane- Data from Reference 31	14
Table 3-1: Silicon Lines seen in the Reaction Flame	36
Table 4-1: Catalogue of Abundant Species in Active Nitrogen (at 3 torr)	61
Table 4-2: Thermodynamic Dissociation Energies of Silane.	64

Chapter I

Introduction

Purpose and Objective of This Study

Silane, SiH_4 , is a gas which has important application in the manufacture of thin films of hydrogenated amorphous silicon (a-Si:H) for solar cells, xerographic photoreceptors, and other imaging detectors. It is also used extensively for the production of thin films of silicon nitride and silicon oxide employed in the fabrication of microelectronic devices. One of the most widely used methods for the production of these films is that of Plasma Enhanced Chemical Vapor Deposition (PECVD). In this production technique, a low pressure electric discharge is applied to a gas mixture containing SiH_4 and a thin film of the desired material (depending on the other gases employed) is grown on a substrate. For example, in the case of amorphous silicon film production, the SiH_4 is diluted in a rare gas (usually argon)¹ and for the production of silicon nitride films, the SiH_4 is mixed with either nitrogen or ammonia². In all of these PECVD systems, one of the key steps in the production process must be the dissociation of SiH_4 since in all cases the films contain proportionally less hydrogen than is present in SiH_4 . The rate of SiH_4 dissociation under PECVD conditions is thus an important parameter governing film growth. The dissociation rate under a given set of conditions is strongly influenced by the mechanism by which SiH_4 is dissociated. These include electron impact, ion-molecule reactions, and reactions involving neutral heavy particles. Interest in the work presented here began in this laboratory in 1983 while studying electron impact dissociation of SiH_4 in a direct current discharge³. While most PECVD reactors involve radio frequency discharges, a dc discharge was chosen to begin the investigation because of its more well understood characteristics. The details of this work will be discussed later in this chapter, but to summarize, it was found that the rate of SiH_4 dissociation when diluted in nitrogen was far greater than expected from electron impact. Some other mechanism had to be responsible for the observed dissociation. In an effort to determine what the driver for the dissocia-

work on SiH_4 reactions in active nitrogen is given at the end of the chapter.

In chapter II, the experimental apparatus is described along with calibration procedures where appropriate. The chapter begins with a description of the flowing afterglow apparatus along with its associated flow and pressure controls. This is followed by a description of the Tunable Diode Laser (TDL) system used to measure SiH_4 density and the calibration procedure used in the measurement. To measure SiH_4 dissociation in the afterglow region, the density was measured from the integrated absorbance of an isolated SiH_4 absorption line. The integrated absorbance was determined by least-squares fitting a Voigt profile to the measured absorption data and then comparing these measurements with data from a known gas mixture. For calibration, the line intensity of the Q(3),A2,1 line of the ν_4 band of SiH_4 was measured absolutely using a known gas mixture of SiH_4 in argon. No detailed line intensity measurements are available in the literature for SiH_4 . The ultraviolet/visible monochromator system with associated photomultiplier and signal processing system are described along with the relative intensity calibration procedure used. Finally, a description is given of the Fourier Transform Infrared (FTIR) spectrometer system with long path absorption cell used for making infrared absorption measurements of the gases leaving the reaction zone.

In chapter III the results of the measurements and the analysis of the data are presented. A general description is given of the behavior of the observed chemiluminescence as it was affected by pressure, SiH_4 flow, and discharge current. These qualitative observations were very important in the overall formulation of the reaction model. Specifically, the movement and shape of the reaction flame and the observations of pulsing of the reaction flame were key indicators of the presence of a chain reaction in the overall scheme. Following the general observations emission spectra of the chemiluminescence are given and key emitting species are identified. The primary spectral features in the reaction flame at pressures above 2 torr are the B-X band system of SiN and a number of lines due to atomic silicon. In addition, there is an unidentified broadband continuum emitter in the range of 450-870nm. No NH_x , H_2 , H , or SiH emission could be identified. Spectra taken over the pressure range 0.5-8 torr are presented. At pressures below 2 torr the dominant spectral feature is the aforementioned broadband continuum while at pressures above 2 torr, the dominant features are the SiN and Si emission. The dominance of both the Si and SiN emissions at higher pressures indicates

that these emissions increase faster than linear with pressure. Difficulties in defining the emitting volume prevented a precise determination of the pressure dependence. Measurements of the SiN B-state vibrational populations observed in the higher pressure chemiluminescence are also presented. At these higher pressures, the measured B-state vibrational populations show a peak in the populations at vibrational level $v=5$. This type of distribution has been seen previously in experiments where SiCl_4 and SiBr_4 were added to active nitrogen. Following this, dissociation measurements of SiH_4 are presented and compared with the first positive emission from the afterglow. The measurements show that the amount of SiH_4 dissociated at the "zero remaining limit" (when the initial SiH_4 density is such that exactly this amount can be dissociated) is shown to be proportional to the square root of the intensity of the N_2 first positive emission in the afterglow. This indicates that the dissociation is proportional to the N-atom density in the afterglow. Absorption spectra taken during the FTIR/long path cell investigation are presented. The only absorption features found in the spectra are due to SiH_4 and an unidentified species with bands at 900 and 2200 cm^{-1} . The very broadband nature of these later features and the positions of the band centers indicate a complex molecule containing Si and N and perhaps some H. Finally, the results of an experiment involving a modification of the original flowing afterglow apparatus to look at SiH_4 dissociation induced by collisions with $\text{N}_2(\text{A}^3\Sigma)$ molecules are presented. In this experiment, argon metastables are created in a dc discharge and allowed to collide with N_2 molecules downstream of the discharge. In the resulting collisions some of the argon metastables transfer their energy to N_2 to form $\text{N}_2(\text{A}^3\Sigma)$ metastables which can then react further downstream with SiH_4 . If the SiH_4 is dissociated by the collisions with the N_2 metastables, the resulting radical fragments react with SiH_4 to form higher silanes such as Si_2H_6 . The experiment showed conclusively that Si_2H_6 formation was initiated by the reaction of $\text{N}_2(\text{A}^3\Sigma)$ metastables with SiH_4 .

Chapter IV presents development of the reaction mechanism and the justification for the proposed scheme. It begins with a general discussion of the rate-equation approach and discusses the bounds on the general bimolecular reaction rate. Following this, a discussion is given of the general characteristics the reaction scheme must possess in order to describe the observed results. A general cataloging of the most abundant species found in the afterglow is also given. From the fact that N-atoms are the most abundant reactive species present in the afterglow and from the general behavior of the reaction scheme presented in chapter III it is

concluded that the direct reaction of N-atoms with SiH_4 , if finite, must be very slow. This is in spite of the results of chapter III that indicate that SiH_4 dissociation is proportional to the N-atom density in the afterglow. This key observation indicates that in any proposed reaction scheme, N-atoms must be the driver for SiH_4 dissociation but cannot react directly with the molecule. From these observations and the overall characteristics the reaction scheme must possess, a general model of the reaction mechanism is developed. This general model attempts to describe the bulk of the observations available about the behavior of the chemiluminescence and the SiH_4 dissociation. Arguments are then presented to specifically define the species involved in each step of the general model. The arguments are based on how the measured data can be explained while satisfying thermodynamic constraints. At the same time, consideration is also given to realistic densities of species available in the afterglow, and perturbations that the proposed scheme would have on these densities. The steps in the general model include the initial (slow) dissociation of SiH_4 , reaction of N-atoms with SiH_x radicals, formation of electronically excited SiN and Si , and production of a species to drive the later (fast) SiH_4 dissociation. Vibrationally excited, ground electronic state N_2 is proposed as the primary driver for the later stages of the SiH_4 dissociation. The specific set of chemical reactions proposed to describe the reactions of SiH_4 in active nitrogen is summarized at the conclusion of the chapter.

Details of the coupled rate-equation model are presented in chapter V and the results of the model compared with experimental data. The overall model includes a simplified set of reactions to describe the interaction of the various afterglow species, the reactions between the afterglow species and the silicon bearing species, and a complete model of the interaction of the vibrational levels of $\text{N}_2(X^1\Sigma)$. Formulation of these subsets of the overall model, the selection of rate constants for the reactions, and the initial conditions used as input for the model are discussed. When available, literature values for the rate constants are used. When not available in the literature, rate constants are constrained by gas kinetic values. The vibrational state densities are treated as a set of coupled equations which interact through the exchange of vibrational quanta (v-v) and vibration-to-translation exchange (v-T). The rates for these processes are taken from the literature. Following this, the general behavior of the model is presented including a discussion of the SiH_4 dissociation and the behavior of the chemiluminescence. The model is shown to describe the general behavior of the chemiluminescence ob-

served in this work and the time dependence of the N-atom and SiH₄ concentrations measured by mass spectrometer in reference 30. The model results of the time dependence of the vibrational populations in the N₂ electronic ground state are discussed and the chapter concludes with a discussion of the likelihood for the formation of higher nitrides of silicon in the gas phase. Chapter VI presents some conclusions and suggestions for further work.

Background and Motivation for this Work

The SiH₄ molecule possesses tetrahedral symmetry with an Si-H bond distance of 1.46Å. Due to symmetry, the nine vibrational modes of the molecule are reduced to four fundamental modes. There is one non-degenerate stretching mode ν_1 at 2187cm⁻¹, one doubly degenerate bending mode ν_2 at 978cm⁻¹, and two triply degenerate bending and stretching modes ν_3 at 2183cm⁻¹ and ν_4 at 910cm⁻¹. Formally, only the ν_3 and ν_4 modes are infrared active but due to the small differences in frequency between the ν_1 and ν_3 modes and the ν_2 and ν_4 modes, vibration-rotation interaction between these modes results in all four modes being active.⁵ The electronic states of SiH₄ are not well known. The molecule possesses no strong absorption bands in the visible or ultraviolet. Some extremely weak absorption bands seen in the visible have been attributed to $\Delta v=6-9$ overtones of the ground state vibrational levels.⁶ Absorption spectra of the vacuum ultraviolet show an onset at $\approx 160\text{nm}$ (7.8 eV) followed by continuous absorption to shorter wavelengths.⁷ Gordon⁸ has performed *ab initio* calculations of the energies of the vertical excited states of SiH₄ and these calculations place the first excited state at ≈ 9 eV above the ground state. Gordon, however, states that the calculations tend to overestimate the excitation energies by ≈ 1 eV.

As mentioned at the beginning of this chapter, interest in SiH₄ began in this laboratory in 1983 while studying the dissociation of SiH₄ in a dc discharge as part of an effort to study the plasma chemical reactions associated with PECVD of amorphous silicon³. In that work, measurements of the rate of dissociation of SiH₄ diluted in either argon, helium, or nitrogen was measured using the TDL system, mentioned earlier, to monitor the SiH₄ density downstream of the discharge. The density was determined by measuring the absorbance of an isolated rotation-vibration line of the ν_4 band. Premixed gases containing 1%-5% SiH₄ were flowed through the discharge under controlled mass flow conditions so the residence time in the discharge was well known. From the downstream

density measurements, the fractional dissociation was measured for a fixed residence time and a fixed discharge current. By varying the SiH_4 residence time in the discharge an effective "rate" of dissociation could be measured. These measurements were then compared with calculated rates due to electron impact. The rates were calculated by solving the Boltzmann transport equation for the electrons in the positive column to arrive at an electron energy distribution which was then folded with a model cross section for SiH_4 dissociation. The model cross section was assumed to have a threshold of 7.8 eV corresponding to the onset of vacuum u.v. absorption. For He/SiH_4 and Ar/SiH_4 mixtures, the measured rates and the calculated rates agreed within a factor of 2. Considering the fact that no attempt was made in the calculations to include the effects of the sheath regions of the discharge, this was considered reasonable agreement. From these results, the conclusion was drawn that for SiH_4 diluted in these rare gases, the dissociation rate in a dc discharge was set by electron impact⁹. In the case of N_2/SiH_4 mixtures, reasonable agreement between the calculated and measured rates could not be achieved. For example, in the case of 1% SiH_4 in N_2 , the measured rate was a factor of 70 larger than the calculated rate. In this case it was concluded that other processes besides electron impact must be occurring in the discharge to lead to such a large rate of dissociation¹⁰. As discussed in the beginning of this chapter, it was the purpose of this work to determine what some of these other processes might be.

Silane Dissociation

Probably because of the lack of detailed knowledge of the electronic states of SiH_4 , the mechanisms by which the molecule is dissociated are not well known. The earliest studied dissociation process is that of pyrolysis. These early studies of pyrolysis lead to the development of the first method of amorphous silicon production known as Chemical Vapor Deposition (CVD). This process is based on the thermal decomposition of SiH_4 at atmospheric pressure on a hot (typically 450-700°C) substrate. This is in contrast with PECVD of amorphous silicon which is done at pressures of less than a torr, requires a (usually RF) gas discharge, and employs substrate temperatures of less than 200°C. There have been a number of measurements of pyrolysis of SiH_4 made in both heated vessels and shock tubes. The most important pyrolysis work using a heated vessel is probably the work of Purnell and Walsh¹¹. They found that both H_2 and Si_2H_6 were formed at a pressure dependent rate which exhibited an

activation energy of $E_a=55.9\pm0.5$ Kcal/mole (2.43 eV/molecule). The pressure dependence found by Purnell and Walsh was given as $P^{1.5}$. Pressures in their experiment ranged from 35-400 torr and temperatures ranged from 650-700°C. The most significant shock tube measurements are probably those of Newman et al.¹². Under the shock conditions estimated at $P_{total}\approx 4000$ torr and $T=1035-1184^\circ\text{K}$ they found an activation energy of $E_a=52.7\pm1.4$ Kcal/mole (2.29 eV/molecule). Recently Coltrin et al.¹³ have published a unimolecular decomposition rate for SiH_4 , based on an unpublished RRKM analysis by O'Neal of reference 12's original data. Their Arrhenius expression for the rate is given as

$$k(T,P) = (a+bP)AT^\beta \text{EXP}(-E_a/RT) \quad (\text{s}^{-1}) \quad (\text{eq. 1-1})$$

where $a=0.0504$, $b=0.9496$, P is in atmospheres, $A=2.54\times 10^{38}$, $\beta=-7.95$, and $E_a=62.0$ Kcal/mole (2.69 eV/molecule). Coltrin et al.¹³ claim the expression is valid over the pressure range of 5 torr to 1 atm. For a typical CVD reactor case of $T=500^\circ\text{C}$ and $P=1$ atm, eq. 1-1 gives a unimolecular decomposition rate of $k=8.46\times 10^{-3} \text{ s}^{-1}$. With the exception of a 1984 paper by Robertson, Hils, and Gallagher¹⁴, who claimed that SiH_4 pyrolysis was initiated by surface decomposition, the pyrolysis of SiH_4 is considered a unimolecular, *homogeneous* process. Both Purnell and Walsh¹¹ and Newman¹² propose the decomposition proceeds via the reaction,



From the heat of formation data given in appendix B, the enthalpy change in the above reaction is $\Delta E=+59.9$ Kcal/mole, thus the activation energy given by Coltrin et al.¹³ is consistent with this picture of thermal dissociation.

Dissociation of SiH_4 in discharges can occur by reactions with ions. For example, reactions of SiH_4 with rare-gas ions can result in dissociation by reactions such as



Since Ar is often used as a buffer gas in amorphous silicon deposition, reactions such as eq. 1-3 could be important in governing the overall SiH_4 dissociation under discharge conditions. Ion-molecule reactions involving

silane and ionized fragments from the break up of silane can also be important. Reactions such as



and



where $n=2$ or 3 and $m=0,1,2$, can increase the rate of silane dissociation under discharge conditions. Haaland¹⁵ has recently discussed a number of ion-molecule reactions that can occur in silane discharges. Haaland's work includes measurements of reaction rates of SiH_4 with the noble-gas ions He^+ , Ne^+ , Ar^+ , Kr^+ , and Xe^+ and a number of ion-molecule reactions that can occur among dissociated fragments. Also, Chatham, et al.¹⁶ measured reactions rates for SiH_4 with Ar^+ , He^+ and Ne^+ while Turbin, et al.¹⁷ and Haller¹⁸ have looked at ion-molecule reactions among silane fragments. It is assumed in the work presented here that ion densities in the afterglow are sufficiently small that ion-molecule reactions of this type can be neglected.

Likewise electron impact dissociation of SiH_4 will not be considered in this work, but under discharge conditions this process is significant. Measurements of electron impact dissociation of SiH_4 have been made under discharge conditions and with low energy electron beams. Nolet¹⁹ measured the rate of disappearance of SH_4 diluted in argon in a flowing-gas D.C. discharge, while Perrin and Aarts²⁰ measured dissociative excitation of electronically excited fragments of SiH_4 using a low energy electron beam. Perrin, et al.²¹ used a multipole reactor and a mass spectrometer to measure the rate of disappearance of SiH_4 in a flowing-gas system. The narrow energy spread of the electrons in the multipole reactor allowed Perrin et al.²¹ to measure a total dissociation cross section as a function of electron energy from ≈ 17 eV to 110 eV. As mentioned earlier, DeJoseph, et al.³ used a method similar to Nolet¹⁹ to measure the rate of silane dissociation under D.C. discharge conditions and used a modelling approach to arrive at a dissociation cross section. The model cross section was assumed to have a threshold coincident with the vacuum ultraviolet absorption threshold. This threshold is also very close to the ≈ 8 eV threshold arrived at by extrapolation of the data of Perrin, et al.²¹ It thus seems reasonable that the threshold for electron impact dissociation of SiH_4 is very close to, if not coincident with, the threshold for vacuum ultraviolet absorption of 7.8 eV. The products formed from the

electron impact dissociation are dependent on the electron energy, but in the case of vacuum u.v. absorption at 147 nm (8.4 eV), Perkins, et al.²² suggest the products are primarily SiH₂ (83%) and SiH₃ (17%). However the product distribution from photodissociation may differ from electron impact dissociation since the electrons can induce transitions which are not necessarily optically allowed.

Heavy particle dissociation of silane can be divided into two types of collisions. In a *reactive* collision, the colliding species chemically bonds to one of the atoms of the silane molecule. The hydrogen abstraction reaction of atomic hydrogen with silane is of this type:



The second type of collision to consider is a super elastic collision in which the internal energy of the colliding species is sufficient to dissociate silane, but the reacting species maintains its identity (but with less internal energy) after the collision. The reaction of Hg(³P₁) with silane is such a reaction:



Reaction 1-6 has been studied by a number of authors. Kushner²³, has recently reviewed the rate measurements and gives a rate constant of 2.7x10⁻¹² cm³/s. Reaction 1-7 is known from experiments with mercury sensitization of silane. In these experiments, a gas mixture of SiH₄ and Hg is irradiated with 257 nm (4.8 eV) resonance radiation from a Hg lamp resulting in SiH₄ decomposition and hydrogen evolution. While this reaction has been known since the observations of Emeleus and Stewart²⁴ in 1936, it has only been recently that details of the reaction have been studied²⁵. In particular, it has not been clear whether the reaction involved the Hg(³P₁) state, which is excited by the 257 nm radiation, or whether the reaction involved the metastable Hg(³P₀) state formed in the reaction



where M is any gas species. The two states differ in energy by only 0.2 eV²⁶, thus reaction 1-8 might be expected to be reasonably fast. Perrin and Allain²⁵ measured the rate of *quenching* of both the metastable Hg(³P₀) state and the Hg(³P₁) state by silane and report quenching rates of

$7.3 \pm 1.3 \times 10^{-10}$ and $8.3 \pm 0.7 \times 10^{-10}$ cm³/s respectively for the two states. Furthermore, they suggest that the quenching of both states is primarily by electronic-to-electronic transfer to SiH₄, followed by dissociation of SiH₄. In particular, they rule out the *reactive* collision



and suggest that for M=SiH₄ reaction 1-8 is very slow. This is in spite of the lack of any known electronic states of SiH₄ below 7.8 eV. This points up a difficulty with proposing reaction schemes involving silane. From the energetics alone, one would be tempted to conclude that reaction 1-9 would be more likely than reaction 1-7. If one were then to consider the lack of excited states of SiH₄ below 7.8 eV, one would most surely rule out reaction 1-7. The difficulty with this reasoning lies in the details of the collisions. Because of the thermal energies involved, the colliding particles can spend a relatively long time in close proximity and thus there is some probability that a collision *complex* of the colliding pairs will be formed. The subsequent breakup of this unstable complex may lead to the formation of species that might not be expected to be formed in a brief, or *direct* collision²⁷. Reactions of heavy particles with SiH₄ must therefore be considered a difficult area to predict *a priori* rates of reaction and details of the reaction channels.

Previous Work

Active nitrogen has been studied for more than 100 years and the reader is referred to the book by Wright and Winkler for a good historical perspective up until 1968⁴. While extensively studied (Wright and Winkler list 1529 references) active nitrogen remains for the most part a poorly understood subject. Wright and Winkler summarize the difficulties associated with this enigma in the following quote²⁸:

"Active nitrogen and its behavior stand revealed as more complex than generally recognized. Moreover, apparent contradictions in observations and interpretations are indicated as reflecting a greater sensitivity of the systems to experimental conditions than has generally been appreciated. As a consequence, assessment of much of the available data, at the present time, is likely to be arbitrary"

Unfortunately, there has been little done since 1968 to change the above assessment.

One of the earliest and most performed experiments with active nitrogen involved the introduction of various compounds into the afterglow, studying the resulting changes in the afterglow (if any), studying the spectroscopy of any emission from the reaction zone, and studying any new compounds formed during the reaction. Thus while the original idea of introducing the SiH_4 into active nitrogen seemed straightforward, it fell in with a group of experiments which have been extensively studied for many years with many conflicting results and interpretations. Thus it was surprising when this work was begun in 1984 that only one paper, by Dewhurst and Cooper in 1960²⁹, could be found of any study of SiH_4 in active nitrogen. Since this work was begun, two more studies of SiH_4 in active nitrogen have appeared, both in 1986. Horie, et al.³⁰ looked at SiH_4 in active nitrogen in a flowing afterglow similar to the one used in this work. Piper and Caledonia³¹ also used a flowing afterglow experiment but with higher flow speeds than used in this work or reference 30.

Dewhurst and Cooper²⁹ reacted SiH_4 in a glass bulb containing active nitrogen at a pressure of 1.2 torr. A liquid nitrogen trap was positioned downstream of the bulb to trap condensables from the reaction. Experiments were performed at room temperature and 250°K. They described a "lilac colored reaction flame" at both temperatures and reported "an intense blue glow" when the silane flow was stopped and the active nitrogen allowed to reach the downstream LN_2 trap. They also reported "a preliminary examination of the emission spectra" in which they identified atomic silicon emission. Reaction products from the cold trap were later analyzed using infrared absorption and gas chromatography. No ammonia, hydrazine, or other condensable products could be identified in either the room temperature or 250°K data.

Horie et al.³⁰ used a small flowing afterglow system similar to the one to be described in this work. Pressures in their experiment were kept near 3 torr. They published spectra of the reaction flame over the range 450-800nm and discussed some observed features in the range of 200-450nm. Spectra were not corrected for system response. Emission spectra from Si^* , SiN^* , and an unidentified continuum from 450 to 810nm were discussed. Changes in the continuum when deuterated silane (SiD_4) was substituted were also discussed. They specifically stated that no emissions from SiH , Si_2 , NH , or NH_2 could be identified. In addition to spectra

of the most intense region of the flame, spatially resolved emission was presented for Si^* , SiN^* , $\text{N}_2(1^{\text{st}} \text{ positive})$, and at two wavelengths in the continuum. Mass spectroscopy was used to measure the density of N-atoms, SiH_4 , and H_2 as a function of time in the reaction zone. The mass spectrometer was also used to search for reaction products. Only H_2 could be found. One very interesting observation by Horie et al. was the measurement of chemiionization in the reaction flame. Attempts to determine the mass of the ions were unsuccessful, but they claimed the magnitude of the ion current was comparable to that due to NO^+ when NO was introduced into the afterglow. Lastly, Horie, et al. proposed a sketchy reaction scheme to explain their observed results. More details of their proposed scheme will be discussed later, but essentially a chain reaction was proposed triggered by the reaction of $\text{N}_2(\text{A}^3\Sigma)$ metastables with SiH_4 resulting in SiH_4 dissociation. In their proposed scheme $\text{N}_2(\text{A}^3\Sigma)$ metastables were produced by exothermic reactions which further reacted with SiH_4 . They also invoked $\text{N}_2(\text{A}^3\Sigma)$ to explain the Si^* emission by collisions of the second kind with Si.

Piper and Caledonia³¹ also measured emission spectra of the chemiluminescence in a flowing afterglow system. Pressure in their experiment ranged from 1.5 to 2 torr. While there is no detailed data to support this, it appears from the spectra presented in references 30 and 31 that Piper and Caledonia had higher sensitivity in their spectrometry. The spectral features identified by Piper and Caledonia differed in both species identified and relative intensity from those of Horie, et al. Like Horie et al., Piper and Caledonia identified a number of lines from Si^* and identified some SiN^* emission. On the other hand, while the SiN^* emission was a dominant feature in the spectra of Horie et al., the emission was very weak in the spectra of Piper and Caledonia. Unlike Horie, et al., Piper and Caledonia observed emission from both SiH and NH , the NH emission being one of the strongest features in their spectra. Piper and Caledonia also observed emission from CN , which was not mentioned by Horie, et al. There is also disagreement between the two on the observed continuum emission. Piper and Caledonia reported a continuum between 280 and 430nm, with no emission above 430nm. As previously discussed, Horie, et al. observed continuum emission from 450 to 810nm with no emission seen below 450nm. Piper and Caledonia also discuss spectra taken under different afterglow conditions. By changing the configuration of their experiment, they were able to produce active nitrogen that only contained $\text{N}_2(\text{A}^3\Sigma)$, and also varying densities of N-atoms. The results of these measurements were that no emission was seen with only $\text{N}_2(\text{A}^3\Sigma)$ present

and the intensity of the emission was stronger as the N-atom density was increased. Finally, Piper and Caledonia reported reaction rates for a number of afterglow species to react with SiH_4 . These rates were determined by measuring the rate of loss of a particular species due to reactions with SiH_4 . The table below summarizes their results.

Table 1-1: Rate Coefficients for Various Nitrogen Species with Silane.
Data from Reference 31.

<u>Nitrogen Species</u>	<u>Rate Coefficient ($10^{-11}\text{cm}^3/\text{s}$)</u>
$\text{N}_2(\text{A}^3\Sigma, v=0)$	0.59 ± 0.11
$\text{N}_2(\text{A}^3\Sigma, v=1)$	0.78 ± 0.17
$\text{N}_2(\text{a}'^1\Sigma, v=0)$	14.5 ± 3.5
$\text{N}(\text{D})$	4.0 ± 0.9
$\text{N}(\text{P})$	0.06 ± 0.02
$\text{N}(\text{S})$	<0.006

The reaction rate for $\text{N}(\text{S})$ was set by the smallest rate they could measure in their experiment. No reaction of $\text{N}(\text{S})$ with silane could be observed. Besides the three references given here, one might be tempted to compare the reaction of SiH_4 in the afterglow to that of CH_4 . Wright and Winkler⁴ give a number of references for CH_4 in active nitrogen. While the results of the investigations (emission spectra, species formed) are similar, interpretation of the reaction mechanism is an open question. Thus one is in much surer waters by staying with the problem at hand. In the following pages, this problem will be presented.

Chapter II

Description of the Experiment

Most flowing afterglow experiments have used either a "condensed" dc discharge or a microwave discharge to produce the afterglow (see reference 4). The condensed discharge is produced by placing a capacitor (formerly a condenser) in parallel with the discharge electrodes to produce an oscillating voltage discharge which yields a high concentration of nitrogen atoms in the afterglow. The microwave discharge is typically made up of a small microwave cavity driven at a few GHz. For this investigation, a conventional dc discharge with current regulation was used. The reason for using the dc discharge was twofold. First, since it was desired to measure the dissociation of SiH_4 as a function of discharge parameters, the dc discharge offered a more easily measurable and reproducible set of parameters (current and voltage) than the microwave discharge. Second, the positive column of the dc discharge appeared to be simpler (but not simple) system for modeling the afterglow and hence predicting what species and their concentrations would be present. As will be discussed later, modeling even the dc discharge proved to be so difficult that this latter advantage failed to materialize. Figure 2-1 is a schematic of the experiment. The basic experiment consisted of a flowing afterglow with associated flow and pressure controls, an absorption cell and Tunable Diode Laser (TDL) system for measuring the silane density downstream of the afterglow, and a visible/ultraviolet monochromator for recording the spectrum of the radiation from the reaction zone. Details of the system will be described below.

Description of the Experiment- Flowing Afterglow System

Pure nitrogen (Matheson ultrahigh purity, 99.999% min.) was flowed through an 8 mm i.d. pyrex discharge tube with electrodes out of the flow as shown in the figure. The spacing between the side arms housing the electrodes was 25 cm. The electrode material was Kovar. The power supply was a current regulated dc supply capable of 6 kV maximum

SCHEMATIC OF THE EXPERIMENT

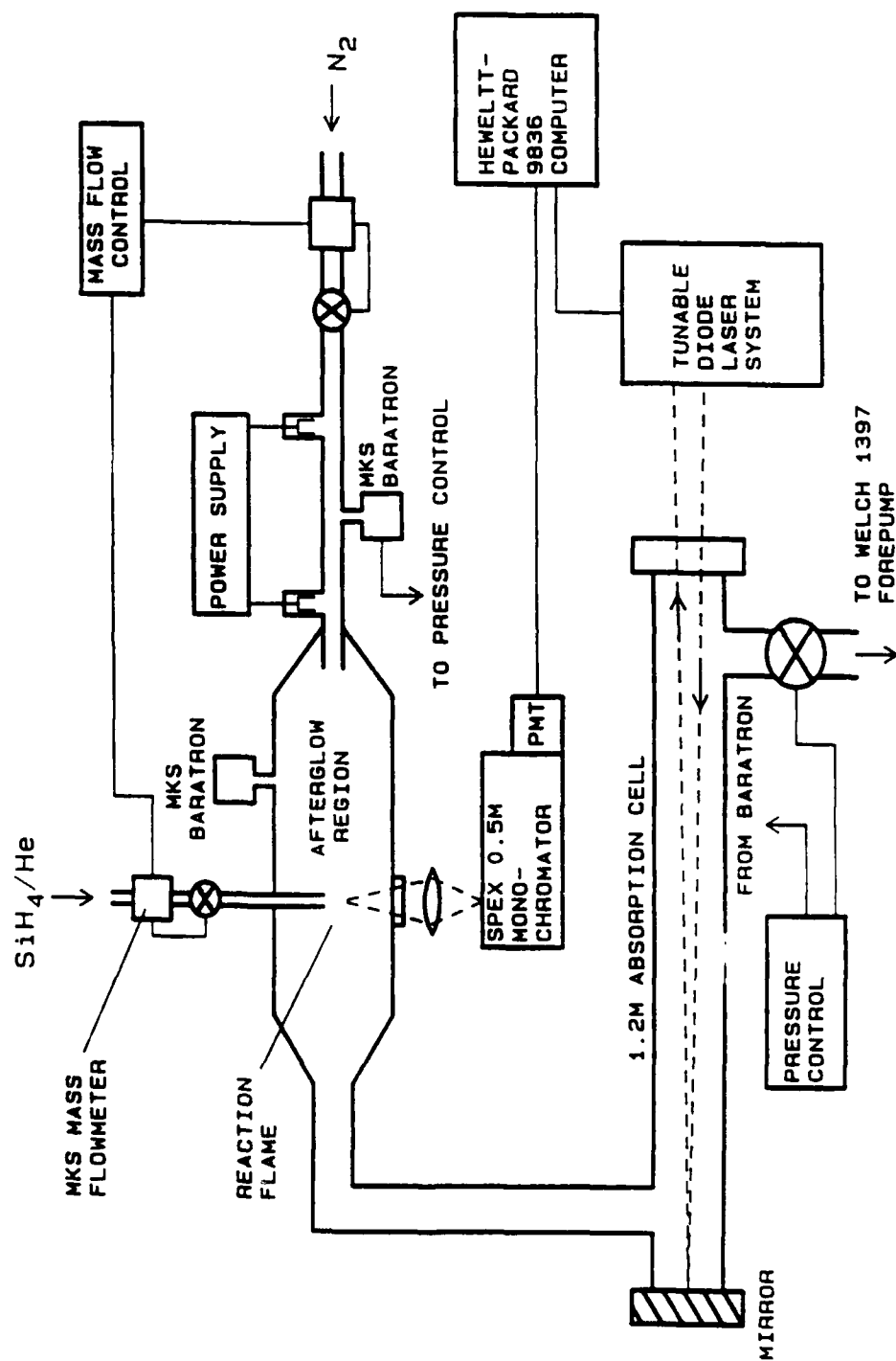


Figure 2-1: Schematic of the Experiment

voltage. A Weston model 911 analogue milliammeter was used to measure discharge current. Discharge voltage measurements used a Fluke model 80K-40 probe (1000 Mohm input resistance) and a Fluke model 8050A 4 1/2 digit DMM were used. The nitrogen mass flow was controlled by an MKS model 254 Mass Flow Controller. This unit would maintain a preset mass flow of up to three gases by measuring the mass flow of each gas with an MKS model 258 flow meter and via a feedback loop control the flow with an MKS model 248A flow control valve. The mass flow meters were of the thermal conductivity type and the model 254 allowed gas-correction factors to be entered via front panel switches so that true mass flow could be read out and controlled for any gas. This system also controlled the silane/helium mixture which was introduced into the afterglow. A mixture of $0.9 \pm 0.1\%$ silane in helium was used throughout the experiment so that small amounts of silane could be titrated using the mass flow meters. Flow rates of pure silane would have been too small to be accurately measured and controlled. Since its lowest energy level is at 19.8 eV, helium is assumed to not interact with the afterglow or silane in the experiment. Pressure in the system was measured at two points using MKS capacitance manometers. A model 315BHS (10 torr head) was used in the afterglow region and a model 220BHS (10 torr head) was used to measure the pressure in the discharge region. The pressure signal from the discharge region was fed to an MKS model 252A Exhaust Valve Controller which in turn controlled an MKS model 253A Throttling Valve. This system thus allowed independent control and good stability of both the mass flow and the pressure. It should be pointed out that over the pressures and flows of the experiments run, the pressures recorded by the two capacitance manometers never differed by more than a few percent.

Nitrogen flowing out of the discharge then entered a 36 mm i.d. pyrex section where the straw-yellow Lewis-Rayleigh afterglow⁴ could be seen. This larger i.d. section extended about 45 cm from the end of the discharge tube. The silane/helium mixture could be introduced into the afterglow at a point 25 cm from the end of the discharge tube. During the course of the investigation, the silane injection tube was moved to a point at the edge of the discharge tube, but most of the data was recorded with the tube at the 25 cm position. A 2.5 cm quartz window was cemented to the side of the 36 mm section at the silane injection port to allow recording of emission spectra down to 220 nm in the u.v. During the course of the experiment, an identical flow tube was constructed entirely of quartz to allow less restricted viewing, but most of the spectra that will be presented here were taken with the quartz window. The visible/u.v.

spectrometer will be described later. Gas flowing out of the 36 mm i.d. section then entered a 1.2 m absorption cell fitted with a barium fluoride window on one end and a mirror on the other. This allowed the gases leaving the reaction zone to be probed with the Tunable Diode Laser (TDL) system which is described below. By monitoring the infrared absorption of silane, its density could be measured downstream of the reaction zone. The gas then left the absorption cell and was pumped by a Welch model 1397 mechanical pump (425 liters/s @ 1 torr) equipped with an oil trap. Due to the low concentrations of silane used in the experiment, no special precautions were taken with the pump except to vent the exhaust to the outside. A blower with an enclosed motor was used to draw the exhaust gases from the pump.

The design of the experiment was based to some extent on ease of fabrication and, unfortunately, characterization of the flow velocity was difficult. The flow velocity of gas in a cylindrical tube is given by³²

$$v = \frac{Q}{PA} = \frac{12.7 \cdot Q(\text{sccm})}{P(\text{torr}) \cdot A(\text{cm}^2)} \text{ (cm/sec)} \quad (\text{eq. 2-1})$$

where Q is mass flow, P is pressure, and A is the cross-sectional area of the tube. While mass flow and pressure could be accurately measured, the abrupt change in tube diameter from the 8 mm i.d. discharge section to the 36 mm i.d. reactor section meant that the flow velocity dropped by the ratios of the areas or $(8/36)^2 \approx 1/20$. Thus there was a transition region in which the flow velocity changed by approximately a factor of 20. At low pressures (below 3 torr) the flow velocity was limited by the conductance of the lines to the pump so that at 1 torr the maximum mass flow of N_2 was limited to 40 sccm. At higher pressures, the mass flow measurements were constrained to the limit of the mass flow meter which was 400 sccm. The maximum flow velocity in the small diameter section ranged from ≈ 1000 cm/s at 1 torr to ≈ 3000 cm/s at 3 torr to ≈ 1000 cm/s at 10 torr. From observations of the straw-yellow afterglow, it was apparent that at high pressure (8-10 torr) and high mass flow, the transition region extended beyond the point of introduction of the silane/helium mixture. Thus it was not possible to accurately know the flow speed in the reaction zone at all values of mass flow and pressure. When measurements were to be compared at different pressures, the quantity Q/P was held constant.

Tunable Diode Laser (TDL) System

A schematic of the TDL system is shown in figure 2-2. The system is a commercial system built by Laser Analytics, Inc. The system centers around a small ($\approx 0.025 \text{ mm}^3$), low power, continuous wave solid-state semiconductor laser composed of lead salts such as PbS, PbSe, PbTe, and PbSnTe³³. These lasers emit in the wavelength range 2-30 microns in the infrared with the wavelength range of a particular laser fixed by its composition. A single laser may only cover 0.05 micron, hence many lasers are needed to cover the total range of the system. The advantages of these lasers over other infrared techniques are their very narrow linewidth ($\approx 3 \times 10^{-4} \text{ cm}^{-1}$) and high brightness compared to a standard blackbody source at 1500°K. The narrow linewidth allows the true Doppler profile of an absorption line at low pressure to be seen which results in high sensitivity for detecting species by absorption. In addition, the narrow linewidth allows the true profile of the line to be measured and hence no correction for instrument resolution is needed. The high brightness of the lasers allow rapid data acquisition using fast solid state infrared detectors. A major disadvantage is that the lasers operate at temperatures below that of liquid nitrogen, hence either liquid helium or a helium refrigeration system must be used to cool the lasers. This system used a closed-cycle helium refrigeration system which is indicated in figure 2-2 by "Lines to Compressor". Another disadvantage (although minor) is that the lasers usually run multimode so that some form of mode selection is necessary to achieve narrow linewidth operation. This is accomplished in this system by passing the laser through the half-meter monochromator shown in figure 2-2. The wavelength of a particular composition laser is varied by changing the temperature of the diode¹². In practice, this is accomplished in two ways. First, a wavelength range of interest is selected by changing the temperature of the heat-sink on which the diode is mounted using a small resistive heater with a feedback circuit to control the heat-sink temperature. Once the heat-sink temperature has stabilized, the diode temperature is varied about this point by changing the current through the diode. The current can either be swept rapidly and the laser output observed with an oscilloscope or the current can be swept slowly while the laser beam is mechanically chopped and phase sensitively detected. All of the data taken in this work used this latter mode operation. The laser beam was chopped with a tuning fork chopper at 400 Hz (figure 2-2) and the beam detected with a liquid nitrogen cooled HgCdTe detector with matched preamp. The preamp output was fed to

**TUNABLE DIODE LASER SYSTEM
(FROM LASER ANALYTICS, INC.)**

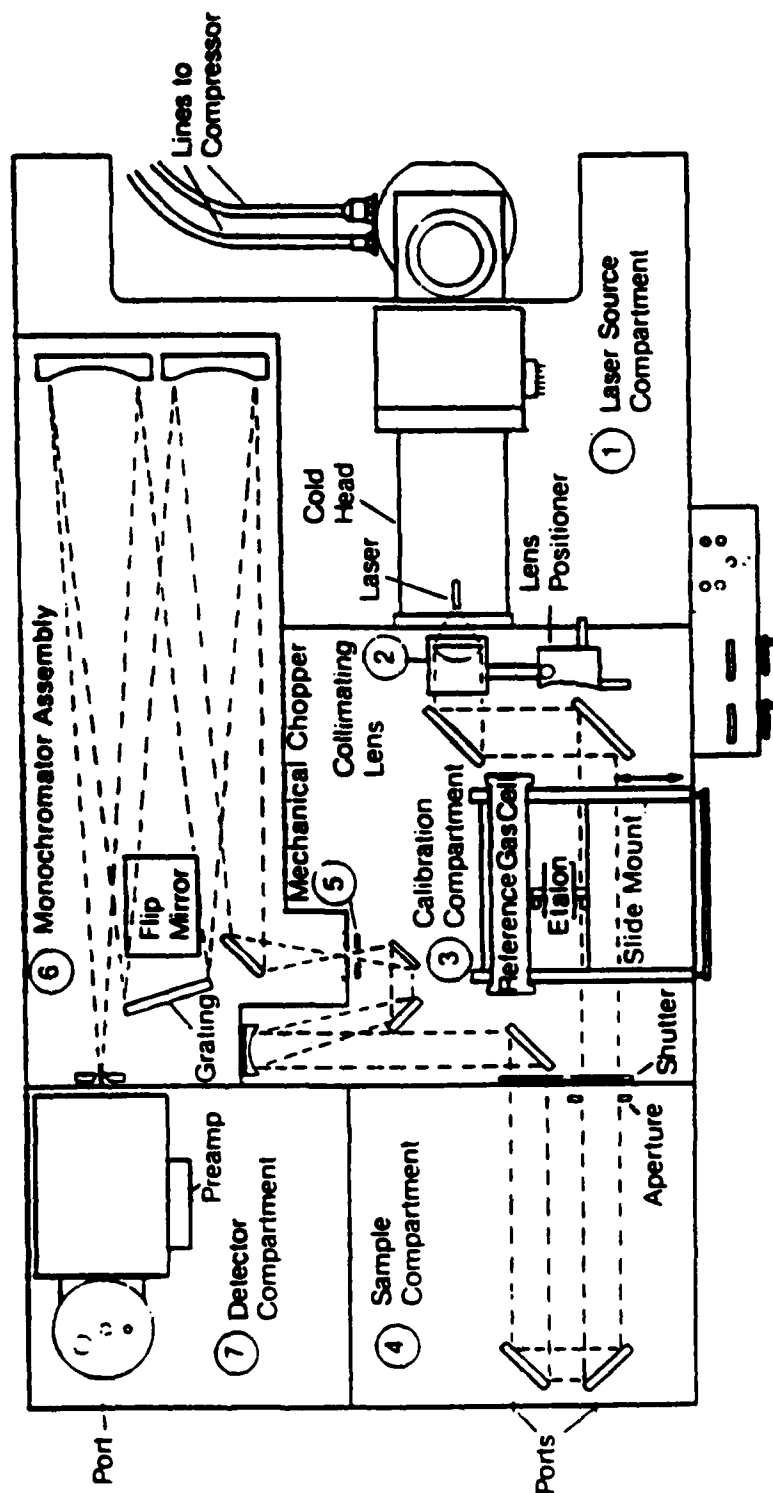


Figure 2-2: Tunable Diode Laser System

a PAR model HR-8 lockin amplifier. The output from the lockin was then digitized and sent to the H.P. 9836C computer (see figure 2-1). The diode current was swept by the computer using a digital-to-analogue converter (DAC) to drive an external current drive on the laser system. For the experiments here, the system was operated in the 'external beam mode' with the two beam turning mirrors removed from the sample compartment (see figure 2-2). Thus the beam was directed out of the instrument through the lower sample compartment port (figure 2-2), through the absorption cell, and then back into the instrument through the other sample compartment port. To measure the silane density in the absorption cell, a pair of PbSnTe diodes were chosen which covered the wavelength range of 10.5 to 11.7 microns. These lasers were mounted in the system cold head and either one could be selected by physically shifting the cold head in its mounts. With these diodes, the ν_4 band of silane could be scanned. This band was chosen for monitoring the silane density primarily because of the availability of stable diodes in this wavelength range which exhibited good tuning characteristics with little 'mode hopping' (see reference 33).

Calibration of the TDL System

Before silane density measurements could be made, the system had to be calibrated. The basic principle behind the density measurement is straightforward; the density is determined by measuring the absorption of the laser radiation by an isolated absorption line of the gas. The intensity of the laser radiation transmitted through an absorption cell of length l which contains a gas of density n is given by (neglecting window losses) Beer's law³⁴ as

$$I(\nu) = I_0(\nu) \cdot \text{Exp}[-n \cdot l \cdot k(\nu)] \quad (\text{eq. 2-2})$$

where $I_0(\nu)$ is the intensity of the radiation on the cell, ν is the wavenumber of the radiation, and $k(\nu)$ is the absorption coefficient of the gas. Figure 2-3 shows a transmittance spectrum of the ν_4 band of SiH_4 taken at 1 cm^{-1} resolution* with a Fourier Transform Infrared (FT-IR) spectrometer by the author. The band is overlapped by the much weaker ν_2

*For those not familiar with units of cm^{-1} , it is the reciprocal of the wavelength expressed in cm ($1 \text{ cm}^{-1} = 10^4/\lambda_{\text{microns}}$).

**SILANE ABSORPTION NEAR 900 cm^{-1} AT 1 cm^{-1} RESOLUTION
(1% SiH_4 IN NITROGEN AT 100 TORR, 75 cm PATHLENGTH)**

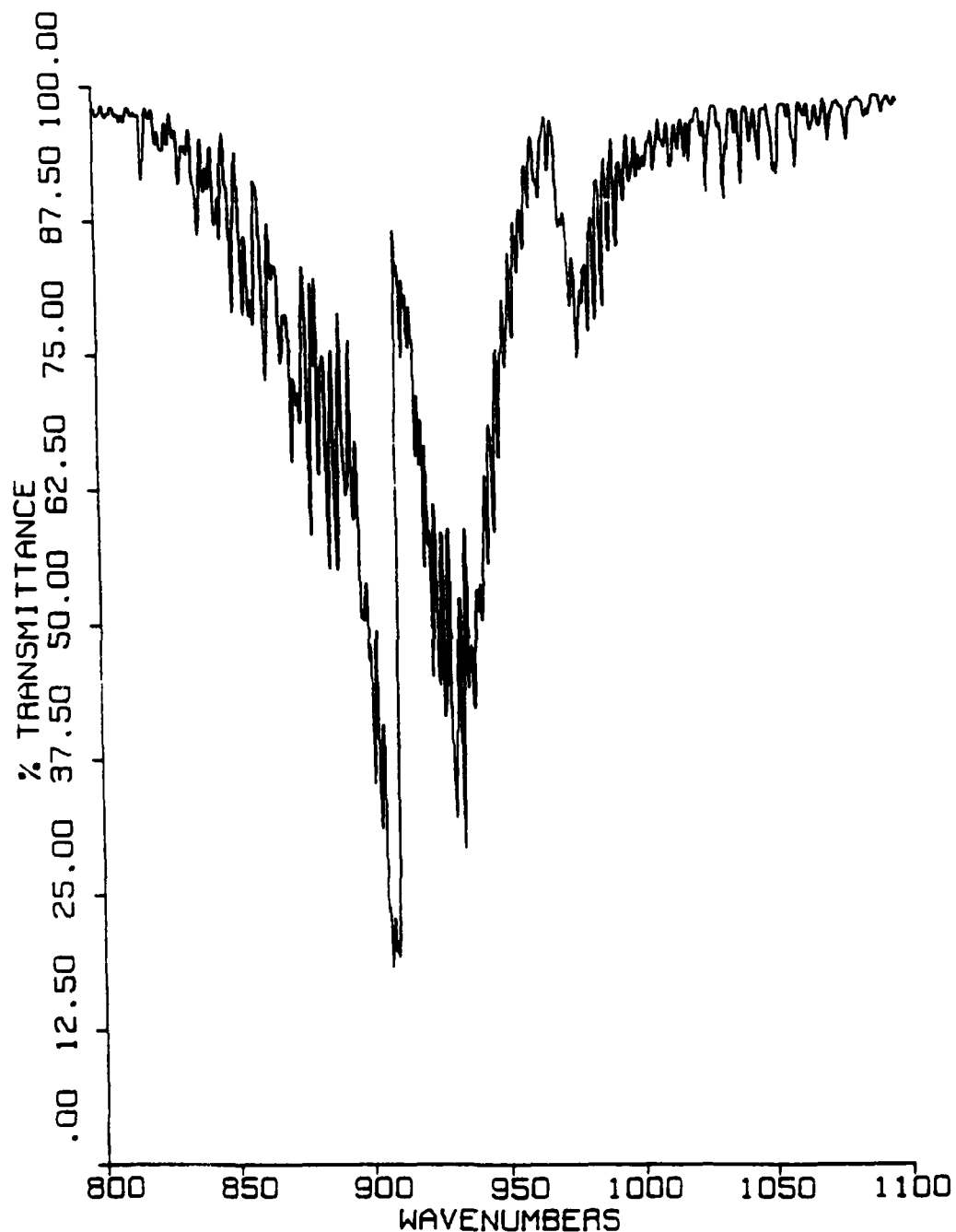


Figure 2-3: Silane Absorption Near 900 cm^{-1} (1 cm^{-1} Resolution)

band which is centered approximately 59 cm^{-1} above the ν_4 band.³ The transmittance is defined by

$$T(\nu) = I(\nu)/I_0(\nu) \quad (\text{eq. 2- 3})$$

Thus the transmittance spectrum is directly related to the absorption coefficient. As can be seen, the absorption coefficient is an extremely complex function of wavelength (or wavenumber). If the resolution is improved to 0.06 cm^{-1} as shown in figure 2-4 (FT-IR in this laboratory), still more features are revealed. Finally, if one scans the region at edge of the Q-branch near 910.7 cm^{-1} with the diode laser as in figure 2-5, individual absorption lines can be seen. The lower trace in figure 2-5 is an etalon fringe pattern made by inserting a 1 inch germanium etalon (see figure 2-2) into the TDL beam and repeating the scan. The etalon scan gives a means of calibrating the wavelength range of the TDL scan. In figure 2-5, the spacing of the etalon peaks is 0.04855 cm^{-1} . It should be pointed out that figure 2-5 is not a transmittance spectrum but is simply a plot of $I(\nu)$ vs. ν from the diode laser. The density of silane was determined by measuring the absorption of one of these isolated lines. For an isolated line with both Doppler and pressure broadening, the absorption coefficient is described by the Voigt function³⁴:

$$k(\nu) = S/\gamma_D [\ln(2)/\pi]^{1/2} \cdot V(x, y) \quad (\text{eq. 2-4})$$

where S is the line intensity, γ_D is the Doppler half-width at half maximum, and $V(x, y)$ is the Voigt function given by

$$V(x, y) = \frac{y}{\pi} \int_{-\infty}^{\infty} \frac{\exp(-t^2)}{[y^2 + (x-t)^2]} dt \quad (\text{eq. 2-5})$$

with x and y given by

$$x = [\ln(2)]^{1/2} \gamma_c/\gamma_D \quad (\text{eq. 2-6})$$

**SILANE ABSORPTION NEAR 900 cm^{-1} AT 0.06 cm^{-1} RESOLUTION
(1% SiH_4 IN NITROGEN AT 100 TORR, 75 cm PATHLENGTH)**

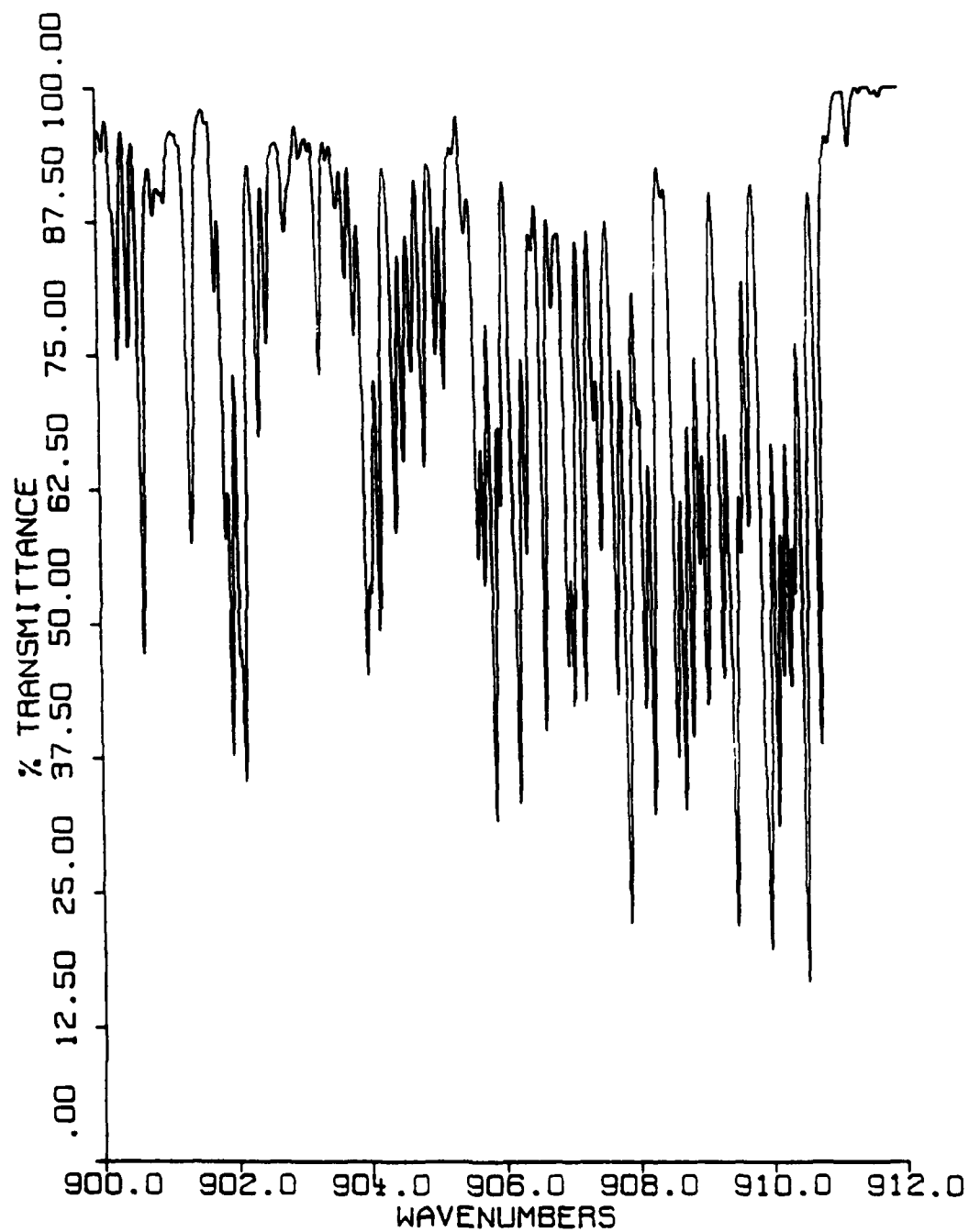


Figure 2-4: Silane Absorption Near 900 cm^{-1} (0.06 cm^{-1} Resolution)

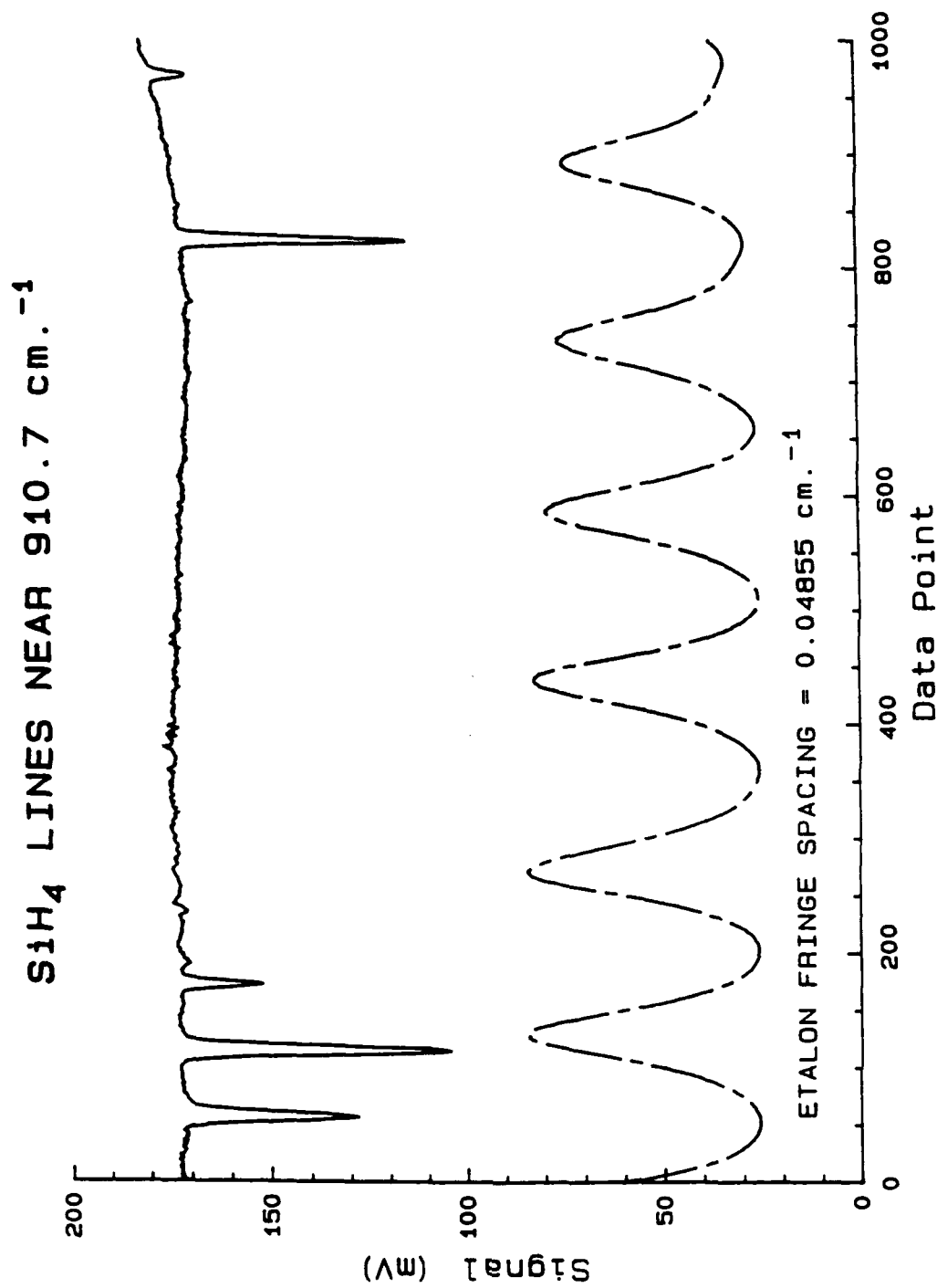


Figure 2-5: Tunable Diode Laser Scan of Silane Lines Near 910 cm⁻¹

$$y = [\ln(2)]^{1/2} \cdot (v - v_0) / \gamma_D \quad (\text{eq. 2-7})$$

where γ_D and γ_c are the Doppler half-width at half maximum and the pressure broadened half-width at half maximum for the line, and v_0 is the line center. γ_c is given by

$$\gamma_c = \sum_{i=1}^N \Gamma_i \cdot P_i \quad (\text{eq. 2-8})$$

where Γ_i is the broadening coefficient of the i th species in the gas mixture and P_i is the partial pressure of the i th species. Thus from this equation it is clear that the absorption coefficient $k(v)$ in equation 2-2 depends on the pressure and composition of the surrounding gas. This means that under conditions where the gas composition or the total pressure vary significantly, a measurement of the peak absorption of an isolated line is not sufficient to determine the density of the absorbing species. On the other hand, the integral of $k(v)$ over the full extent of the line, given by

$$S = \int_0^{\infty} k(v) dv \quad (\text{eq. 2-9})$$

i.e. the line intensity is a function of the gas temperature but independent of pressure. Thus, if the absorbance

$$a(v) = -\ln[T(v)] \quad (\text{eq. 2-10})$$

is measured over the full extent of the line, its integral will be proportional to the density of the absorbing species. Thus, if the line intensity is known, or can be measured from a known density (and pathlength) of the gas, then the density can be measured in an unknown sample. This was the method chosen for measuring the silane density.

A calibration was performed by operating the system shown in figure 2-1 in a static fill mode (no gas flowing) without a discharge. For the calibration, a gas mixture of 0.95% silane in argon was used. This gas mixture was supplied by Matheson and was guaranteed to be within 10% of the most significant figure in the mixture specification. Hence the mix

was guaranteed to be $0.95 \pm 0.005\%$ silane in argon. Next, a line was chosen to be the calibration line for the measurements. The strong line on the right of figure 2-5 was chosen as a calibration line because it was strong enough to give good sensitivity and isolated from other interfering lines. This line has been identified by Johns and Kreiner³⁵ as the Q(3),A₂,1 line at a position of $910.759 \pm 0.003 \text{ cm}^{-1}$. The system was filled to a known pressure with the mixture, then nitrogen added (to simulate conditions in the experiment) and a scan of the line taken. The diode output was adjusted so that the zero-gas background intensity was flat across the width of the line and on either side for at least four full widths of the line. After much trial and error, it was found just as accurate to fit a straight line across the top of the line and to use this as the zero-gas reference as to scan the region twice (with and without gas) and ratio these files. The measured $I(\nu)$ was then ratioed against this constructed reference to obtain a transmittance spectrum. An absorbance spectrum was then calculated, and two procedures were then used to obtain the line intensity. First, the absorbance spectrum was integrated numerically over the full extent of the scan. Since the path length and silane partial pressure were known, the line intensity S could be measured. The second procedure was to perform a least-squares fit of a Voigt function to the measured absorbance. The method used for the least-squares fit was the Marquardt algorithm which is described in Bevington³⁶. Voigt functions were generated using an algorithm described by Drayson³⁷. This later method gave much more consistent results. Five measurements were made with the result

$$S[\text{Q}(3),\text{A}_2,1] = 9.74 \pm 0.44 \text{ cm}^{-2}\text{atm}^{-1}.$$

The two procedures described above were then used along with this value of the intensity to measure silane density downstream of the afterglow.

Visible and U.V. Spectrometer

The spectrometer used to acquire visible and u.v. emission spectra of the reaction flame was a 0.5 meter Spex monochromator with independently adjustable entrance and exit slits. The reaction zone was imaged 1:1 on the entrance slit using a 50 mm diameter CaF_2 lens of 150 mm focal length. A 1200 lines/mm grating blazed at 500nm was used throughout the measurements. With this blaze the system could respond down to about 220 nm. The photomultiplier used was an RCA C31034 which is

sensitive over the range of about 200 to 890 nm. This photomultiplier has a GaAs photocathode and should be cooled for optimum performance. Cooling was supplied by a Products for Research thermoelectric cooler which in turn was water cooled. This system allowed the photocathode to be cooled to -20°C which resulted in a reduction in dark current to less than 2 nA. Two different systems were used to measure the PMT output during the course of the experiment. Early in the experiment, the PMT anode was simply connected to ground through a 20 Mohm resistor which had a 0.01 μf capacitor in parallel. The voltage across the resistor was measured with a Hewlett Packard model 3478A digital voltmeter operated in the auto range mode. The output of the voltmeter was sent to the 9836 computer over an IEEE 488 line. The second system for measuring the PMT output consisted of a Photochemical Research Associated model 1770 dual channel photon counting system with an interface module for transfer of data to the 488 bus. In this configuration, the PMT dark counts were on the order of 5 cps. Both systems worked very well and gave good dynamic range and signal-to-noise in the spectra. The latter system only became available near the end of the experiment.

Relative Calibration of the Spectrometer

Early in the experiment, it was found that intense emission was observed in the wavelength range 220-500 nm. It was decided to calibrate the spectrometer for relative response over this wavelength range. Unfortunately no standard sources were available in our laboratory that possessed sufficient intensity below 300 nm to allow calibration. Hence the system was calibrated between 300 and 500 nm. To perform the calibration, a tungsten ribbon standard lamp (Eppley Laboratories) was placed at the focus of the lens in figure 2-1 in place of the discharge tube. The difficulty with this calibration lies in the fact that at 300 nm the scattered light in the instrument is about a factor of 3 larger than the radiation from the standard lamp. To determine the scattered light contribution at a given wavelength, two sharp cutoff colored glass filters from Corning were used. Filter #3-75 transmitted down to 380 nm and filter #3-72 cutoff at 430 nm. For wavelengths up to 400 nm, the procedure was to record the signal from the PMT without any filters, then with filter #3-72 and then with filter #3-75. With a particular wavelength blocked, it was assumed that the signal was due to scattered light. But this was the scattered light present with the filter in place. To arrive at a value for the scattered light present with no filter in place, it

was assumed that up to 400 nm the ratio of scattered light with a filter to that without a filter was a constant. Measurements were then made of the scattered light at 200 and 220 nm (where the lamp output is negligible) with and without the filters in place. The ratios of these signals were then used to scale up the values measured for scattered light in the wavelength range of interest. An attempt was made to use a third filter, #3-67, which cutoff at 550 nm to determine the scattered light contribution in the wavelength range 400-500 nm. Unfortunately, the data indicated that the filter cutoff too much of the radiation from the lamp to accurately determine the scattered light contribution without the filter in place. Hence it was decided to treat the scattered light contribution as a constant over the range 400-500 nm and set the value at that measured for 400nm. Fortunately, the lamp signal in this wavelength range was greater than a factor of 25 larger than the scattered light, hence the error from treating the scattered light value incorrectly should be less than 4%. A calibration sheet supplied with the standard lamp gave only seven values of the lamp output between 300 and 500 nm. Signals were measured at each of these wavelengths, scattered light contributions removed, and the result ratioed to the radiance of the standard lamp. The resulting seven 'sensitivity values' for the system were then least-squares fit to a third order polynomial to allow the relative response of the system to be calculated at any wavelength between 300 and 500 nm.

Fourier Transform Spectrometer/Long Path Cell

During part of this work, the 1.2 m absorption cell shown in figure 2-1 was replaced by a 20 m absorption cell of the White-type³⁸. The base length of the cell is 0.75 m, but by reflecting the radiation entering the cell back and forth, a maximum path length of 20.25 m can be achieved. This cell is a commercially made unit from Wilks. Absorption spectra of species in the cell were obtained using a broadband infrared emitter (glowbar) and an FT-IR spectrometer. The cell, spectrometer, and associated optics are shown in figure 2-6. The detector used was a liquid nitrogen cooled HgCdTe. The FT-IR system is a commercial system built by EOCOM and interfaced to a Nicolet 1180 minicomputer. The system is capable of achieving a resolution of 0.06 cm^{-1} and with the KBr beamsplitter installed, could cover the wavelength range from 2.5 to 14 microns ($4000\text{-}400\text{ cm}^{-1}$). The reason for using the FT-IR system instead of the diode laser is for its great scanning range. The diode laser can typically only be scanned $\approx 0.5\text{ cm}^{-1}$ without changing the heat-sink temperature.

FT-IR/LONG PATH GAS CELL SYSTEM

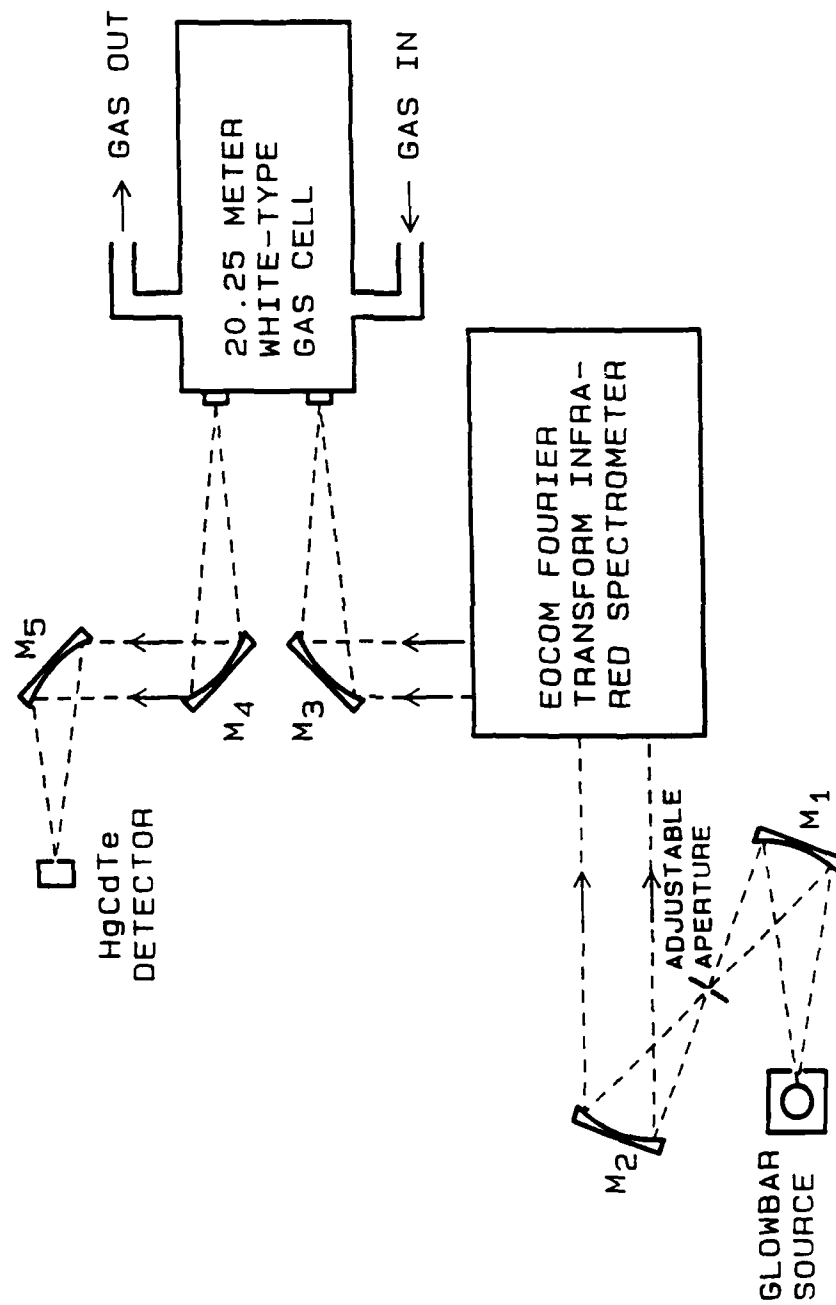


Figure 2-6: FT-IR/Long-Path Absorption Cell System

Thus the diode laser is useful when the species of interest is well identified, but for survey work the FT system is far superior. The 20 m cell was needed to give the FT system a comparable sensitivity to the diode laser for low pressure gases. Since the typical linewidth of an isolated line at 1 torr is on the order of 10^{-3} cm^{-1} , even at its highest resolution the FT system is a factor of 20 larger in FWHM. Thus peak absorbances measured with the FT system for an isolated line are typically a factor of 20 smaller than those measured with the diode laser.

Chapter III

Experimental Results

As stated in chapter I, this work began with the question of whether silane would be dissociated in active nitrogen. After the apparatus described in chapter II was assembled, the first observations made were aimed at answering that question. With nitrogen flowing, no discharge, and a small amount of the silane/helium mixture flowing, the diode laser was scanned across the wavelength region shown in figure 2-5 to observe the silane absorption. With the diode laser signal displayed in real time on an oscilloscope, the discharge was initiated and the silane absorption almost disappeared. Indeed, silane was dissociated in the afterglow. If that was all that had happened, the experiment probably would have stopped with a measurement of the rate of dissociation of the silane. But before any quantitative measurements were made, a number of general observations indicated that this was a very interesting system for study.

General Observations of the Reaction

The first surprising observation was that at the point where the silane was introduced, a bright lavender reaction flame was produced which could be seen with the room lights on if the pressure was of the order of few torr or higher. In addition, downstream of the reaction flame the straw-yellow afterglow was no longer visible. This reaction flame had also been described by Dewhurst and Cooper²⁹ but at the time of these first observations the author was unaware of that reference. After observing the reaction flame for only a few minutes, a white powder could be seen coating the walls of the reaction vessel and also the silane injection port. However, more striking than the flame itself was its behavior with pressure, silane flow, and discharge current. For example, at a few torr the flame could be made to move far downstream of the silane injection port by reducing the discharge current or the silane flow, yet the physical extent of the flame remained about the same. If the flame was moved far enough downstream that it moved out of the absorption cell

toward the pump, no silane dissociation was observed. Under slow nitrogen flow conditions, the flame shape changed to a disk which moved upstream of the silane injection port. Under some conditions of pressure, discharge current, and silane flow the reaction flame could be made to pulsate at about 1 Hz or less, and these pulsations could be seen in the silane dissociation. While this qualitative behavior was very repeatable, quantitatively many of the observations appeared to be influenced by the powder on the tube walls. In general, as the tube walls became coated, the reaction seemed to occur more slowly (reaction flame moved downstream) for the same discharge conditions and mass flow settings. Because of the effects of powder buildup on the tube walls, frequent cleaning of the flow tube was required. From these general observations, the conclusion was drawn that some kind of chain reaction must be involved in both the production of the chemiluminescence and the silane dissociation. Silane dissociation by direct reaction with a single afterglow species was ruled out from the complex behavior of the reaction flame. Though not quantitative, these general observations would later become a strong guiding force behind the description of the overall reaction process.

Reaction Flame Emission Spectra

Figure 3-1 shows a spectrum of the reaction flame taken at a background pressure of 2 torr. Resolution (FWHM) is about 0.5 nm and the spectrum is not corrected for system response. The strongest features in the spectrum are atomic silicon lines at 250, 290, and 300 nm, SiN emission between 390 and 430 nm, and an unidentified broadband continuum emitter between 450 and 870 nm. Close inspection actually shows that the continuum extends down to about 300 nm. Figure 3-2 shows a more detailed spectrum of the Si emission at a resolution of 0.1 nm. In figure 3-2, the log of the intensity is plotted so the weaker lines near 250 nm can be more easily seen. Table 3-1 lists the Si lines observed. The wavelengths and transitions are from Striganov and Sventitskii³⁹. Jevons⁴⁰ has observed the same Si lines in the reaction of SiCl_4 in active nitrogen. Jevons also observed an additional group of lines between 220 and 222 nm, but in that wavelength range, the sensitivity in the work reported here is almost zero. The only other lines reported by Jevons besides those given in table 3-1 are lines at 243.8, 244.3, 245.2, and 253.2 nm. Jevons reports that for each of these lines, the intensity is "weaker than in a discharge" of SiCl_4 vapor. Since these lines are listed as

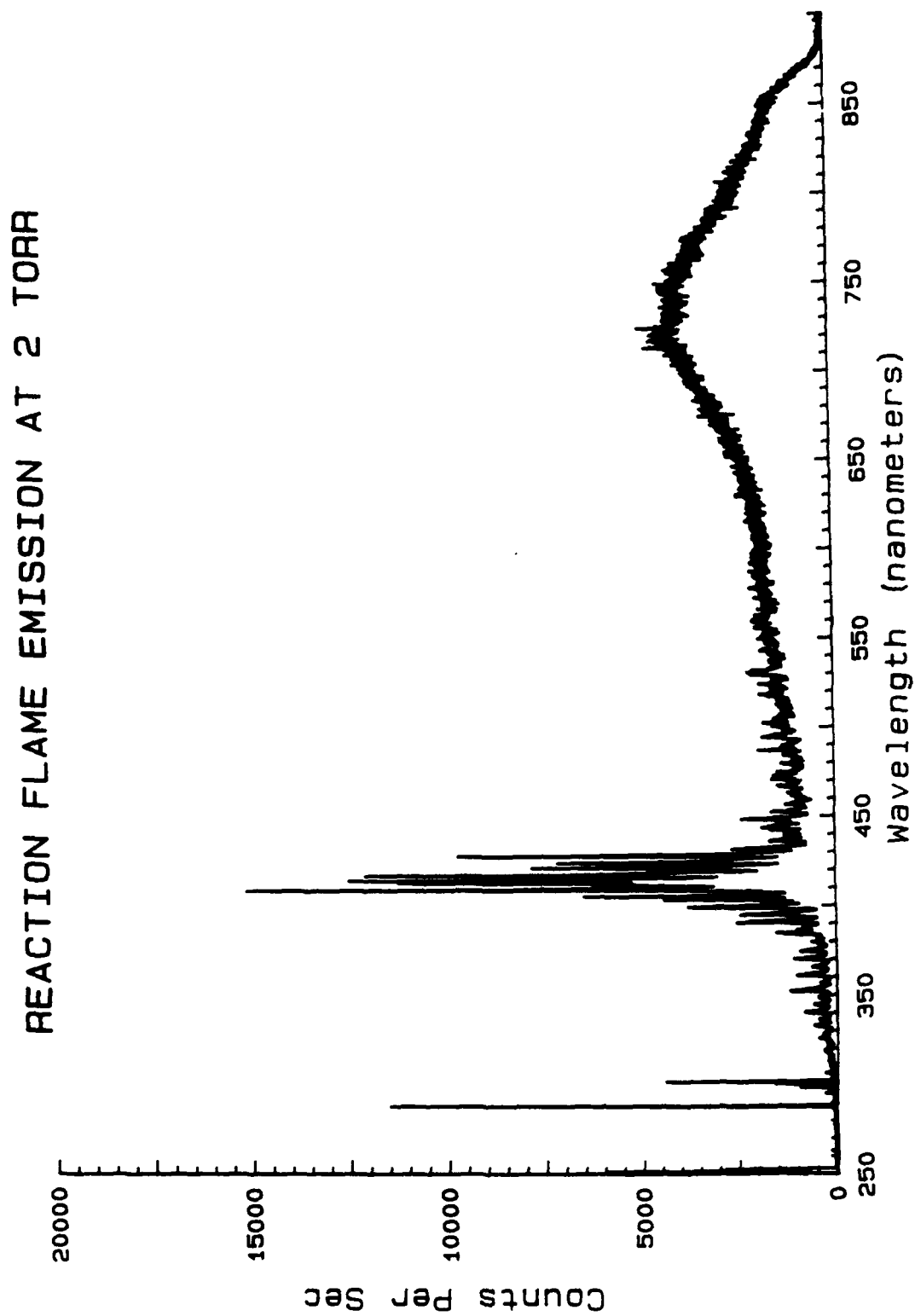


Figure 3-1: Emission Spectrum of Reaction Flame at 2 torr

MOST INTENSE Si LINES

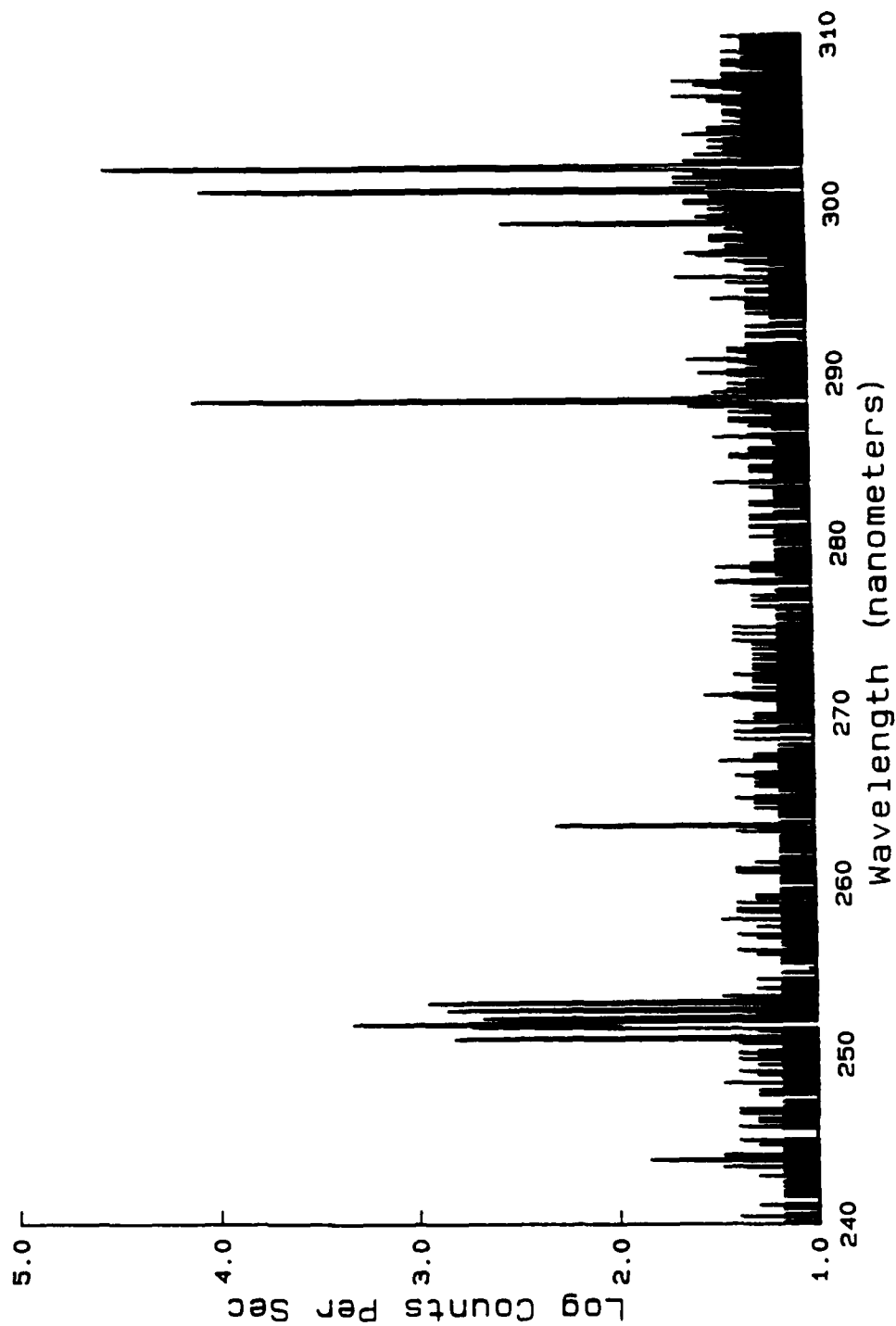


Figure 3-2: Most Intense Silicon Lines Seen in Flame

very weak in Striganov and Sventitskii, they may have been too weak to observe in this work.

Table 3-1: Si Lines Seen in Reaction Flame

<u>Wavelength (nm)</u>	<u>Transition¹</u>	<u>J²</u>	<u>Relative Intensity³</u>
243.52	3p ² ¹ D-3d ¹ D°	2-2	67
250.69	3p ² ¹ D-4s ³ P°	1-2	656
251.43	3p ² ³ P-4s ³ P°	0-1	536
251.61	3p ² ³ P-4s ³ P°	2-2	2100
251.92	3p ² ¹ D-4s ³ P°	1-1	466
252.41	3p ² ³ P-4s ³ P°	1-0	700
252.85	3p ² ³ P-4s ³ P°	2-1	874
263.13	3p ² ¹ S-3d ¹ P°	0-1	200
288.16	3p ² ¹ D-4s ¹ P°	2-1	12300
298.76	3p ² ¹ D-4s ³ P°	2-1	334
300.67	3p ² ³ P-3p ³ ⁵ S°	1-2	10825
302.00	3p ² ³ P-3p ³ ⁵ S°	2-2	32325
390.55	3p ² ¹ S-4s ¹ P°	0-1	2548

¹Transition listed as lower state-upper state

²Total J vaules are upper J-lower J

³Measured from data at 10 torr; not corrected for spectrometer response

As in the work here, Jevons was unable to identify any Si lines above 390.5 nm in the afterglow. Jevons does, however, point out that lines above 390.5 nm are seen very clearly in a discharge of SiCl₄. Figure 3-3 shows a more detailed spectrum of the SiN emission which originates from the B-X transition of SiN⁴¹. Vibrational band assignments are given as (v'-v'') and are from reference 43. Besides the unidentified broadband emitter, only Si and SiN emission could be identified. No NH_x, H₂, H, or SiH emission could be observed despite careful attempts to identify emission from these species. Dewhurst and Cooper²⁹ also reported that no ammonia, hydrazine, or other liquid nitrogen condensable products were formed. Comparing the spectra shown here with the recent work of references 30 and 31, who also looked at silane in active nitrogen, the spectra in this work agree qualitatively with those of Horie, et al.³⁰, but differ

DETAILS OF SiN EMISSION

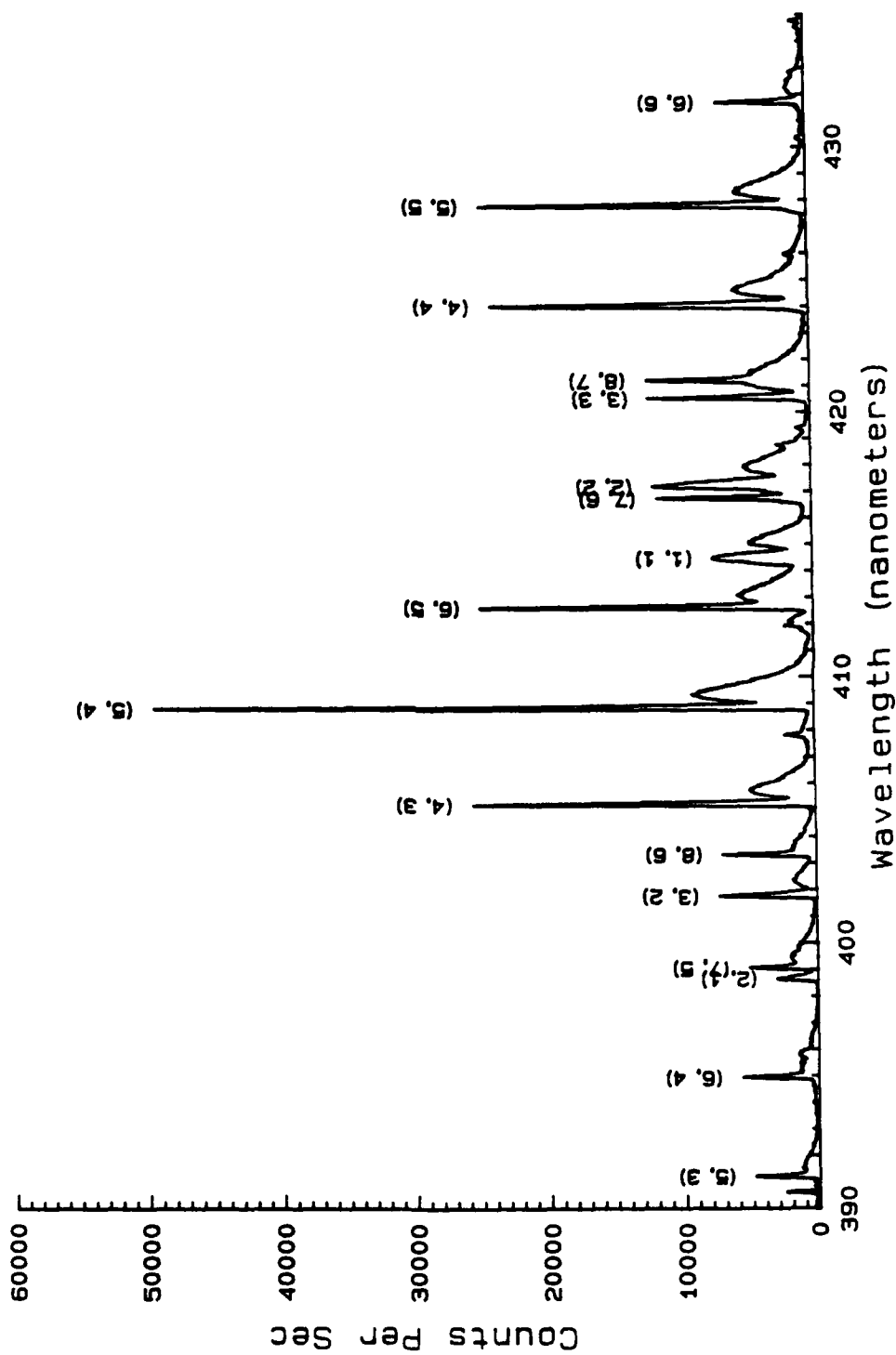


Figure 3-3: Detail of SiN Emission Seen in Flame

significantly from those of Piper and Caledonia³¹. Piper and Caledonia observed rather strong NH emission and weak SiH emission while Horie, et al. could not detect either of these species. The SiN emission observed by Piper and Caledonia was very weak while in the work of Horie, et al. the SiN emission was a dominant feature as in this work. In addition, Piper and Caledonia do not show any broadband emission above 450 nm, but show continuum emission between about 280 and 430 nm. On the other hand, Horie, et al. observe strong continuum emission between 450 and 810 nm but show no broadband emission below 450 nm. The differences in the experiments are primarily in the construction of the flowing afterglow systems. Horie, et al. used a system very similar to the one used here which used relatively slow gas flow while Piper and Caledonia used a much higher flow speed system. Specifically, the spectra presented in reference 30 were taken about 60 ms after the silane was injected, while the spectra presented in reference 31 were acquired at about 10 ms into the reaction. The pressures in the two experiments were 3 torr and 1.5-2 torr respectively. Thus, Piper and Caledonia are observing the chemiluminescence from very early times in the reaction, while in the work of both Horie, et al., and this work, the observed chemiluminescence is from much later in the reaction. Scans of the reaction flame given in reference 30 indeed show that for early times in the reaction both the Si and SiN emission are very weak. The inability to characterize the flow conditions in this work prevented quantitative measurements of the time dependence of the chemiluminescence, but spectra taken at different points in the reaction flame also indicated a buildup of the Si and SiN emission. These data support the idea that the differences in the observed spectra are a result of the measurements being made at different times in the reaction history. On the other hand, it was found in this work that the broadband emission recorded at 800 nm preceded both the Si and SiN emission. This was also observed by Horie, et al., yet as mentioned earlier Piper and Caledonia show no long wavelength continuum in their data. In a phone conversation with Piper, he stated that looking carefully at his data it appeared "the chart recorder pen did not go to zero" above 450 nm. This statement together with the fact that they used a grating blazed for the u.v., may have lead to the continuum being overlooked. It appears reasonable, therefore, that the qualitative differences between the spectra observed in this work and reference 30, and those observed in reference 31 are probably due to differences in the time of observation of the reaction history. The failure of reference 30 to see the origin of the continuum closer to 300 nm may have been the result of the pressure used

in their experiment. This pressure effect will be discussed in the following section.

Pressure Effects on the Emission

Figures 3-4 through 3-7, along with figure 3-1 show emission spectra obtained between 0.5 torr and 8 torr total pressure. Resolution is approximately 0.5nm. In each case the nitrogen flow was adjusted to maintain constant flow speed. The silane/helium mixture was adjusted so that the afterglow was fully quenched downstream of the reaction zone. The spectra show how the continuum emission decreases relative to the Si and SiN emission as the pressure is increased. Because of this, positive identification of the SiN emission at 0.5 torr was difficult. The spectra also show that the SiN emission increases faster than the Si emission at the higher pressures. Beyond these observations, it is difficult to draw too many quantitative conclusions from the data due to the behavior of the reaction flame. At higher pressures (8-10 torr) the flame is very intense and very compact, much like a bunsen burner flame. As the pressure is decreased, the intensity of the flame decreases and the flame becomes more diffuse. For example, at 0.5 torr the 'flame' completely fills the 36 mm section of the flowing afterglow system (see figure 2-1), appearing as a very diffuse glow. On the other hand, the emitting volume sampled by the spectrometer was essentially fixed by the collection optics and slit area. This volume was roughly 2 cm x 0.3 mm (slit height x width) x 3.6 cm (diameter of flow section). For good quantitative data, some kind of integration over the full extent of the flame would be needed, and this was not available. As can be seen by comparing figures 3-4 and 3-5 with figure 3-6, it is much clearer in the spectra taken at less than 2 torr that the continuum emission extends down to $\approx 300\text{nm}$. This may explain the failure of Horie, et al.³⁰ to observe any continuum below 450nm, as all of their data were taken at pressures very close to 3 torr. Besides pressure, another possible explanation for the increased intensity would be the increase in N-atom density with pressure in the experiment. If the chemiluminescence is driven by N-atoms, then this increased density might explain the increased intensity of the emission. To determine the relative increase in N-atom density, the intensity of the N_2 first positive emission in the afterglow was used. Figure 3-8 is a spectrum of a typical afterglow from this experiment taken at 2 torr. The intense emission of the first positive system gives the afterglow its straw-yellow color. While there are numerous theories that attempt to explain the origin of

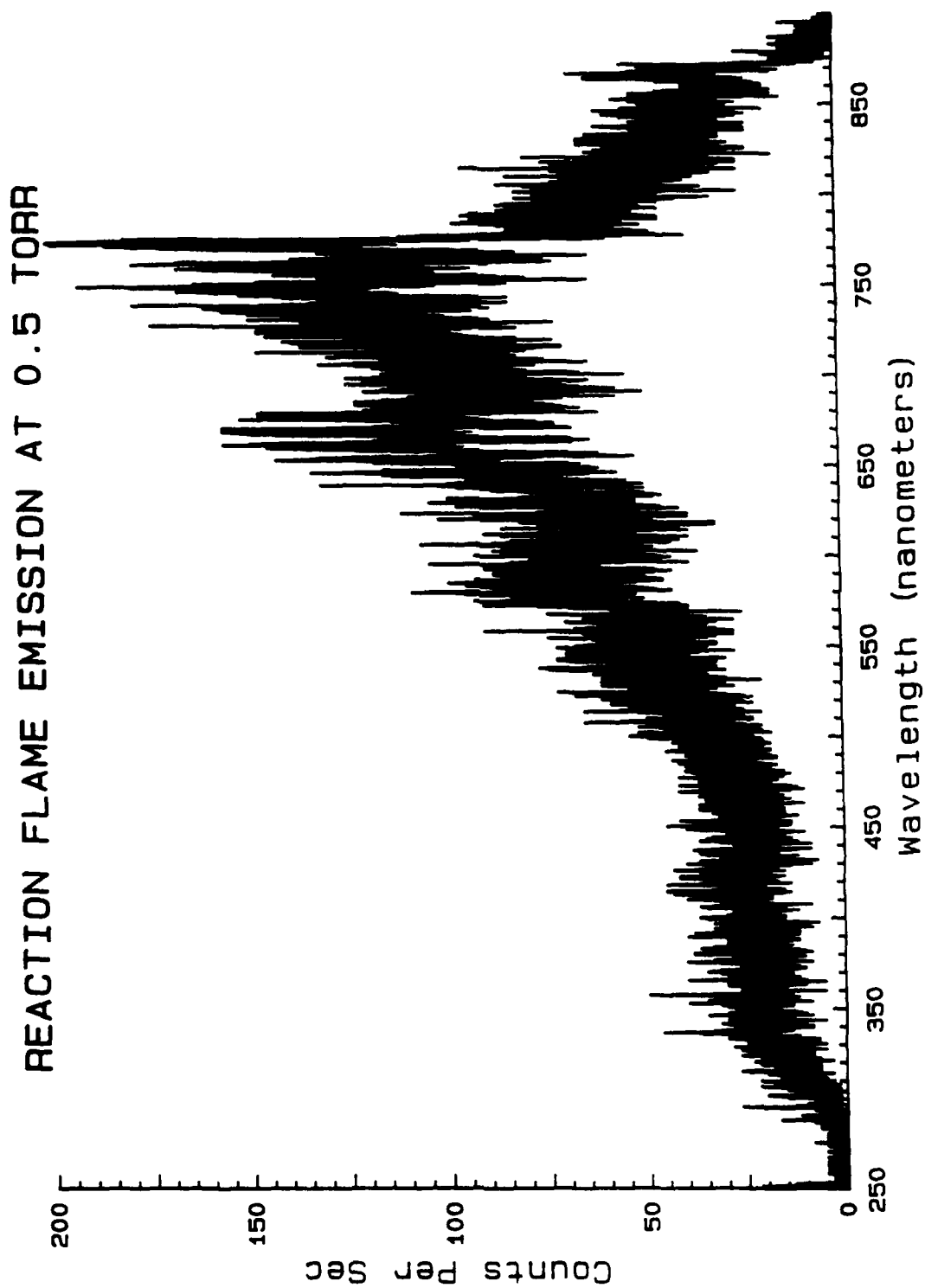


Figure 3-4: Emission Spectrum of Reaction Flame at 0.5 torr

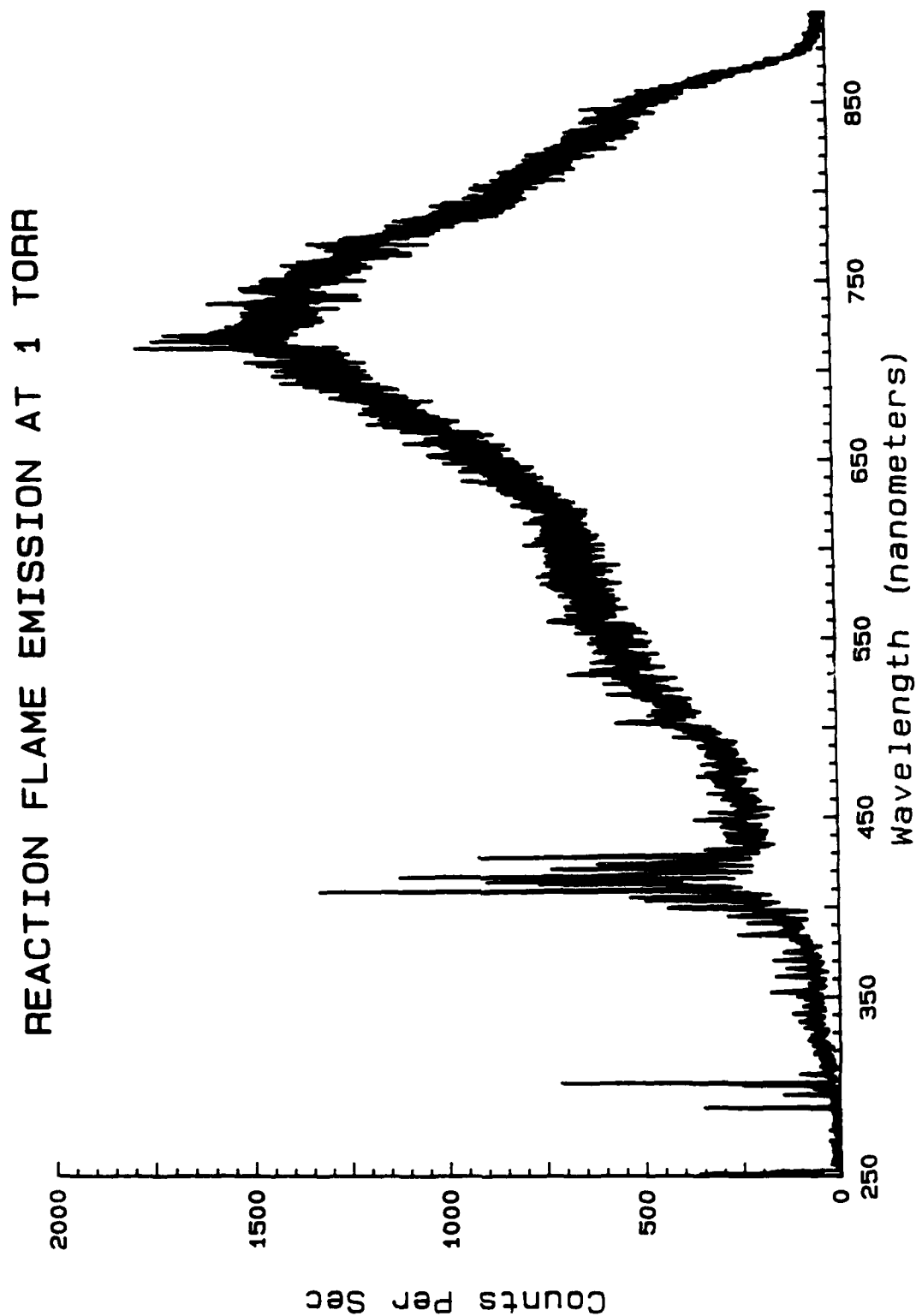


Figure 3-5: Emission Spectrum of Reaction Flame at 1 torr

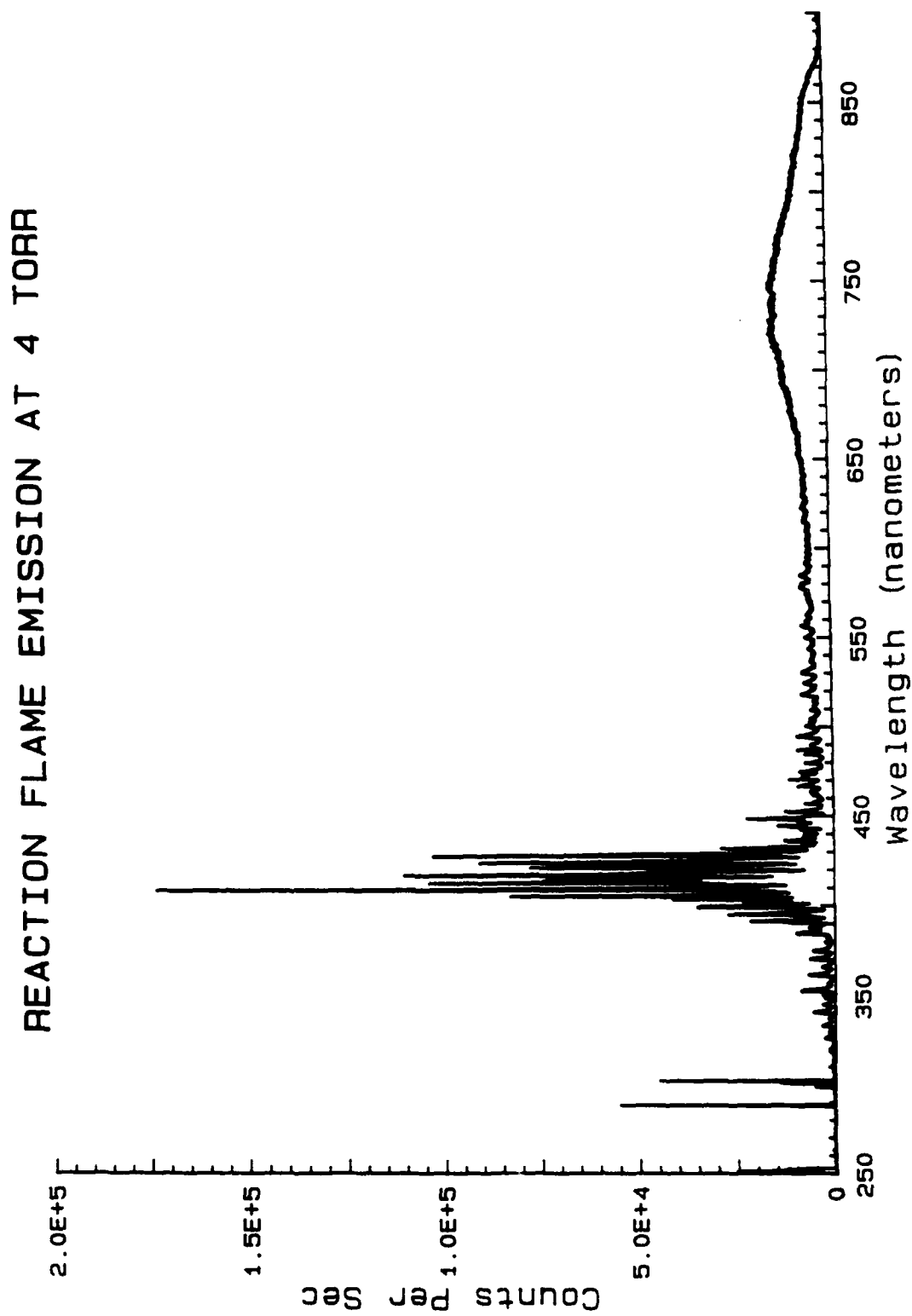


Figure 3-6: Emission Spectrum of Reaction Flame at 4 torr

REACTION FLAME EMISSION AT 8 TORR

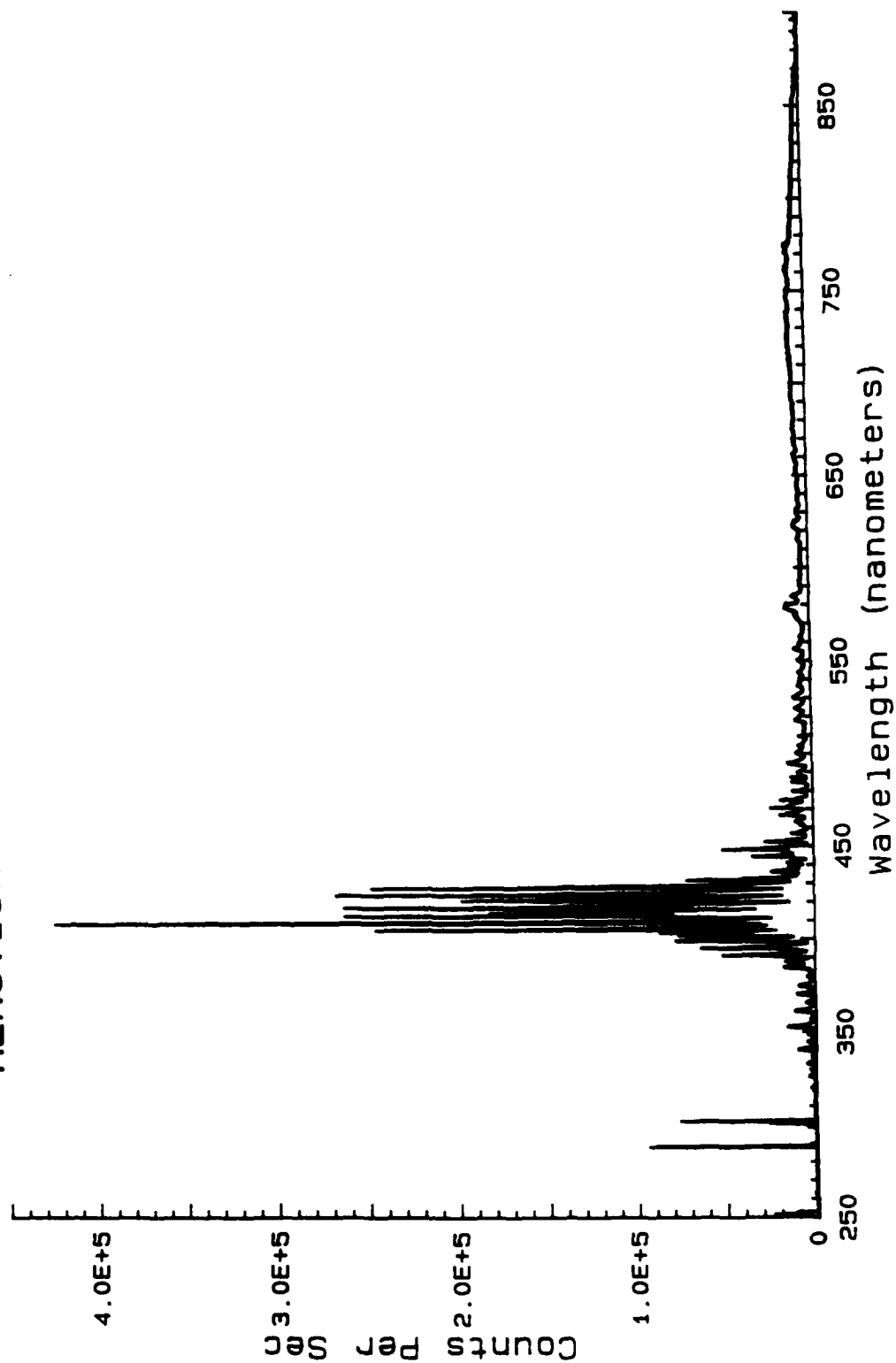


Figure 3-7: Emission Spectrum of Reaction Flame at 8 torr

NITROGEN AFTERGLOW EMISSION AT 2 TORR

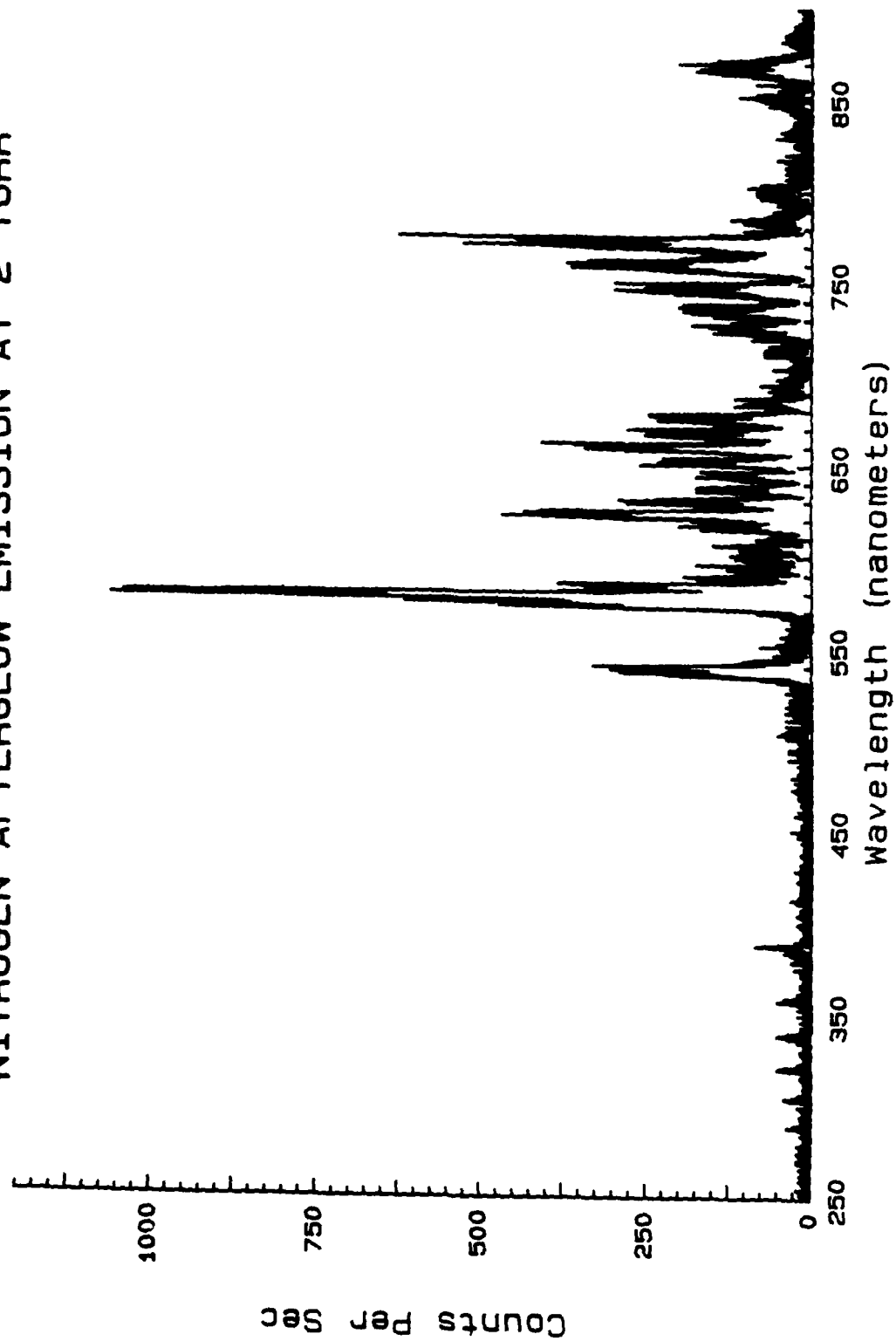


Figure 3-8: Emission Spectrum of Nitrogen Afterglow at 2 torr

the first positive emission, experimentally it is observed that in the pressure range of 1-10 torr, the intensity of the first positive afterglow emission is proportional to the square of the N-atom density.⁴² Thus measurements of the first positive intensity before silane was introduced could be related to the N-atom density in the afterglow. Before each of the spectra shown in figures 3-4 through 3-7 (and 3-1) were taken, a spectrum of the first positive emission was recorded without silane flowing. The first positive spectra were then numerically integrated from 565nm to 610nm and this integral used as a measure of the first positive intensity. For example, between 1 and 8 torr the SiN emission increased by a factor of 360 while the first positive intensity only increased by a factor of 68. This indicates that the N-atom density only increased by a factor of 8.2. The Si emission likewise increased more than the first positive intensity. This indicates that there is an effect of total pressure on both the Si and SiN emission which exceeds the rate of increase one might expect from increased N-atom density at higher pressures. While it is difficult to be very precise in any quantitative analysis of the emission data for the reasons stated above, it does appear that **both the Si and SiN emission increase faster than linear with pressure**, even when scaled to the increased N-atom density.

SiN B-State Vibrational Populations

Figure 3-9 shows a set of Morse potentials for SiN constructed from the molecular constants given by Foster⁴³. Foster does not, however, give values for the dissociation limits. The dissociation limits were taken from Breuohl, et al.⁴¹ who extrapolated the ground state potential to a value of $D_0=5.77$ eV. The ground state dissociation energy given by Herzberg⁴⁴ is $D_0=4.5$ eV. Since the dissociation energy of SiN is important for determining the energetics of various reactions in the afterglow, a more detailed discussion of the dissociation energy is given in appendix A. As stated earlier, the emission shown in figure 3-3 is from the B-X transition. Bands originating from the first 10 vibrational levels of the B-state could be identified in spectra taken during the experiment. Using available Frank-Condon factors⁴⁵, the relative populations of the B-state were calculated from the measured intensities of the B-X emission. These relative populations are shown in figure 3-10. These data were obtained from intensity measurements taken at 10 torr total pressure. The procedure used to obtain the data was to first correct the spectra for the

MORSE POTENTIALS FOR SiN

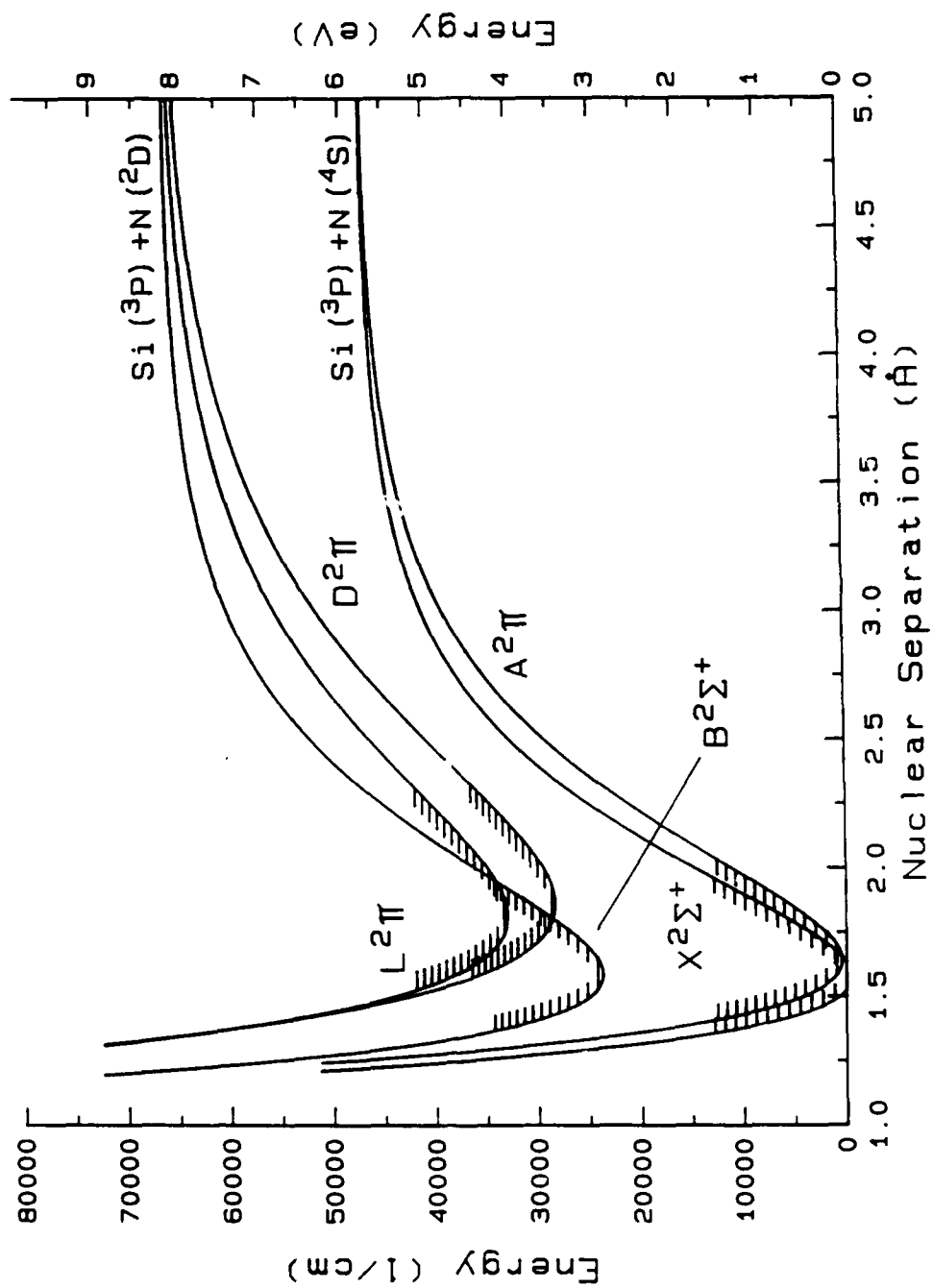


Figure 3-9: Morse Potentials for SiN

MEASURED RELATIVE SiN B-STATE VIBRATIONAL POPULATIONS IN THE N₂ AFTERGLOW

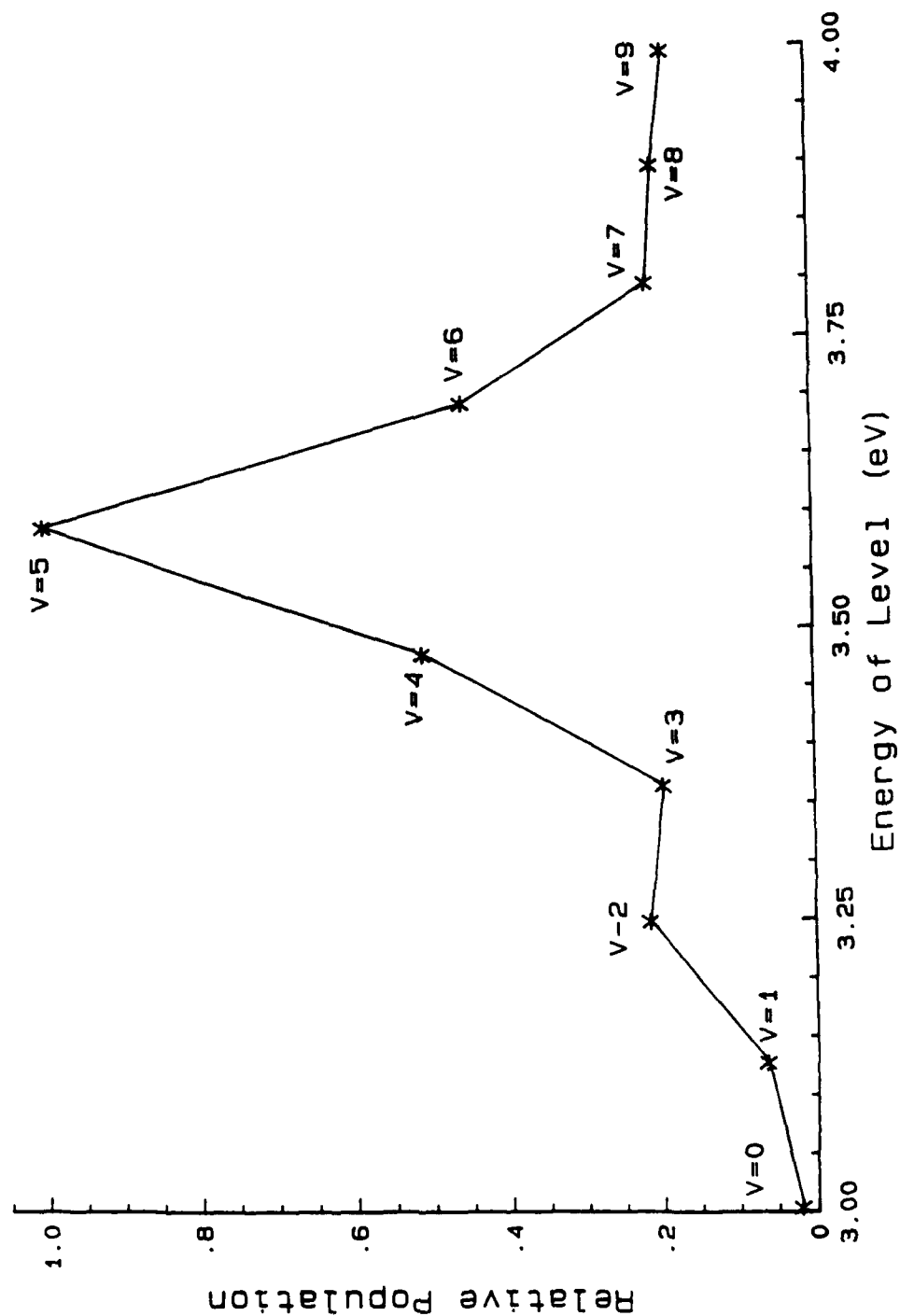


Figure 3-10: Measured Relative SiN B-State Vibrational Populations

relative response of the spectrometer system using the calibration procedure described in chapter 2. Next, intensities of the R-branch bandheads were recorded for each transition that could be observed. Each resulting intensity value was then divided by the corresponding Frank-Condon factor to arrive at a set of relative populations. Finally, relative populations having a common upper level were grouped and a weighted average taken. The weights were set proportional to the intensity of the transition. These average values of the relative populations of the upper levels were then scaled to the maximum value of the population of $v=5$. No error bars are given in figure 3-10, but reference 45 gives the Frank-Condon factors as accurate to between 5% and 10%. Probably an error of 10%-20% is reasonable for the data of figure 3-10. As can be seen, the data clearly shows a peak at $v=5$ of the B-state. This distribution is unusual in that one would normally expect the $v=0$ state to be the most populated. What is perhaps even more unusual is that an almost identical vibrational population distribution has been seen by Broida⁴⁶ in the SiN emission from the reactions of SiCl_4 and SiBr_4 in active nitrogen. Thus, **the vibrational populations in the B-state of SiN follow the same distribution whether the starting 'fuel' is SiH_4 , SiCl_4 , or SiBr_4 .**

Silane Dissociation Measurements

As discussed at the beginning of this chapter, silane was indeed dissociated in the reaction with active nitrogen. Since a dc discharge was used to produce the afterglow in this experiment, it was first decided to measure the amount of silane dissociation as a function of the discharge parameters such as current, voltage, and pressure. Early on in the investigation, it was felt that the afterglow produced from the dc discharge could be modeled with available data from the literature; therefore, measurements of the discharge parameters could be later correlated to specific characteristics of the afterglow. Unfortunately, the modelling proved to be unreliable at predicting **detailed** behavior of the afterglow so that it was very difficult to draw conclusions from the measurements of the dissociation as a function of discharge parameters. For example, model predictions of the N-atom density were as high as 10% while measurements by Caledonia, et al.⁴⁷ give typical densities of less than 1%. It was then decided to try and correlate the dissociation measurements with some other parameters of the experiment which were more easily related to some characteristic of the afterglow.

As discussed earlier, the N_2 first positive intensity in the afterglow is proportional to the square of the N-atom density. It was therefore decided to measure the silane dissociation as a function of the first positive emission intensity. To do this, the apparatus shown in figure 2-1 was modified slightly. To monitor the first positive intensity, a small side-looking photomultiplier with a slit and narrow band filter was placed just upstream of the silane injection tube. Using this system, the afterglow intensity could be measured before the silane was introduced into the reactor. The PMT was a Hamamatsu R106 and the filter was a Baird Atomic #10-30-6 which had a center wavelength of 578 nm and a bandwidth of approximately 13 nm. It was found necessary to locate the PMT slightly away from the silane injection port because first positive emission from the discharge was scattered from the injection tube and overwhelmed the afterglow signal. Even with the offset of the PMT, a small amount of scattered light from the discharge still entered the PMT and had to be corrected for in the measurements. The correction procedure involved quickly reducing the nitrogen mass flow while allowing the pressure control to maintain constant pressure in the system. When gas flow reached zero, the afterglow intensity effectively reached zero and the PMT reading was taken as the scattered light from the discharge. This value was then subtracted from the reading taken with nitrogen flowing. The PMT signal was read out through a current-to-voltage converter connected to a digital voltmeter. To measure the silane dissociation, the following procedure was used. After the discharge had stabilized and the afterglow intensity measured, a small amount of silane/helium mixture was introduced and the downstream silane density measured with the TDL system. The density was determined using the procedures described in chapter 2, particularly the method of least-squares fit to the Voigt profile. Depending on the strength of the absorption, the silane/helium mass flow was either increased or decreased so as to give a set of downstream silane densities that could be accurately measured but as close to zero as possible. This procedure followed the approach of a titration measurement to determine what silane/helium mass flow would yield zero silane density downstream. The data were then plotted as in figure 3-11 and least-squares fit to a straight line. The intercept was then taken as the maximum helium/silane mass flow for complete silane dissociation. This raw value of mixture mass flow was then multiplied by 0.009 to convert to silane mass flow. This value was taken as the 'dissociated silane'. Figure 3-12 shows a log-log plot of the first positive intensity vs. the dissociated silane. The straight line is a least-squares

HELIUM/SILANE MASS FLOW VS. SILANE DENSITY DOWNSTREAM OF REACTION ZONE

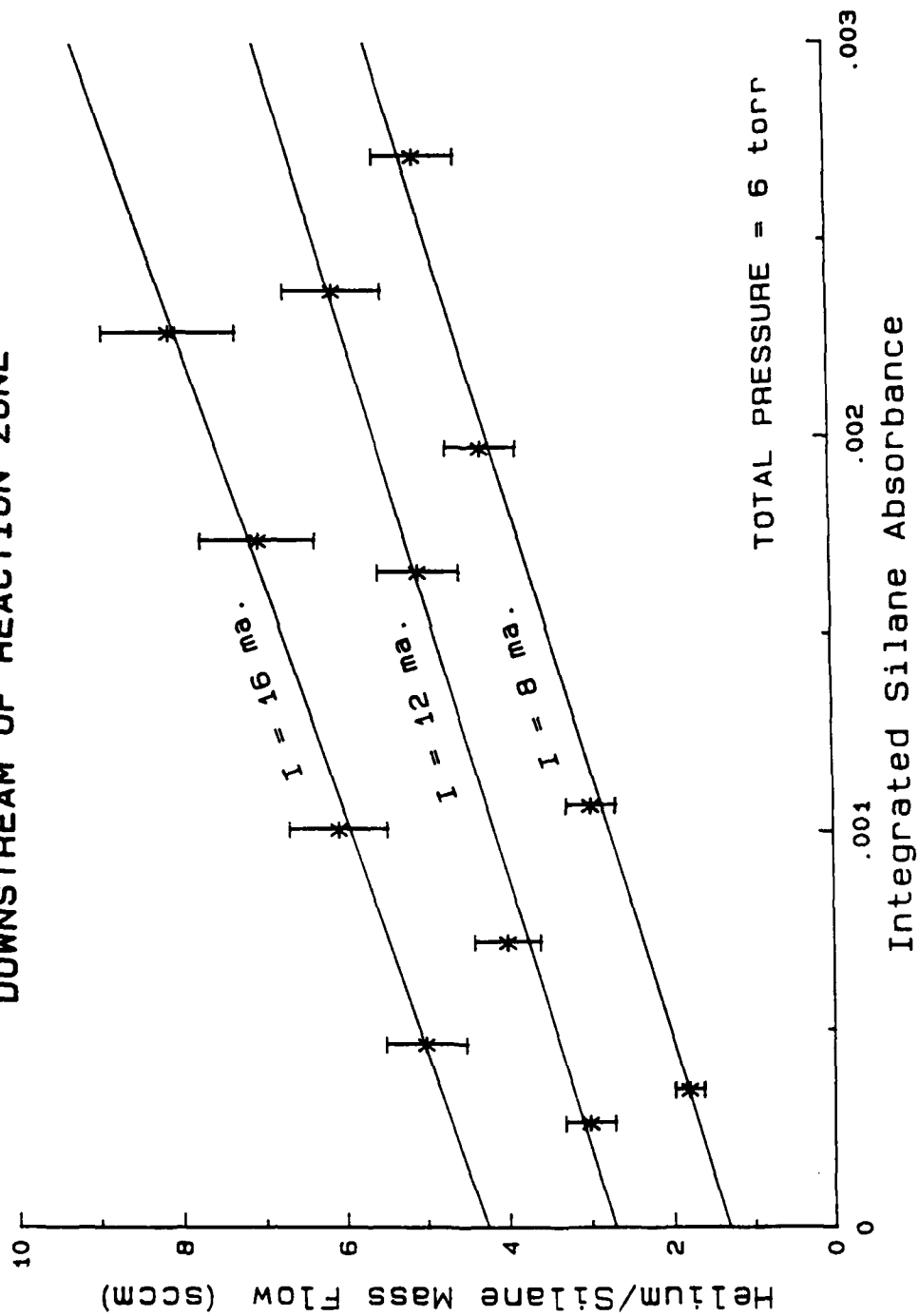


Figure 3-11: Helium/Silane Mass Flow vs. Downstream Silane Density

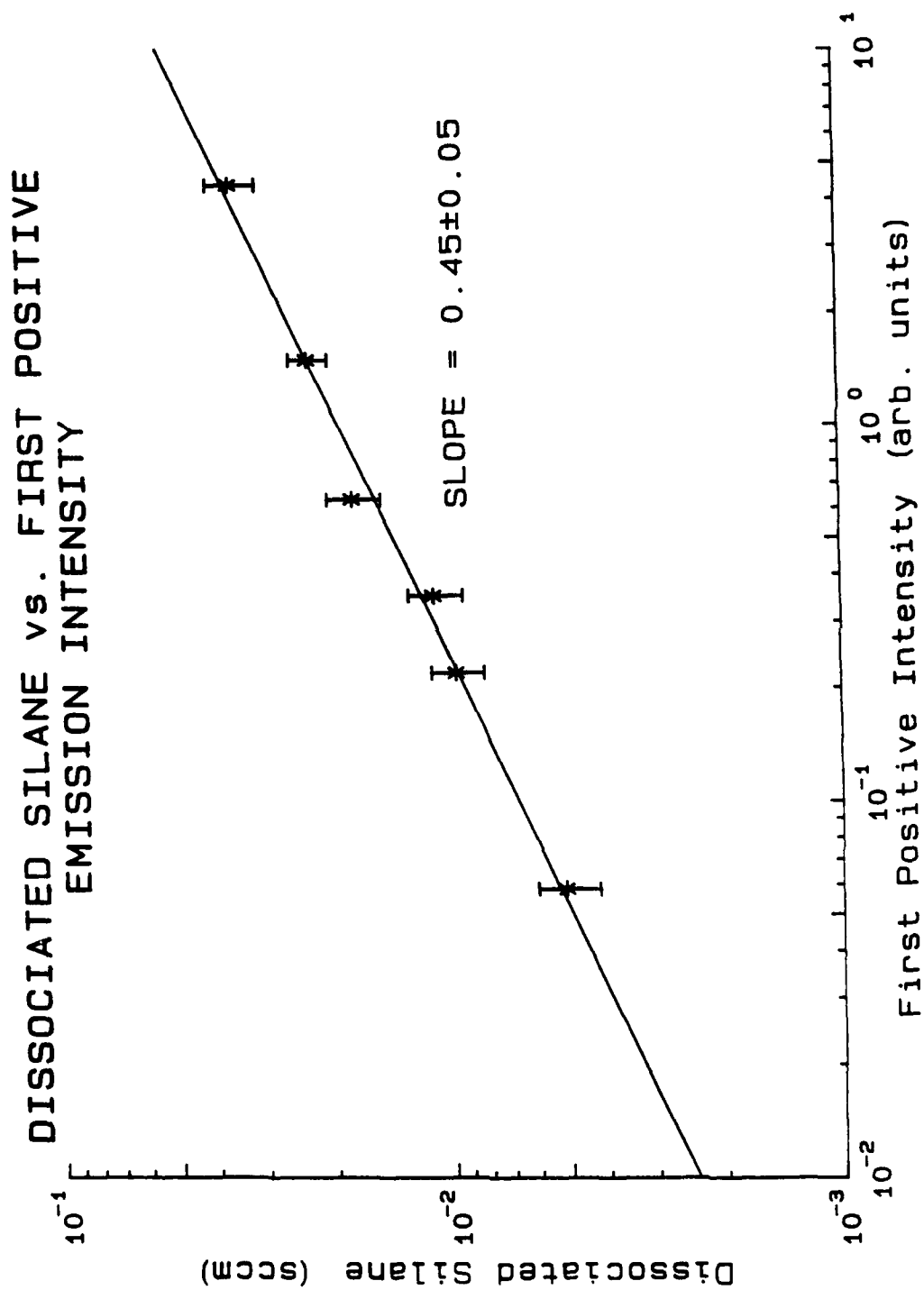


Figure 3-12: Dissociated Silane vs. First Positive Emission Intensity

fit which yields a slope of 0.45 ± 0.05 . This indicates that the silane dissociation is proportional to the first positive intensity to the 0.45 power. Since the first positive intensity is proportional to the square of the N-atom density, these data indicate that to within the uncertainty of the measurements, and for small amounts of silane, **the amount of silane dissociated is proportional to the N-atom density in the afterglow.**

FT-IR Absorption Measurements

As discussed in chapter 2, during this part of the experiment the 1.2 m absorption cell in figure 2-1 was replaced with the FT-IR/Long Path Cell system shown in figure 2-6. The purpose of these measurements was to survey the species leaving the reaction zone with absorption spectroscopy in hopes of identifying species which might not emit in the visible. Initially, measurements were made at 4 cm^{-1} resolution with the path length at 20.25m. Figure 3-13 is a transmittance spectrum of the reaction products taken at a total pressure of 10 torr and with the silane flow adjusted to ensure more silane than could be dissociated by the afterglow. The sharp features at $\approx 910 \text{ cm}^{-1}$ and $\approx 2180 \text{ cm}^{-1}$ are due to unreacted silane. Likewise, the rapidly varying structures on each side of the sharp feature at 2180 cm^{-1} are also due to silane. The structure centered at about 1500 cm^{-1} is due to residual water vapor in the lab air which did not "ratio out" when the transmittance spectrum was calculated. The broad features at 900 and 2200 cm^{-1} which overlap the silane are due to new species. Figure 3-14 shows that if the silane/helium flow is reduced so that all of the silane is reacted, these broad features remain. Absorption spectra taken at 0.06 cm^{-1} resolution, though much noisier, show the same broad features. No structure beyond what is seen at 4 cm^{-1} resolution could be identified. Experiments run at total pressures of 6 torr and 5 torr also showed these features; however, at 5 torr the absorption was approaching the detection limit of the system. The lack of structure in the observed absorption indicates the species is probably a complex molecule with many degrees of freedom. Positive identification of the absorbing species has not been made at this time, but some suspected species have been ruled out. The features do not agree with published spectra of ammonia or hydrazine⁴⁸. This is consistent with the results of Dewhurst and Cooper²⁹. Comparison with absorption spectra of trisilylamine, $\text{N}(\text{SiH}_3)_3$, has ruled out this species even though it possesses absorption bands centered in exactly the same locations as the

**ABSORPTION SPECTRUM OF REACTION PRODUCTS IN
LONG-PATH CELL AT 10 TORR, 4 cm^{-1} RESOLUTION
(RESIDUAL SiH_4 SEEN AT 910 AND 2180 cm^{-1})**

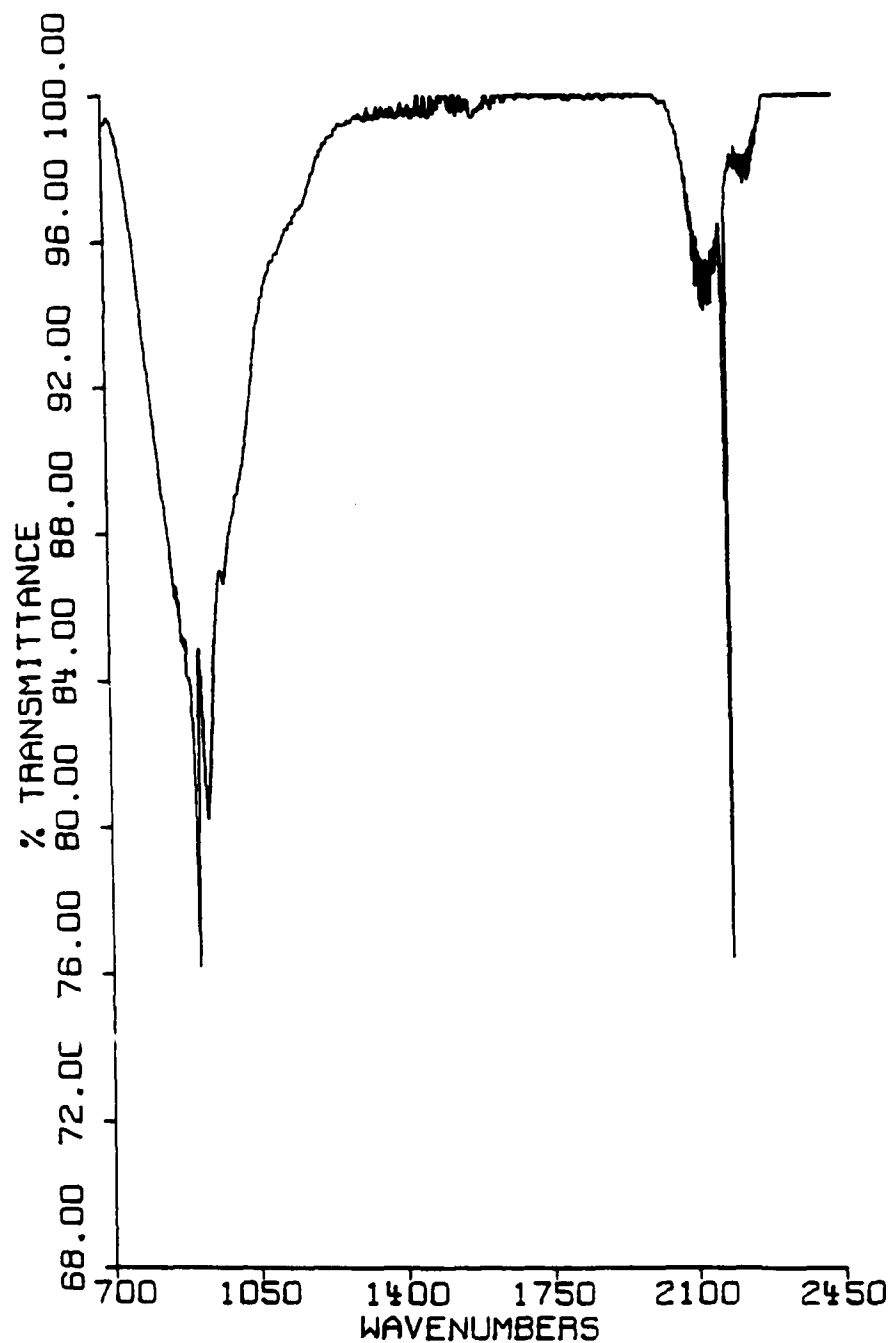


Figure 3-13: Long-Path Absorption of Downstream Reaction Products
(residual silane present)

**ABSORPTION SPECTRUM OF REACTION PRODUCTS IN
LONG-PATH CELL AT 10 TORR, 4 cm^{-1} RESOLUTION**

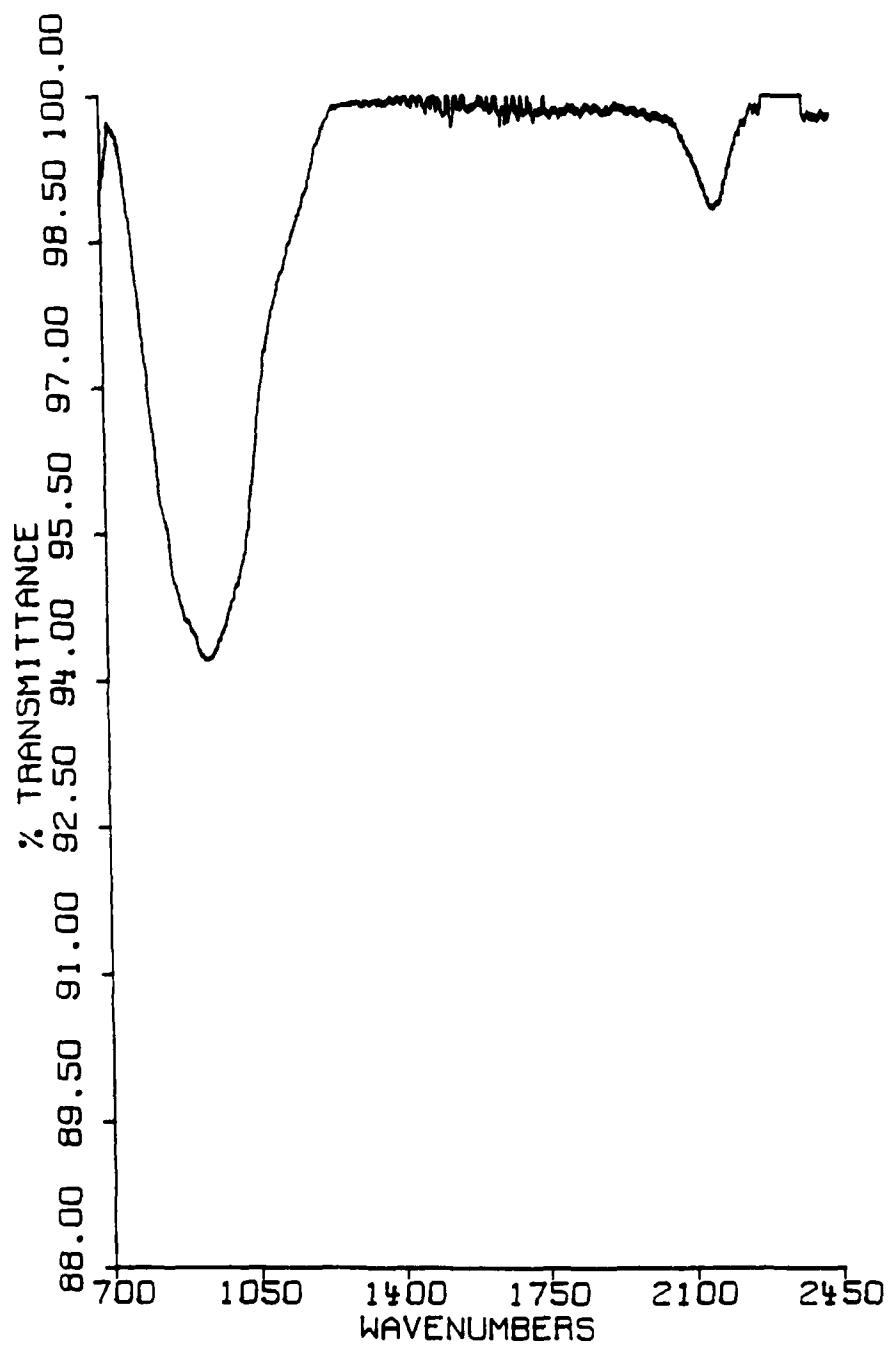


Figure 3-14: Long-Path Absorption of Downstream Reaction Products
(reduced silane flow)

observed features.⁴⁹ It does seem reasonable that the unidentified species contains Si, N, and H since the band at 2180 cm^{-1} is characteristic of an Si-H bond stretching vibration and the Si-N bond stretching is at about 1100 cm^{-1} . It is very tempting to assign the absorption feature to Si_3N_4 which possesses a strong band⁵⁰ between 600 and 1250 cm^{-1} , however the band seen here at 2180 cm^{-1} would indicate that some hydrogen is also present in the unidentified species or perhaps the absorption is the result of multiple species. Therefore, at this point the species cannot be positively identified; however, it appears reasonable to assume the species is a higher nitride of silicon with perhaps some hydrogenation. This indicates that **some higher nitrides of silicon are formed in the reaction and remain in the gas phase at pressures as low as 5 torr.**

Disilane Production by Silane Reaction with Nitrogen Metastables

While the FT-IR/Long Path Cell system was still in place, one more set of measurements was made with a modified flow reactor. The modified reactor is shown in figure 3-15. In this system, pure argon was flowed through the discharge to produce argon metastables. The Ar flow was then intersected with a flow of pure nitrogen. The gas was then reacted with the silane/helium mixture further downstream. Stedman and Setser⁵¹ have shown that argon metastables will readily transfer energy to the $\text{C}^3\Pi$ state of nitrogen which will eventually radiate down to the metastable $\text{A}^3\Sigma$ state of N_2 . This reaction is fast enough that conditions could be adjusted so that all of the argon metastables could be quenched by the time the flow reached the helium/silane port. Thus at the point of silane injection, the gas flow only contained groundstate Ar and N_2 , and some metastable $\text{N}_2(\text{A}^3\Sigma)$. All measurements made with this configuration were at a total pressure of 10 torr. An attempt was made to measure any chemiluminescence from the reaction, but to the sensitivity of the experiment, no chemiluminescence could be detected. Piper and Caledonia³¹ also attempted to measure chemiluminescence from the reaction of N_2 metastables with silane, but likewise were unsuccessful. From the description of their experiment, it is felt that the overall sensitivity of Piper and Caledonia's experiment was better than this work below about 400 nm but above that wavelength, the experiment described here was more sensitive. In an attempt to observe whether any reaction occurred, absorption spectra were taken of the gases leaving the reaction zone and entering the 20.25 m cell. Initial inspection of the absorption spectra showed only SiH_4 present in the cell. Using a background subtraction

ARGON METASTABLE TRANSFER EXPERIMENT

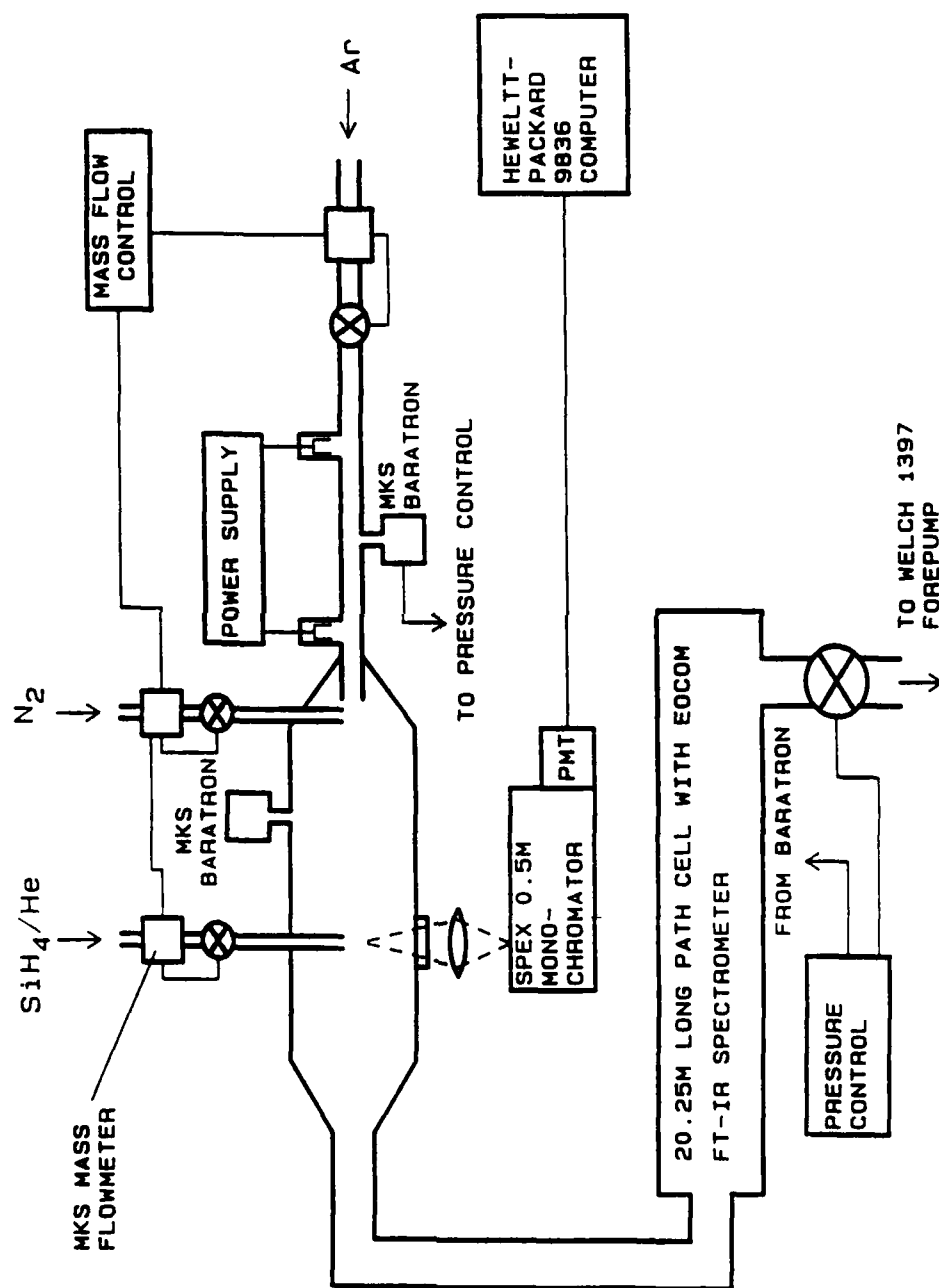


Figure 3-15: Schematic of Argon Metastable Transfer Experiment

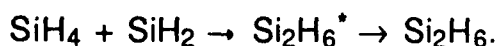
scheme, the feature shown in figure 3-16 (recorded at a resolution of 1 cm^{-1}) was uncovered. In this subtraction scheme, an absorbance spectrum taken without a discharge was subtracted from a spectrum with a discharge. Before the subtraction was performed the 'no discharge' spectrum was multiplied by a constant less than 1. This constant could be varied about 1 while the difference spectrum was observed interactively. When the value of the constant was such that a flat background in the difference spectrum was obtained, the difference spectrum was stored. This 'absorbance difference spectrum' was then converted back to the transmittance spectrum shown in figure 3-16. While the feature is small (note the vertical scale in figure 3-16), the absorbing species could be positively identified as disilane, Si_2H_6 . Previous work in this lab with disilane made possible an estimate of the partial pressure of the species from the measured absorbance. Using a value of the Q-branch peak absorption coefficient, measured in this lab at a resolution of 1 cm^{-1} by Chaney, et al.⁵², of $k_0 = 0.105 \pm 0.008 \text{ torr}^{-1} \text{ cm}^{-1}$ gives a value of

$$P_{\text{Si}_2\text{H}_6} = 9.5 \pm 2.5 \times 10^{-5} \text{ torr}$$

in figure 3-16. The positive identification of disilane clearly shows that some silane is dissociated by $\text{N}_2(\text{A}^3\Sigma)$ and the dissociated products react to form disilane. The most likely scheme for the disilane production is



followed by



**Si₂H₆ ABSORPTION SEEN IN LONG-PATH CELL AFTER
SUBTRACTION OF RESIDUAL SiH₄ ABSORPTION**

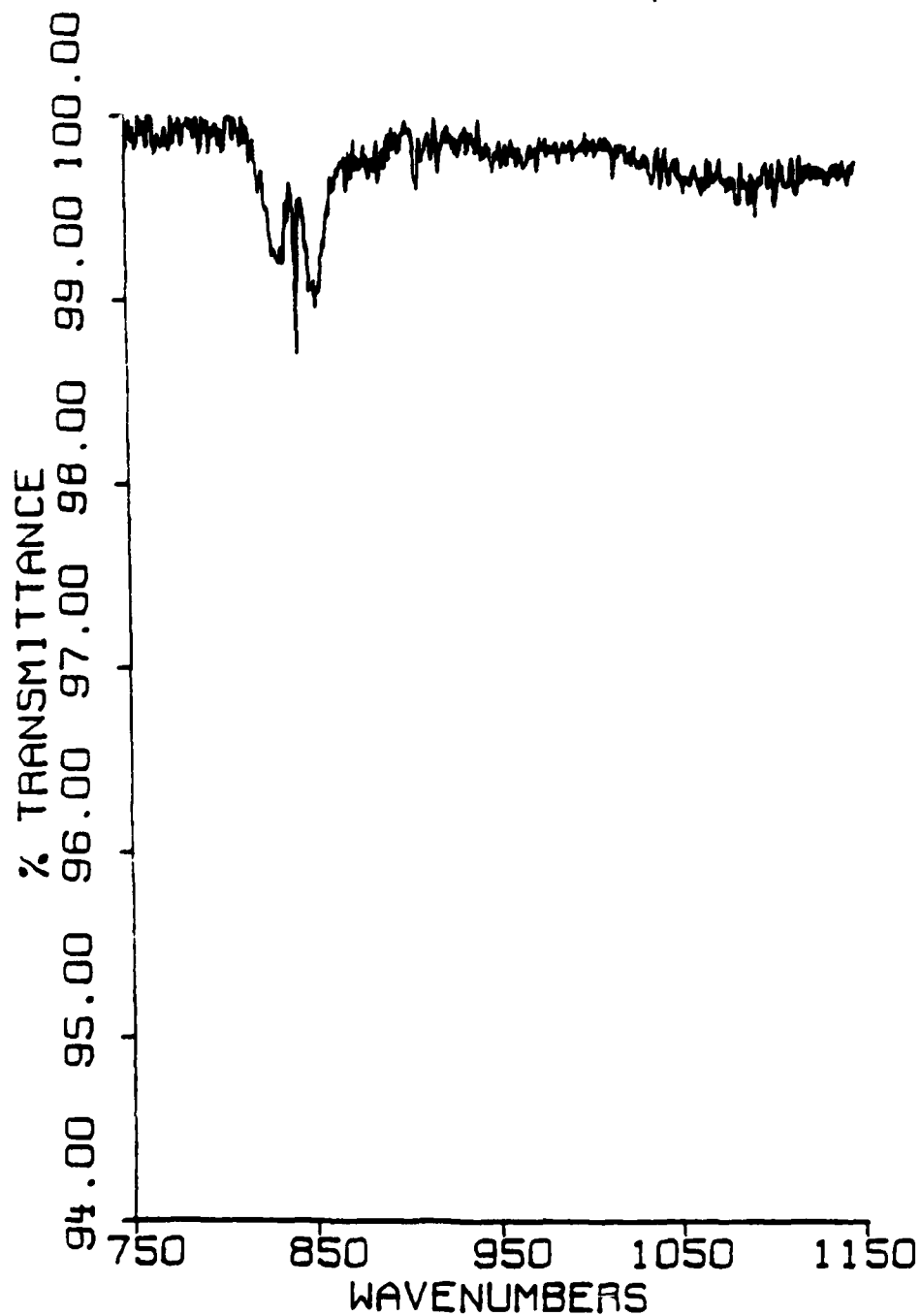


Figure 3-16: Disilane Absorption After Substraction of Residual
Silane Absorption

Chapter IV

Development of the Reaction Model

To fully understand the behavior of silane in active nitrogen, it is necessary to know what chemical reactions take place and the rates of those reactions. In general, this is a very difficult problem. In light of the lack of detailed understanding of the nitrogen afterglow alone, it would be foolhardy to suppose that such a detailed picture would emerge from this investigation. On the other hand, it might be possible to propose some likely reactions that could explain the observed results. Thus an effort to "model" the reactions was begun. Almost by definition, this part of the work is very speculative. Any proposed reaction scheme might not be the only scheme that would describe the results, however, if a proposed scheme is plausible, does not violate any laws of physics, and describes the observed results, it is viable until some new result or other data rules it out. Therefore, the goal of this part of the investigation was to arrive at a plausible set of chemical reactions which would explain the bulk of the observations. Guidance for this part of the work comes from a number of sources. Wright and Winkler⁴ give a good compilation of work involving the introduction of various species into active nitrogen. Many of the references therein give suggested models of reaction schemes for different species. More recently, Horie et al.³⁰ have suggested a reaction scheme based on their measurements of silane in active nitrogen and their work has guided the work here. Since this is the only known data on the reaction mechanism of silane in active nitrogen, comparisons will be frequently made between their work and the work reported here. When the work of Horie et al. is cited, it should be understood this refers to reference 30.

General Rate Equation Approach

The "model" of the reaction will be a set of coupled rate equations which govern the time dependence of the various species and processes (such as chemiluminescence) involved in the reaction. The rate equations are essentially a set of coupled differential equations which can be solved

numerically and the solutions compared with observations. For example, suppose the following reaction occurs in a system:



The rate equations governing the species would be

$$\begin{aligned} d[A]/dt &= -K \cdot [A] \cdot [B] \\ d[B]/dt &= -K \cdot [A] \cdot [B] \\ d[C]/dt &= +K \cdot [A] \cdot [B] \end{aligned} \quad (\text{eq. 4-2})$$

where $[A]$, $[B]$, and $[C]$ are number densities of the species and K is the rate constant for that reaction. For a given set of initial conditions one can solve this set of coupled equations to get the time dependence of the species involved. From this simple example, one can see that the number of coupled equations is equal to the number of species, and the number of rate constants is equal to the number of reactions. In the case of modeling a completely new system one is faced with putting together both a set of proposed reactions and a set of proposed rates (if measured values do not exist). What makes it possible to bring some reality to such a model is that the rates one can choose are not arbitrary. The rate constants basically are a measure of the collision rate of the species involved in a reaction. This means the rates can not exceed the "gas kinetic rate", i.e. the rate constant calculated by assuming the particles move at thermal velocities and collide with a "hard sphere" collision cross section⁵³. Specifically for two particles of molecular weight m_1 and m_2 at a temperature T , the "gas kinetic rate" is given by⁵³

$$K(\text{gas kinetic}) = \sigma_{12} \left[8\pi kT / m_{12} \right]^{1/2} \quad (\text{eq. 4-3})$$

where

$$\sigma_{12} = 0.5(\sigma_1 + \sigma_2) \quad (\text{eq. 4-4})$$

with σ_1 and σ_2 the hard sphere diameters, m_{12} is the reduced mass and k is Boltzmann's constant. For example, if one assumes for each colliding partner a hard sphere diameter of 2.5 Å, a molecular weight of 30amu, and a gas temperature of 300°K, the gas kinetic rate is

$$K = 1.3 \times 10^{-10} \text{ cm}^3/\text{s}.$$

Therefore, if a reaction scheme is proposed with the binary collision rate set by equation 4-3, and the predicted time dependance of an observed phenomenon is slower than measured, the scheme is in trouble. Another characteristic of this system that makes the modeling effort tractable is that for the most part only binary collisions need be considered due to the low pressures involved in the reactor.

General Characteristics of the Reaction Scheme

Before any reaction schemes to explain the behavior of silane in active nitrogen could be developed, some knowledge of the characteristics of active nitrogen was needed. Caledonia, et al.⁴⁷ have made measurements of various species present in a 'typical' afterglow and table 4-1 gives estimates of densities of various species one might expect to be present at a pressure of 3 torr.

Table 4-1: Catalogue of Abundant Species in Active Nitrogen
(at 3 torr)

<u>Afterglow Species</u>	<u>Approximate Density (cm⁻³)</u>
N(⁴ S)	10 ¹⁴
N(² D)	10 ¹¹
N ₂ (A ³ Σ)	10 ¹⁰
N(² P)	10 ¹⁰
N ₂ (a' ¹ Σ)	<10 ¹⁰

Table 4-1 must be taken only as a guide because conditions such as gas purity, cleanliness of the flowing afterglow system, type of discharge used for excitation, and a host of other factors can dramatically affect the number densities given in the table. Table 4-1 is probably a reasonable guide to the various rankings of the species with respect to number

density. One species not listed in table 4-1 is vibrationally excited, ground electronic state N_2 . The number densities of the various vibrational levels depend strongly on the level and with the ground state potential capable of supporting approximately 70 vibrational levels, there are too many for a brief table. More discussion concerning vibrationally excited N_2 will be given later. Thus, table 4-1 indicates that in most nitrogen afterglows, the dominant 'active' species is atomic nitrogen. Using these general characteristics of the afterglow and the results presented in chapter III, a number of conclusions about the reactions occurring in the afterglow were formulated.

The following is a list of the results and the conclusions drawn:

1) From the general observations of the reaction flame: The overall reaction scheme consisted of some kind of chain reaction involving more than one species in the reaction with silane. The chemiluminescence can take place in time short compared to the 'induction period', i.e. the time before the chemiluminescence begins.

2) From the observations of Si and SiN emission and comparisons with reports using other silicon compounds as 'fuel': The Si emission and SiN emission resulted from reactions only involving species present in the afterglow, atomic silicon, and species formed from atomic silicon and some form of nitrogen.

3) From the general observations, the dissociation measurements and the N-atom density in the afterglow: The silane dissociation is driven by N-atoms; **however**, silane does not readily react directly with N-atoms.*

4) From the FT-IR absorption measurements and the results of Dewhurst and Cooper²⁹: The densities of any NH_x species must be very low.

* The latter part of conclusion 3), i.e. silane does not react directly with N-atoms has recently been confirmed by Piper and Caledonia (ref. 31) who measured the reaction rate of N-atoms with silane and found the rate was smaller than they could measure with their apparatus:
 $R < 0.006 \times 10^{-11} \text{ cm}^3/\text{s}$.

5) From the results of emission measurements at various pressures: The intensity of the Si and SiN chemiluminescence increases faster than linear with pressure.

These general conclusions about the reaction lead to a very general scheme for the reaction mechanism. This general scheme is given below:

- 1) Some species, [A], present in the afterglow slowly dissociates SiH_4 .
- 2) The resulting silicon-bearing radicals react rapidly with N-atoms.
- 3) A series of reactions with N-atoms produces the observed chemiluminescence and produces a species, [B], which can dissociate SiH_4 .
- 4) The species produced in step 3) feeds back to step 1) to dissociate more SiH_4 .

In the above scheme the two unknown species, [A] and [B], can in fact be the same; however, this is not required. The problem now becomes one of filling in the details of the above and checking if indeed the results predicted agree with observations.

Initial Silane Dissociation in the Afterglow

To determine which species in the afterglow might be responsible for the initial dissociation of SiH_4 , some energetics of silane dissociation are needed. The energies needed to dissociate silane thermodynamically into various radicals are shown in table 4-2. The dissociation energies are given in electron volts. The dissociation energies are calculated from heat of formation data of Ho, et al.⁵⁴ Since one is interested in dissociating silane by collision with some energetic species in the afterglow, table 4-2 is somewhat misleading in that the energies apply to conditions of thermodynamic equilibrium. In a collision of silane with an energetic particle, equilibrium may not be established among the degrees of freedom of the particles. As discussed in chapter I, the threshold energy for dissociation of silane by electron impact is believed to be ≈ 7.8 eV, even though there are lower energy channels as shown in table 4-2.

Table 4-2: Thermodynamic Dissociation Energies of Silane

<u>Dissociation Channel</u>	<u>Energy (eV)</u>
SiH ₄ → SiH ₂ + H ₂	2.60
→ SiH ₃ + H	3.98
→ Si + H ₂ + H ₂	4.32
→ SiH + H ₂ + H	5.89
→ SiH ₂ + H + H	7.13
→ Si + H ₂ + H + H	8.84
→ SiH + H + H + H	10.41
→ Si + H + H + H + H	13.37

Data to support the hypothesis that dissociation can take place at the lower energies shown in table 4-2 comes from two sources. In chapter III it was shown that Si₂H₆ was formed in the reaction of SiH₄ with N₂(A³Σ) metastables. The Si₂H₆ is most probably produced from the reaction of SiH₄ with either SiH₂ or SiH₃ produced by the dissociation of SiH₄ by collision with N₂(A³Σ). Figure 4-1 is an energy level diagram of N₂ based on the data from Huber and Herzberg⁵⁵, and as can be seen, the N₂(A³Σ) state lies approximately 6.1 eV above the ground state of N₂. The other indicator of lower energy dissociation comes from experiments with mercury sensitization of silane²⁴. Silicon deposition by mercury sensitization of silane⁵⁶ involves deposition by irradiating a mixture of silane and mercury with 254nm resonance radiation from a mercury lamp. It is believed that the deposition is driven by dissociation of SiH₄ by collisions with the Hg(6p³P₁^o) excited state which lies at 4.9 eV. From these results, it appears that dissociation of silane by heavy particle collisions can occur at lower energies than observed for electrons. It will be assumed then that the energies shown in table 4-2 are valid threshold energies for

MORSE POTENTIALS FOR N₂ (simplified)

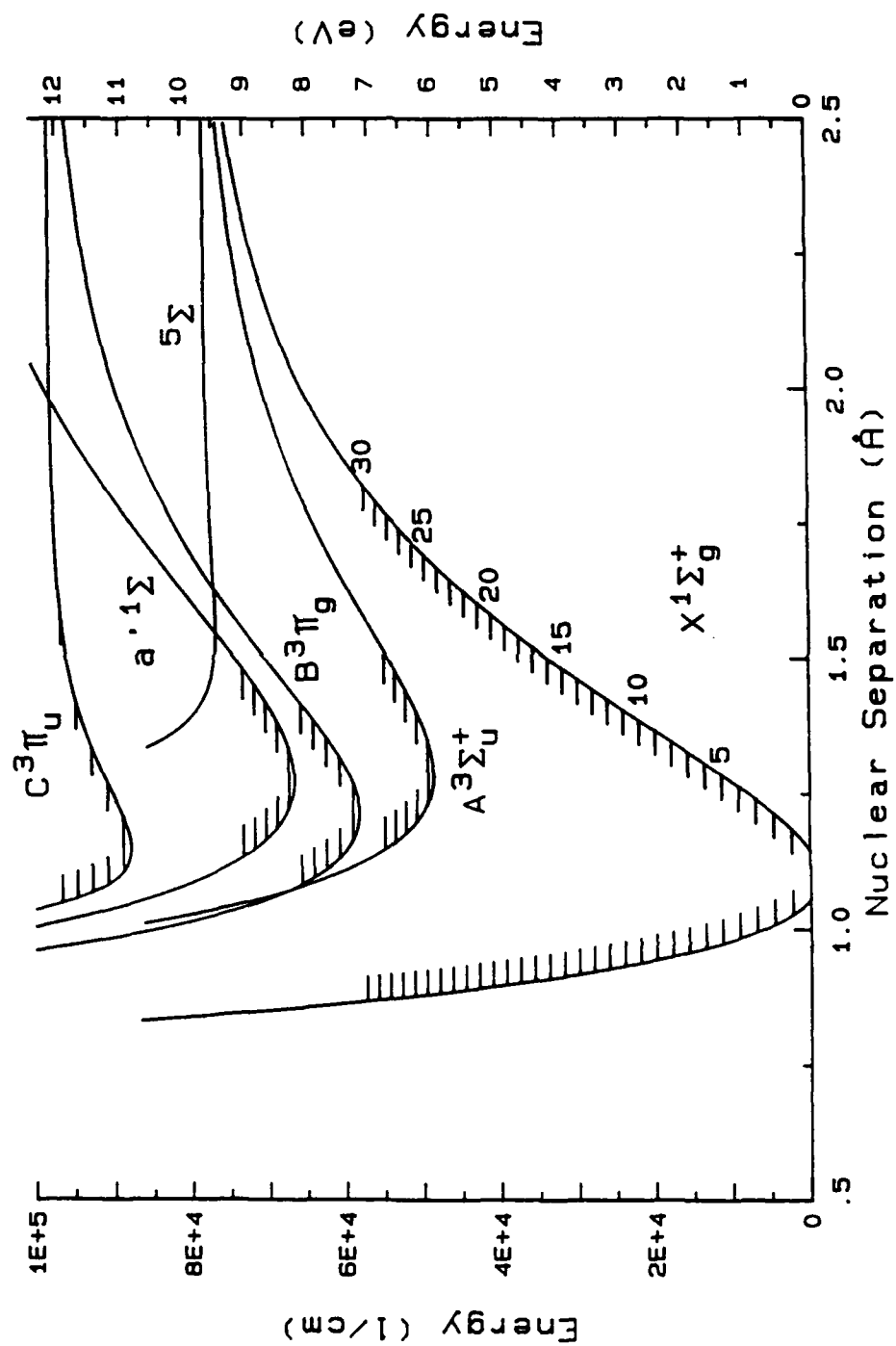


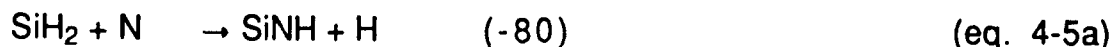
Figure 4-1: Morse Potentials for Nitrogen (simplified)

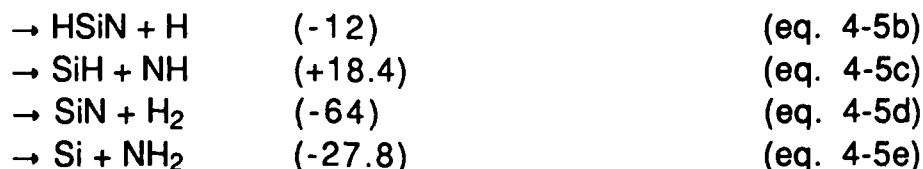
dissociation of silane by heavy particle collisions. From this assumption and figure 4-1, it is clear that a number of energetic species of N_2 are available to dissociate SiH_4 . Both the metastable $A^3\Sigma$ and the $a'^1\Sigma$ possess sufficient energy as does the vibrationally excited $X^1\Sigma$ state. An $N_2(X^1\Sigma)$ molecule at $v=10$ or above possesses sufficient energy to dissociate SiH_4 by the low energy process shown in table 4-2. In a collision of this type, the N_2 molecule gives up a large number of vibrational quanta to an electronic state of SiH_4 which then dissociates. This "v to E transfer" has been observed as both an intramolecular (within the same molecule) and as an intermolecular (from one species to another) process. Intramolecular transfer has been observed by Dunnwald, et al.⁵⁷ in nitric oxide, and by DeLeon and Rich⁵⁸ and Farrenq et al.⁵⁹ in carbon monoxide. Intermolecular transfer has been observed by Rich and Bergman⁶⁰ in collisions of vibrationally excited CO (and N_2) with C_2 and CN, and by Star⁶¹ in collisions of vibrationally excited N_2 with sodium. Thus, there is significant evidence to suggest that vibrationally excited nitrogen may be capable of dissociating silane by the process of v to E transfer. Silane might also be dissociated by v-v pumping in collisions with vibrationally excited N_2 . In this case, a collision is expected to exchange only one vibrational quanta between N_2 and SiH_4 . By repeated collision with $N_2(v)$, SiH_4 could be vibrationally "pumped" until the molecule reached the dissociation limit. As mentioned in chapter I, SiH_4 has a non-degenerate stretching mode ν_1 at 2187 cm^{-1} , one doubly degenerate bending mode ν_2 at 978 cm^{-1} , and two triply degenerate bending and stretching modes ν_3 at 2183 cm^{-1} and ν_4 at 910 cm^{-1} . Exchange of vibrational quanta between $N_2(v)$ and SiH_4 would be expected to occur at the fastest rate between similarly spaced vibrational levels. Thus one might expect near-resonant transfer between either ν_1 or ν_3 of SiH_4 and $v=6$ of $N_2(X^1\Sigma)$. The lower energy modes of SiH_4 do not come into resonance until $v=50$ of N_2 , which is too high to be considered in this initial dissociation step. To model this v-v pumping between N_2 and SiH_4 would require knowing a large number of rates for both the exchange of quanta between the molecules along with rates for quenching of the vibrational energy of SiH_4 by various gas phase s in the afterglow. Due to the complexity of this calculation and the lack of rate data, it was simply assumed that $N_2(X^1\Sigma, v\geq 10)$ would have sufficient energy to dissociate SiH_4 . The exact mechanism was assumed to be v-to-E transfer, but it must be emphasized that v-v pumping may also be playing a role. In addition to the energetic species of N_2 , the metastable $N(^2P)$ state of atomic nitrogen resides at 3.57 eV above the $N(^4S)$ level, thus it may also be capable of dissociating SiH_4 . With the exception of

vibrationally excited nitrogen, the estimated densities from table 4-1 of the remaining species are on the same order. Calculations which will be discussed in the next chapter indicate that the density of $N_2(X^1\Sigma, v=10)$ is also on the order of 10^{10} , so at least in this initial model, the assumption is made that any of the four species just discussed may contribute to the initial dissociation of silane.

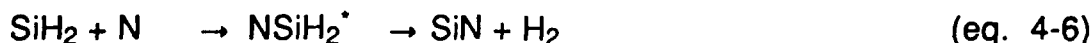
Reactions of N-atoms with Silane Radicals

The next step in the proposed reaction scheme involves direct and rapid reaction of N-atoms with radicals produced from the initial dissociation of SiH_4 . The logic behind this proposed step is twofold. First, the observed results indicate that by approximately 60ms the reaction is complete (at 3 torr). Looking at table 4-1 and assuming a gas kinetic rate, it is clear that N-atoms must be involved early in the reaction or the reaction will evolve too slowly. Second, it is well known that the radicals produced from SiH_4 and N-atoms are all (usually) very reactive. Hence, what is contrary to logic is that N-atoms react so slowly with SiH_4 . Table 4-2 shows that the three silicon bearing radicals and atomic silicon may be produced in the dissociation of silane. To simplify the situation somewhat, the assumption is made that the most likely radicals produced are those originating from reactions that occur at the lowest energies and require the fewest hydrogen-silicon bonds to be broken. For example, it is difficult to visualize a collision between an energetic particle and SiH_4 in which all four hydrogen-silicon bonds are broken to give Si, and then two hydrogen-hydrogen bonds reassembled to give two H_2 molecules. Using these guidelines, the two most likely radicals to be produced are SiH_3 (by line 2 of table 4-2) and SiH_2 (by line 1 of table 4-2). The possible reactions to consider in this step will therefore involve N-atoms on either SiH_2 or SiH_3 . The enthalpy changes for each suggested reaction will be given beside each equation (Kcal/mole). The enthalpy changes are calculated from the heat of formation data given in appendix B. If the enthalpy change is less than zero, the reaction is exothermic, and if the change is greater than zero, the reaction is endothermic. Since this reaction scheme is to be self propagating, reactions which are endothermic will be ruled out as possible steps in the chain. For SiH_2 , some possible reactions are:

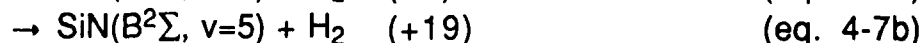




From energy considerations reaction 4-5c can be eliminated from the reaction scheme. Also from an energetics standpoint, it is clear that reactions 4-5a and 4-5d are most favored. The difficulty with reaction 4-5a is that it produces H-atoms. Since no H-atom emission was seen in this experiment one is tempted to conclude that the H-atom density must be low; however, no H_2 emission is seen either, and Dewhurst and Cooper²⁹ found approximately stoichiometric formation of H_2 from SiH_4 . Still better data come from the work of Horie, et al. who measured the time dependence of the SiH_4 dissociation and the time dependence of H_2 density during a reaction. **Their measurements show that throughout the time history of the reaction, the H_2 formed is equal to twice the SiH_4 reacted.** So that even early on in the reaction scheme, the density of atomic hydrogen must be low. Therefore, reactions that produce H-atoms are considered secondary in importance to reactions which produce H_2 . Thus, between reactions 4-5a and 4-5d, reaction 4-5d is considered the dominant pathway. Reaction 4-5e is considered to be secondary due to the lack of any observed NH_2 emission (not a positive indicator), no identifiable NH_x absorption in the long path data, and the lack of any condensable NH_x compounds by Dewhurst and Cooper²⁹. Therefore the primary reaction step for N-atoms on SiH_2 is considered reaction 4-5d. More realistically, this step probably proceeds through an intermediate so the reaction becomes



It should be pointed out that eq. 4-6 does not energetically allow the formation of the B-state of SiN i.e.,

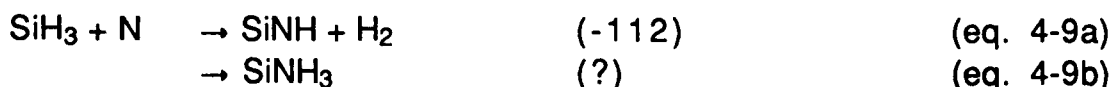


Thus the reaction given in eq. 4-6 cannot account for the SiN^* chemiluminescence, but the breakup of the NSiH_2^* complex could possibly give rise to some broadband continuum emission. Horie et al. have also proposed reaction 4-5d as a key reaction in the chain, however no mention

is made of a possible complex as suggested in reaction 4-6. Reactions involving SiH_3 are probably occurring in the SiH_4 reaction, but it is difficult to produce a scheme which does not either produce H-atoms or some NH_x compound which have been previously ruled out. In addition, the reaction of H-atoms on SiH_3 is considered to occur at a near gas-kinetic rate²³, so that any SiH_3 produced by the reaction given in line two of table 4-2 will be converted to SiH_2 by the reaction



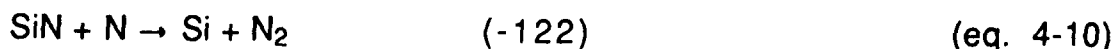
using the H-atoms produced in the initial SiH_4 dissociation. Thus one concludes that SiH_3 molecules do not play a primary role in the reaction kinetics. This does not mean that any SiH_3 produced in SiH_4 dissociation does not react with N-atoms. Reactions of the type



may very well take place, but the assumption made here is that they do not participate in the primary chain reaction that leads to SiH_4 dissociation. Due to the large exothermicity of reaction 4-9a, there is again the possibility that the species may be formed in an excited state which could possibly contribute to the unidentified chemiluminescence.

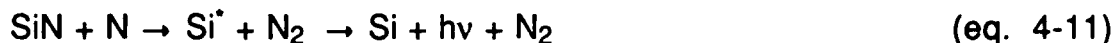
The Si and SiN Chemiluminescence

As stated earlier, the emission produced from Si and SiN is assumed to originate only from species containing Si and N-atoms. The SiN produced in reaction 4-6 is probably formed in a lower energy state which has been suggested to be one of the quartet states from spin considerations⁶². If the quartet states are involved, relaxation to the ground state can only occur through collisions with other species in the afterglow. The assumption is made that most of the SiN is relaxed to the ground state before collisions with an N-atom can occur. The most likely reaction for the formation of Si^* is



which is exothermic by ≈ 5.3 eV. With the exception of the lines at 243.5 nm and 263.1 nm, all of the lines listed in table 3-1 have upper levels that

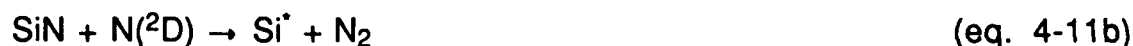
range in energy between 4.13 and 5.08 eV above the ground state. For the lines originating from levels below 5.3 eV, reaction 4-10 can supply the energy for Si excitation. The Si emission is produced by



For lines originating from states with energies above 5.3 eV another mechanism must be proposed. Two possible reactions may be involved to supply this excess energy. The first reaction involves the reaction of N-atoms with vibrationally excited SiN, i.e.,



The vibrational spacing of SiN is ≈ 0.1 eV so that $V=5$ would yield an additional 0.5 eV for reaction 4-11a. The line at 263.1, however, originates from a 6.62 eV level which is very high for vibrationally excited SiN. The second proposed reaction to explain the higher lying Si levels involves reactions of SiN with metastable N-atoms. These are



These species supply an additional 2.38 eV and 3.57 eV respectively to the reaction. One other possible reaction to explain the higher lying Si energy levels may involve the reaction of N-atoms with an electronic metastable of SiN, but at this time the metastable levels of SiN have not been identified, and thus this mechanism is considered too speculative even for an admittedly very speculative part of the thesis. Horie et al. have proposed collisions of Si with $\text{N}_2(\text{A}^3\Sigma)$ metastables as the mechanism for the production of Si^* ; however, they require reaction 4-10 for the production of Si and there appears to be no reason that the reaction could not produce Si in an excited state. From the energetics of reaction 4-10, it is clear that the reverse reaction of Si on N_2 is energetic forbidden. Horie, et al. have proposed that Si-atoms reassociate with N-atoms by the process

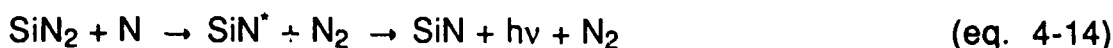


where M is a third body. However, since this reaction involves a three-body process among two species whose densities are comparatively low (N-

atoms are on the order of 0.01 torr), this reaction will be very slow. On the other hand, a reaction of the type



can take place in the times observed because it involves one major species, N_2 . Horie, et al. also mention this reaction but consider it only secondary to reaction 4-12. It is felt that a three-body reaction of this type can be the only three-body reaction that can take place in the necessary time scales needed to match the observations. Thus reaction 4-13 is proposed as the next step in the reaction chain. The next step in the chain is the reaction of N-atoms with the SiN_2 formed in reaction 4-13, specifically, the reaction is



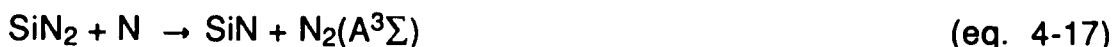
Unfortunately, the heat of formation of SiN_2 is not known so the energetics of reaction 4-14 can not be determined. A consistency check can be made by comparing the energetics of reactions 4-13 and 4-14. From 4-13, the heat of formation of SiN_2 must be less than that of Si, i.e.,

$$H_f(\text{SiN}_2) \leq H_f(\text{Si}) = 107.7 \quad (\text{eq. 4-15})$$

and from equation 4-14,

$$H_f(\text{SiN}_2) \geq H_f(\text{SiN}[\text{B}^2\Sigma, v=5]) - H_f(\text{N}) = 87.1 \quad (\text{eq. 4-16})$$

Therefore, at least the two reactions do not violate any consistency arguments. By contrast, Horie, et al., who also propose a reaction similar to 4-14, suggest the reaction



which requires that the heat of formation of SiN_2 be

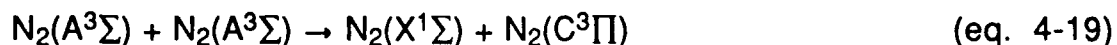
$$H_f(\text{SiN}_2) \geq H_f(\text{SiN}) + H_f(\text{N}_2[\text{A}^3\Sigma]) - H_f(\text{N}) = 146.2 \quad (\text{eq. 4-18})$$

This is clearly inconsistent with equation 4-13, which Horie et al. also indicate can occur.

Reactions 4-11, 4-13, and 4-14 represent a chain reaction which can explain the observed Si and SiN chemiluminescence. The three-body reaction, 4-13, is responsible for the observed pressure dependence of the Si and SiN emission and the involvement of only Si-atom and N-atom bearing compounds satisfies that requirement. Furthermore the chain described by these three equations gives an almost identical time dependence to the Si and SiN emission which is observed by Horie, et al.

Species Generated to Dissociate Silane

In step 3 of the general reaction scheme, it was suggested that during some reaction with N-atoms, a species [B] was generated which would dissociate SiH₄ and speed up the chain reaction. For reactions of this type, a favorite species of workers who have studied active nitrogen is the N₂(A³Σ) metastable (see reference 4). Following this line, Horie, et al. have proposed that N₂(A³Σ) metastables created in reaction 4-17 are available to react back and dissociate SiH₄. The difficulties with this scheme have been discussed above but will be reiterated here. If N₂(A³Σ) are to be generated rapidly, then from equation 4-17, SiN₂ must also be generated rapidly. From the energetics discussed above, the only mechanism available for producing SiN₂ in the Horie, et al. scheme is reaction 4-12. But this reaction will be very slow unless the three-body rate is unusually large. Therefore, it is doubtful that N₂(A³Σ) produced in the scheme suggested by Horie, et al. can be responsible for the further dissociation of SiH₄. Even if some other method for producing N₂(A³Σ) were suggested, it is still doubtful that the metastable is playing a role. As discussed by Caledonia et al.⁴⁷, one of the significant loss mechanisms for N₂(A³Σ) is by the "pooling" reaction



which occurs at a gas-kinetic rate. The N₂(C³Π) state quickly (τ=40 ns) radiates down to the N₂(B³Π), which in turn radiates down to the N₂(A³Σ). Thus two A³Σ molecules react to give back one. The B-A radiation is the familiar first positive emission from the afterglow. Normally, the contribution to the observed first positive emission from the pooling reaction is small due to the low metastable densities. If, however, the N₂(A³Σ) density is raised so as to significantly dissociate the SiH₄, then this increased metastable density would lead to increased first positive intensity during the reaction. This is not observed in this work or the

work of Horie et al. The first positive intensity is seen to decrease monotonically through the reaction zone after the introduction of SiH_4 into the afterglow. To further clarify this point, the data of Horie, et al. can be used. Figure 4-2 is a reproduction of figure 4 from the paper of Horie et al. and shows the the time dependence of N-atoms and SiH_4 (and H_2 in one case) during the reaction. If the SiH_4 is dissociated by some species, [B], then the time dependence of the SiH_4 is given by

$$\frac{d[\text{SiH}_4]}{dt} = -K \cdot [\text{SiH}_4] \cdot [\text{B}]$$

or

$$\frac{1}{[\text{SiH}_4]} \cdot \frac{d[\text{SiH}_4]}{dt} = -K \cdot [\text{B}] \quad (\text{eq. 4-20})$$

For example, measuring the slope of the SiH_4 curve from figure 4-2(c) at a point where the density has gone to ≈ 0.5 gives a value of $\approx 150 \text{ s}^{-1}$ and dividing by 0.5 gives

$$K \cdot [\text{B}] \approx 300 \text{ s}^{-1} \text{ @ } t=25 \text{ ms} \quad (\text{eq. 4-21})$$

Now using the $\text{N}_2(\text{A}^3\Sigma)$ quenching rate measured by Caledonia and Piper³¹ of $5.9 \times 10^{-12} \text{ cm}^3/\text{s}$, and assuming this rate is also the rate for dissociating SiH_4 , gives a value for [B] of

$$[\text{B}] \approx 5 \times 10^{13} \text{ cm}^{-3}$$

which is a more than three orders of magnitude increase over the density expected at 3 torr. This is a very high $\text{N}_2(\text{A}^3\Sigma)$ density and would certainly perturb the first positive intensity in the afterglow. Therefore, the $\text{N}_2(\text{A}^3\Sigma)$ must be ruled out as the species [B] generated in the afterglow which dissociates SiH_4 . The $\text{N}_2(\text{a}^1\Sigma)$ metastable might also be considered as a possible species for dissociating SiH_4 in the latter stages of the reaction. The difficulty with this species is that it lies at 8.2eV above the N_2 ground state, hence for a reaction to produce this state it must be exothermic by $>189 \text{ Kcal/mole}$. No reactions could be postulated that were this exothermic.

FIGURE 4-2: FIGURE 4 OF REFERENCE 30;
[HORIE, ET AL., CHEM. PHYS. LETT., VOL. 4, p. 231 (1986)]

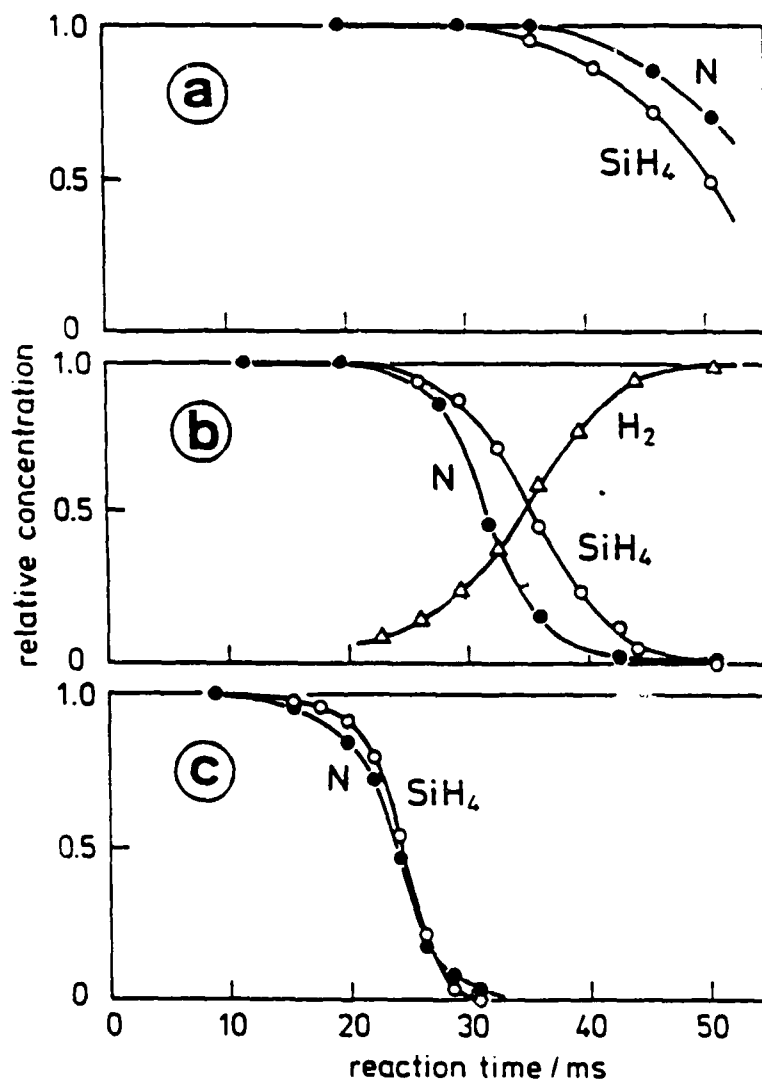


Fig. 4. Concentration profiles of N, SiH₄ and H₂ in SiH₄ + N₂. The relative concentrations are $[N]/[N]_0$, $[SiH_4]/[SiH_4]_0$, and $[H_2]/2[SiH_4]_0$. (a) $p = 416$ Pa, $[N]_0 = 2.38 \times 10^{14} \text{ cm}^{-3}$, $[SiH_4]_0 = 4.21 \times 10^{12} \text{ cm}^{-3}$ ($m = 56$). (b) $p = 416$ Pa, $[N]_0 = 2.38 \times 10^{14} \text{ cm}^{-3}$, $[SiH_4]_0 = 1.04 \times 10^{13} \text{ cm}^{-3}$ ($m = 23$). (c) $p = 390$ Pa, $[N]_0 = 1.47 \times 10^{14} \text{ cm}^{-3}$, $[SiH_4]_0 = 8.8 \times 10^{12} \text{ cm}^{-3}$ ($m = 17$).

One of the first species looked at in this work to fulfill the role of [B] was atomic silicon, thought to react with SiH₄ by the reaction,



This reaction has a rate constant of $5.33 \times 10^{-13} \text{ cm}^3/\text{s}$ calculated by Coltrin et al.⁶³. While the value of this rate constant may have been too small for the results observed here, the uncertainty in the rate was large enough to accommodate the necessary increase. The difficulty with this reaction is that with the recent calculations by Ho et al.⁵⁴ and measurements by Boo and Armentrout⁶⁴ the accepted value for the heat of formation of SiH₂ is now high enough so as to make reaction 4-22 endothermic by $\approx 20 \text{ Kcal/mole}$. In light of this recent data, it is very doubtful that reaction 4-21 is exothermic and hence cannot be used to drive the SiH₄ dissociation.

Another species that might be suspected of driving the SiH₄ dissociation is atomic hydrogen. This can be ruled out using the same arguments used to arrive at eq. 4-21. The rate for dissociation of SiH₄ by H-atoms by the reaction



has been measured at $2.7 \times 10^{-12} \text{ cm}^3/\text{s}$ (see reference 23). Using eq. 4-21, this would give an H-atom density of $\approx 1.1 \times 10^{14} \text{ cm}^{-3}$. The [SiH₄] density at $t=0$ in figure 4-2(c) was only $8.8 \times 10^{12} \text{ cm}^{-3}$, hence the H₂ density measurements made by Horie, et al. would certainly have differed from the $2 \times [\text{SiH}_4]$ result they found.

It may be possible that some other silicon-bearing species formed in the afterglow can dissociate silane; however, since almost nothing is known about possible reactions between many of these species (such as SiN or SiN₂) and SiH₄, the search for the species responsible for SiH₄ dissociation returned to the active nitrogen itself. Earlier, the exothermicity of reactions 4-10 and 4-14 was used to excite Si-atoms and SiN to explain the chemiluminescence from these species. It is also possible that these reactions may leave the N₂ product vibrationally excited, i.e.,



and



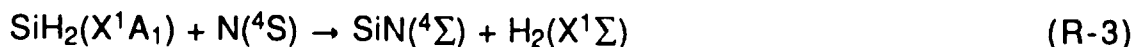
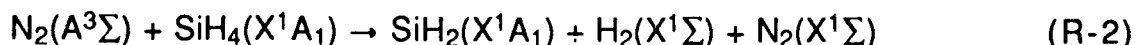
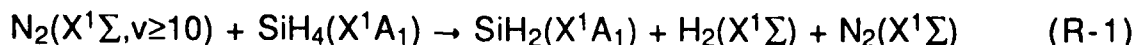
From the energetics of reaction 4-24, there is sufficient excess energy to give $v_{\text{max}}=20$, and since it is assumed that reaction 4-14 is capable of exciting the $\text{B}^2\Sigma$, $V=5$ state of SiN, this yields a value of $v_{\text{max}}=13$. As discussed earlier, vibrationally excited $\text{N}_2(\text{X}^1\Sigma)$ at $v \geq 10$ possesses enough internal energy to dissociate SiH_4 ; therefore, vibrationally excited nitrogen produced in either reaction 4-24 or 4-25 can dissociate SiH_4 . The difficulty with proposing this species as a driver for SiH_4 dissociation lies in the size of typical rate constants for v to E transfer. As pointed out by Rich and Bergman⁶¹, rates for v to E transfer typically range from 10^{-3} to 10^{-4} of gas kinetic. Using a rate of 2.7×10^{-13} in equation 4-21 gives a value for $[\text{B}]$ of

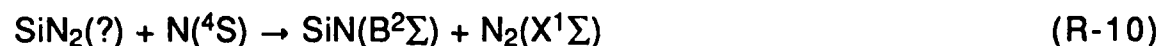
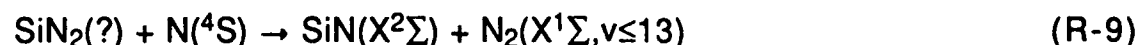
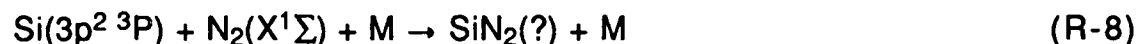
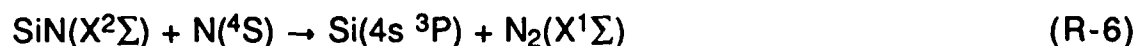
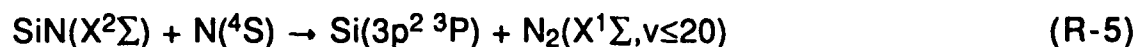
$$[\text{B}] = 1.1 \times 10^{15} \text{ cm}^3$$

at a total pressure of 3 torr. This would represent a fractional vibrational population for $v \geq 10$ of $\approx 1\%$. This is a very high fractional population, and it is very doubtful that this could ever be realized in the afterglow. On the other hand, there have not been any measurements of v to E transfer to a molecule with as many degrees of freedom as SiH_4 , thus it is possible that the rate in this case might be larger than previously measured rates. With a larger v to E rate, a lower vibrational population would be sufficient to dissociate SiH_4 at the rate observed by Horie, et al. **It is therefore proposed that the species $[\text{B}]$, generated in the reaction, which is responsible for SiH_4 dissociation is vibrationally excited, ground electronic state N_2 .**

Summary of the Proposed Reaction Scheme

The proposed reaction scheme is summarized below:





While it is almost certain that additional reactions, besides the ones listed here, are also occurring, the reaction scheme presented here seems capable of describing qualitatively the bulk of the observed results. For simplicity, the above scheme only uses $\text{N}_2(X^1\Sigma, v \geq 10)$ and $\text{N}_2(A^3\Sigma)$ as the initial drivers for SiH_4 dissociation. Since it is assumed this initial process is slow, there is nothing to be gained by including additional species. Also as previously discussed, reactions initially involving SiH_3 are not considered as primary to the reaction scheme. Figure 4-3 is a schematic of the reaction mechanism showing the feedback loops that exist in the scheme. The chemiluminescence occurs in reactions R-7 and R-11 and is generated in a loop composed of reactions R-6, R-7, R-8, R-10, and R-11. The feedback to the SiH_4 dissociation is supplied by reactions R-5 and R-9. All of these reactions are driven by N-atoms yet, as required, there is no direct reaction of N-atoms on SiH_4 . Before the scheme can be quantitatively assessed, the mathematical model described at the beginning of this chapter must be constructed. The next chapter will describe that model.

MECHANISM FOR DISSOCIATION OF SILANE IN ACTIVE NITROGEN

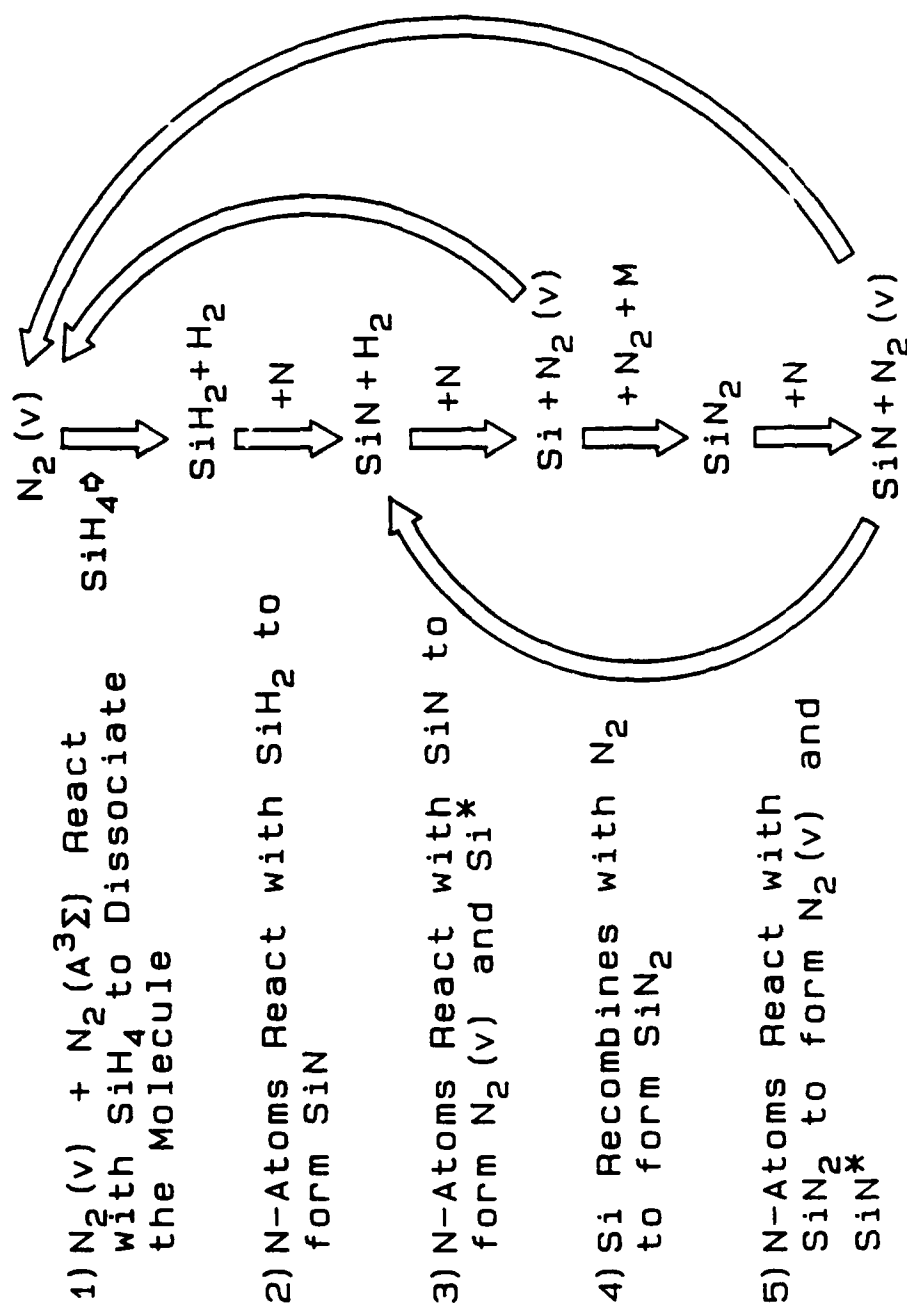


Figure 4-3: Schematic of the Proposed Reaction Scheme

Chapter V

The Reaction Model

As discussed in chapter IV, the reaction is modeled by constructing a set of coupled rate equations, solving these equations, comparing the calculations with observations, and readjusting the model if necessary. Over the course of this work, a large number of models, based on various proposed reaction schemes, have been constructed. While these models were very valuable for guidance towards a "working" reaction mechanism, it was also dominated by long and, for the most part, frustrating excursions down dead end streets. In light of the questionable value of describing in detail the many failures, this chapter will concentrate on the model developed from the reaction scheme proposed in chapter IV. Some background and a brief summary of some of the early modelling efforts will be described below.

Early Models

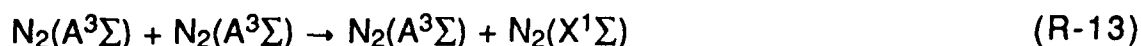
Initially, the modelling effort was to include a model of the nitrogen discharge, which would supply input to an afterglow model, which would be coupled to the silane reaction scheme. The early discharge model and afterglow model were based on the work of Slater, et al.⁶⁵ and modified for the low pressure dc discharge used in this work. It was quickly discovered that the discharge model did not yield excited state densities consistent with measured values in a dc discharge⁶⁶ and measurements in the early afterglow⁴⁷. For example, model predictions of the N-atom density were as high as 10% while measurements by Caledonia, et al.⁴⁷ give typical densities of less than 1%. The densities were also a strong function of the residence time of the N₂ in the discharge, and steady state values were not reached for very long times (>10 s). It was suspected that the electron impact dissociation rate of N₂ suggested by Slater et. al.⁶⁵ was too large to accurately model the data. During this discharge modelling effort, comparisons were attempted between discharge parameters and quantities measured in the reactor. This proved to be fruitless, and

the discharge model was abandoned. For input into the afterglow model, excited state densities measured in early afterglows were taken as the initial conditions and the afterglow model was allowed to "relax" for approximately 30ms before introducing the silane. The afterglow model contained the reactions used by Slater et al.⁶⁵ with updated rates from Caledonia et al.⁴⁷. It was during this part of the modelling that the significance of the pooling reaction to the first positive intensity was clearly identified and was key in eliminating the $N_2(A^3\Sigma)$ metastable from consideration as the species driving the silane dissociation. The next modelling effort involved adding a complex model of the neutral silane/hydrogen chemistry developed by Kushner²³. This model was very complex and contained as many possible reactions between silane and active nitrogen species as could be reasonably imagined. The complexity of this model and the many unknown rates made evaluation of the various processes in the model very difficult. In spite of this, it was during this modelling effort that the significance of the atomic silicon-silane reaction discussed in chapter IV was identified. Inclusion of this reaction in the model gave the first indications of the chain reaction behavior seen in the observations. When this reaction was eliminated from consideration due to the reevaluation of the heat of formation data for SiH_2 , the complex model was completely scrapped. The reactions that appeared "key" in the complex model were pulled out, along with a very basic afterglow model, and a simpler model was begun. The model discussed in the remainder of the chapter represents the evolution of this simple model.

The Afterglow Model

The afterglow model was made as simple as possible while maintaining the most important reactions among the dominate species present in the afterglow. The species included in the afterglow model were $N(^4S)$, $N(^2D)$, and $N_2(A^3\Sigma)$. The $N(^2P)$ metastable was not included because of a lack of good rate data on this species. To investigate the effects of metastable $N(^2P)$, the $N(^2D)$ was, at times, treated as "typical" and allowed to dissociate SiH_4 as described in chapter IV. However, in the final model this was not the case. Vibrationally excited $N_2(X^1\Sigma)$ was included as a separate set of species and will be discussed later. The $C^3\Pi$ and $B^3\Pi$ state were left out of the model once the dependence of the first positive intensity had been established in the more complex model. Since the first positive intensity is only dependent on the N-atom density through recombination and the $A^3\Sigma$ density through the pooling reaction, the densities of

these species were enough to predict the first positive intensity. Since the N-atom recombination is assumed to proceed into the $B^3\Pi$ state, which radiates down to the $A^3\Sigma$, for the purposes of the model it was assumed that the N-atom recombination proceeds directly to the $A^3\Sigma$ state. Thus for this very simple afterglow, the following reactions were used (the equation numbering continues from chapter IV)



Rates for these reactions were taken from references 47 and 65. The rates used for the above reactions were:

$$R-12: \quad k_{12} = 2.33 \times 10^{-33} \text{ cm}^6/\text{s}$$

$$R-13: \quad k_{13} = 1.0 \times 10^{-10} \text{ cm}^3/\text{s}$$

$$R-14: \quad k_{14} = 5.0 \times 10^{-11} \text{ cm}^3/\text{s}$$

$$R-15: \quad k_{15} = 1.0 \times 10^{-11} \text{ cm}^3/\text{s}$$

$$R-16: \quad k_{16} = 2.0 \times 10^{-16} \text{ cm}^3/\text{s}$$

The initial conditions used at the point of injection of the silane were slightly different from table 4-1. The $N(^4S)$ density could be entered as a parameter in the model, and the $N_2(A^3\Sigma)$ and $N(^2D)$ densities were set as 4.3×10^{-6} and 2.4×10^{-5} times the $N(^4S)$ density. This simple model supplied realistic densities of N-atoms and $N_2(A^3\Sigma)$ metastables which were the primary drivers (plus $N_2(X^1\Sigma, v>0)$) in the silane reaction model.

Vibrationally Excited $N_2(X^1\Sigma)$

In the first stages of this latter modelling effort, vibrationally excited, ground electronic state N_2 was simply treated as a single species which was generated by reactions R-5 and R-9 of chapter IV and dissociated SiH_4 by reaction R-1. While this simple treatment showed the necessary characteristics of a chain reaction, a more realistic treatment

was needed to answer questions about vibrational relaxation and/or vibrational pumping. The method chosen to treat the vibrationally excited molecules was to treat each vibrational level as a different species in the model and supply the rates for vibrational exchange and relaxation. This method is often referred to as the Master Equation Approach. The treatment to be discussed here follows very closely the work of Bailey⁶⁷ and also the work of Capitelli⁶⁸. The equation governing the density of a species in some energy level l is given by

$$\frac{dN_l}{dt} = \sum_{i,j,k} \tilde{R}_{j,i}^{k,i} N_j N_k - \sum_{i,j,k} \tilde{R}_{l,j}^{i,k} N_l N_i \quad (\text{eq. 5-1})$$

where N_l is the density, and the $\tilde{R}_{l,j}^{i,k}$'s represent generalized rate coefficients for the population and depopulation of state l . The above set of equations are commonly referred to as the Master Equation. This set of equations is very difficult to solve due to the many states involved so the following simplifying assumptions are made (see Bailey, reference 67):

1. The translational and rotational degrees of freedom are in complete Boltzmann equilibrium.
2. The molecules in each vibrational state are treated as separate species.
3. Only single quantum vibrational exchanges occur.
4. The molecule is represented as a Morse oscillator rigid rotator system.

With these assumptions the Master Equation becomes

$$\frac{dN_v}{dt} = N_{v+1} R_{v+1,v} + N_{v-1} R_{v-1,v} - N_v [R_{v,v+1} + R_{v,v-1}] \quad (\text{eq. 5-2})$$

where the $R_{i,j}$'s are the rates for change of vibrational quanta from i to j . The $R_{i,j}$'s can be written

$$R_{v+1,v} = N \cdot (VT)_{v+1,v} + \sum_{k=0}^{v-1} (VV)_{v+1,v}^{k,k+1} N_k \quad (\text{eq. 5-3})$$

$$R_{v-1,v} = N \cdot (VTB)_{v-1,v} + \sum_{k=1}^v (VV)_{k,k-1}^{v-1,v} N_k \quad (\text{eq. 5-4})$$

where the $(VT)_{i,j}$'s are the rates for the loss of a quantum of vibration to translation (vibration-to-translation, VT) and the $(VTB)_{i,j}$'s are the rates for the gain of a quantum of vibration from the translational energy pool (VT Back, VTB). The VV's are the rates for exchange of vibrational quanta between molecules in different vibrational states, N is the density of colliding species, and v^* is the maximum vibrational level considered. If the VT and VV rates are known, the set of equations given in 5-2 can be integrated from some initial conditions to give the populations in each vibrational level as a function of time. In general, the VV rates only include vibrational exchange among like molecules, thus in this work only exchanges between two N_2 molecules are considered. On the other hand, the VT rates are strongly affected by all species that collide with the molecule. In this experiment, the dominant species was always N_2 ; therefore, for purposes of the model the only VT rates considered were those involving N_2 - N_2 collisions. It should be pointed out that in cases where other major species are present, the VT rates for collisions between that species and N_2 must also be included.

For most molecules, the VV and VT rates are only known for the very lowest lying vibrational levels. To accurately model the behavior of the ground state vibrational manifold, it is necessary to include a large number of levels, thus rates for high lying vibrational states are needed. The general procedure to obtain these rates is to extrapolate the known rates from the lowest levels to the higher states using a theoretical expression for the scaling of the rates with vibrational quantum number. The theory usually used for this scaling the rates is due to Schwartz, Slawsky, and Herzfeld⁶⁹ and is commonly referred to as the SSH theory. In the SSH theory, the VT transition probability (probability per collision) for a molecule to go from $v+1$ to v is given by

$$P_{v+1,v} = P(T) \cdot (v+1) / [1 - \delta \cdot (v+1)] \cdot F(Y_{v+1,v}) \quad (\text{eq. 5-5})$$

where δ is the anharmonicity of the molecule, $P(T)$ is a parameter related to the 1-0 relaxation, T is the temperature, and $Y_{v+1,v}$ is given by

$$Y_{v+1,v} = (0.5)^{3/2} \cdot \sqrt{\theta/T} \cdot [1 - 2\delta \cdot (v+1)] \quad (\text{eq. 5-6})$$

where θ is a parameter related to the molecule (for N_2 Bray⁷⁰ gives a value of $\theta = 5.39 \times 10^6$ °K). The function F cannot be easily evaluated and is usually approximated by (see reference 70)

$$F(y) = 0.5 \cdot [3 - \text{Exp}(-2/3 \cdot y)] \cdot \text{Exp}(-2/3 \cdot y) \quad (\text{eq. 5-7})$$

The anharmonicity of the molecule, δ , is defined so that the vibrational energy levels of the molecule are given by

$$E_v = E_{10} \left[\left(v + \frac{1}{2} \right) - \delta \cdot \left(v + \frac{1}{2} \right)^2 \right] \quad (\text{eq. 5-8})$$

and for N_2 , $E_{10} = 2358.57 \text{ cm}^{-1}$ and $\delta = 6.127 \times 10^{-3}$ (from reference 55). Using the transition probability, the VT rate is given by

$$(\text{VT})_{v+1,v} = Z \cdot P_{v+1,v} \quad (\text{eq. 5-9})$$

where Z is the gas kinetic collision rate calculated using equation 4-3 from chapter IV (for N_2 , the molecular diameter = 3.35 \AA). For the function $P(T)$, Bray⁷⁰ gives the form

$$P(T) = 1.07 \times 10^{-4} \cdot T \quad (\text{eq. 5-10})$$

however, for this work the function described in appendix C was used for $P(T)$. The (VTB) rates were calculated from detailed balance⁶⁷,

$$(\text{VTB})_{v,v+1} = (\text{VT})_{v+1,v} \cdot \text{Exp}[-(E_{v+1} - E_v)/(kT)] \quad (\text{eq. 5-11})$$

where the E 's are calculated from equation 5-8.

The VV rates are also calculated from the SSH theory. The transition probability (per collision) for the target molecule to go from v to $v+1$ while the colliding molecule goes from $j+1$ to j is given by⁶⁷

$$P_{v,j} = S_{v,j}(T) \cdot \text{Exp}\{[(E_{v+1} - E_v) - (E_{j+1} - E_j)]/(2kT)\} \quad (\text{eq. 5-12})$$

where the E 's are from equation 5-8 and $S_{v,j}(T)$ is given by

$$S_{v,j} = Q(T) \cdot \frac{(v+1)}{[1-\delta \cdot (v+1)]} \cdot \frac{(j+1)}{[1-\delta \cdot (j+1)]} \cdot F(Y_{v,j}) \quad (\text{eq. 5-13})$$

where $F(Y)$ is given by equation 5-7 and $Y_{v,j}$ is given by

$$Y_{v,j} = \frac{\delta}{\sqrt{2}} \cdot \sqrt{\theta/T} \cdot |v-j| \quad (\text{eq. 5-14})$$

where θ is given above. $Q(T)$ is given by Bray⁷⁰ for N_2 as

$$Q(T) = 3.7 \times 10^{-6} \cdot T \quad (\text{eq. 5-15})$$

As in equation 5-9 for the VT rates, the VV rate is given by the product of the transition probability given by equation 5-12 and the gas kinetic rate given in equation 4-3. Again using detailed balance, the reverse rates are given by⁶⁷

$$(VV)_{v+1,v}^{w,w+1} = (VV)_{w+1,w}^{v,v+1} \text{Exp}\{ -[(E_{v+1} - E_v) - (E_{w+1} - E_w)]/kT \} \quad (\text{eq. 5-16})$$

Using equations 5-5 through 5-16 and appendix C, VT and VV rates were calculated for $T=300^\circ\text{K}$. Some typical rates are shown in figure 5-1. One remaining parameter was to set the highest vibrational level to be included in the model. As mentioned in chapter IV, the N_2 ground electronic state can support approximately 70 vibrational levels, but due to the simple expression for the energy of the levels given in 5-8, the number of levels should be set lower. In his work, Bray⁷⁰ used a value of $v_{\text{max}}=47$; therefore, this value was also chosen in this work. Thus a total of 48 vibrational levels were included in the set of equations given by eq. 5-2, along with the calculated VT and VV rates to describe the interaction of the $N_2(X^1\Sigma)$ vibrational manifold.

Finally, a set of initial vibrational populations was needed as input into the model. To arrive at this set, the following procedure was used. A model was constructed which included only the vibrationally excited $N_2(X^1\Sigma)$ species and the VT and VV rates. The initial vibrational populations were set to a Boltzmann distribution with a vibrational temperature of 1500°K . This distribution was then allowed to "relax" for 1 second at

SELECTED V-T AND V-V RATES IN N₂ AT 300 DEG. K

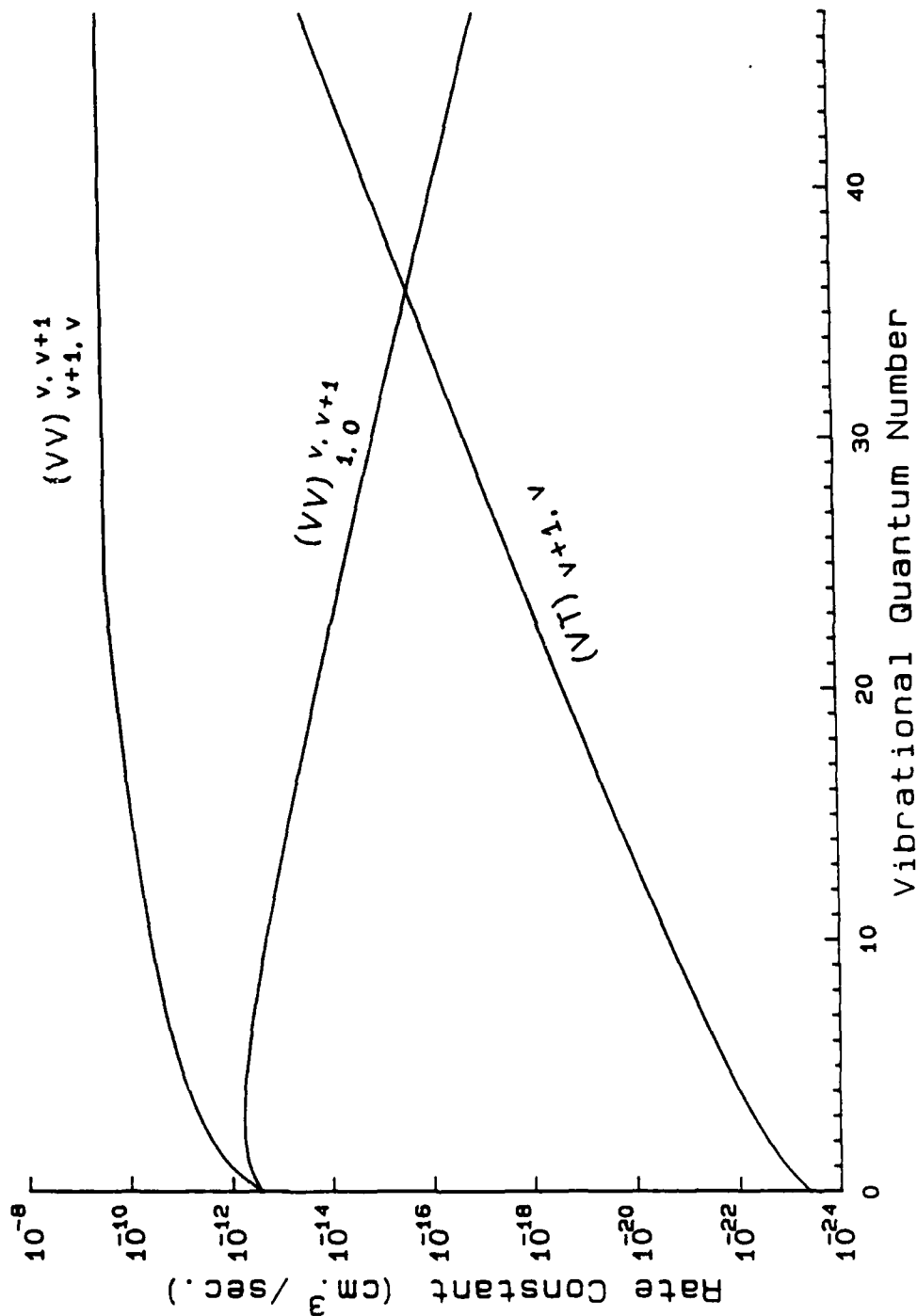


Figure 5-1: Selected V-T and V-V Rates for Nitrogen at 300°K

3 torr. The resulting vibrational populations are shown in figure 5-2, which is a plot of the fraction of molecules in a given level vs. the vibrational quantum number. As can be seen, the distribution is "over populated" with respect to a Boltzmann distribution at the higher levels, but the lower levels are still approximately Boltzmann at the initial 1500°K. Since this vibrational temperature is typical of measurements made on the lowest levels in a nitrogen discharge⁷¹, this distribution was taken as the initial distribution for all runs. It should be pointed out that one would expect the distribution to be affected by pressure, but since only the levels above $v=10$ interacted with silane, details of the distribution were unimportant. The advantage of using this distribution instead of a Boltzmann distribution was that this distribution was relatively stable for times on the order of 1 s, in the absence of any energy input, while the upper levels of the Boltzmann distribution tended to "come up" due to $v-v$ pumping. Therefore, using the distribution in figure 5-2 allowed changes due to chemical kinetics to be more easily seen.

The Silane Reactions

The last step in the model was to integrate the silane reactions R-1 through R-11 given at the end of chapter IV into the model. As discussed in chapter IV, the rate constants can not exceed the gas kinetic rate for a given reaction. When literature values of molecular diameters were available, equation 4-3 was used to set the limiting rate for the model. In cases where molecular diameters were not available, a gas kinetic rate of 1×10^{-10} cm³/s was chosen as a typical value. It should be pointed out, however, that the sum of rates for reactions R-5 and R-6 cannot exceed the gas kinetic rate, since the two only yield different products from the same reaction. The same is true for reactions R-9 and R-10. The v to E transfer rate, R-1, was never allowed to reach the gas kinetic limit, but was limited to 10^{-2} times the gas kinetic. The rate for SiH₄ dissociation by the N₂(A³Σ), reaction R-2, was taken from the work of reference 31 as $k_2 = 5.9 \times 10^{-12}$ cm³/s. The rates R-7 and R-11, which are radiative rates were taken from the literature when possible. For R-7, an average rate of 1×10^7 s⁻¹ was taken for the states of Si. For R-11, the recent measurement of the lifetime of the B²Σ of SiN of 210 ± 10 ns by Walkup, et al.⁷² was used to derive the rate of 4.8×10^6 s⁻¹. An estimate of the gas kinetic three-body rate given in reaction R-8 is difficult. If the process is a true three-body reaction, requiring the three bodies to be present within some

CALCULATED FRACTIONAL VIBRATIONAL POPULATIONS IN THE N_2 AFTERGLOW

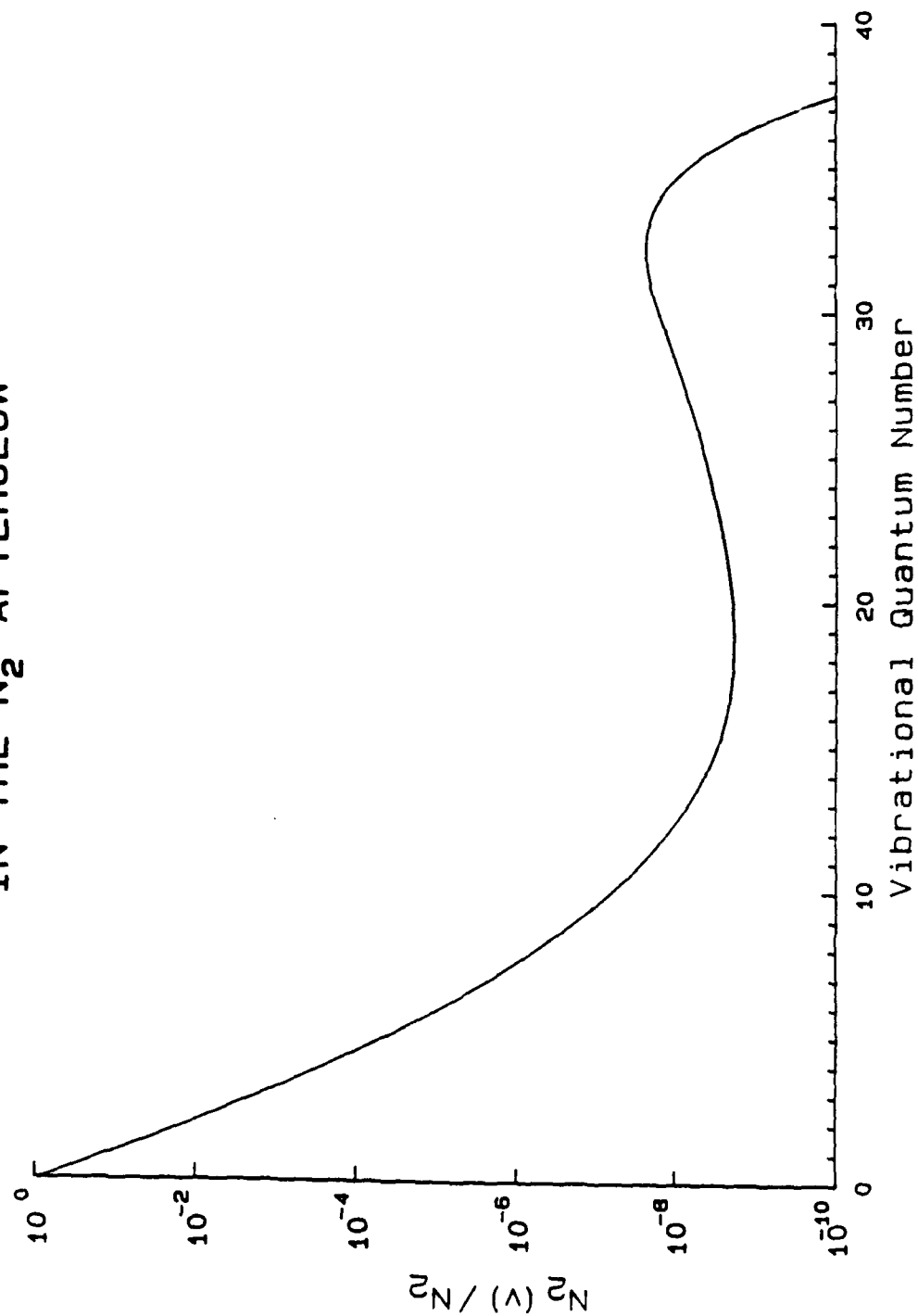


Figure 5-2: Calculated Fractional Vibrational Populations of N_2 in the Afterglow

small volume for the reaction to occur, then a calculation based on the Thompson theory⁵³ can be used. On the other hand, if the reaction is typical of an association reaction, an intermediate state of some finite lifetime is probably involved which must be stabilized by collision with a third body. Depending on the lifetime of this state, the three-body rate in this latter case can be significantly larger than that given by the Thompson theory. In the Thompson theory⁵³, the two reacting species and the third body are assumed to occupy a sphere of radius r_0 for the recombination to occur. The three-body rate scales as r_0^3 so that uncertainties in choosing this radius can affect the rate dramatically. Using available data for the diameters of N_2 and Si and assuming the interaction radius r_0 was equal to the average diameter of the two gave a value of the rate constant of reaction R-8 as

$$k_8 = 6.6 \times 10^{-32} \text{ cm}^6/\text{s} \text{ (Thompson theory)}$$

Because of the nature of the reaction, the above rate was only used as a guideline in the model. For this rate, the rate constant used in the model was allowed to exceed the above rate if necessary. For the vibrational pumping reactions R-5 and R-9, it was assumed that the reactions left the molecules in $v=20$ and $v=13$ respectively. While there is most certainly some distribution of vibrational levels that result from these reactions, with no knowledge of this distribution available, this simple approach was taken. For similar reasons, it was assumed that the v -to- E transfer reaction, R-1, could occur with $v \geq 10$ and the reaction left the N_2 molecule in $v=0$. Again, there is probably some distribution of final states depending on the initial vibrational level involved in the reaction, but this simpler approach was taken. Diffusion was not included in the model although it almost certainly plays a role in the reaction. Changes in the behavior of the reaction as the tube walls became coated, as discussed in chapter III, indicated that diffusion of some species to the wall affected the reaction. Since the proposed reaction scheme involves a number of feedback loops, there are a number of steps where loss of a species to the wall (sticking) could change the behavior of the reaction. The reason for not including diffusion in the model is that very little is known about the sticking coefficients of the various species in the model, hence diffusion would simply add more uncertainty to the modelling effort.

The model as described above contained 11 "reactive" species plus 48 vibrational levels of N_2 for a total of 59 coupled first order differential equations. The number of VV and VT rates needed in the model goes as

$2 \cdot (v_{\text{total}}) \cdot (v_{\text{total}} + 1)$ or 4704 rates for the 48 levels used. Finally, the 16 rates used to describe the afterglow and the silane reaction were also included. The differential equations were integrated using the method of Gear⁷³ which is specifically designed to handle sets of equations which exhibit "stiff behavior"⁷⁴. A detailed discussion of Gear's method is not appropriate here, but it should be pointed out that for stiff sets of equations, use of this method is almost mandatory. For example, it was found by the author, on a much simpler set of stiff equations, that Gear's method was a factor of 1000 times faster than an Adams-Bashforth method for integrating the equations. This is a significant savings in computer time and as a result of this savings, the calculations presented here could be performed on a desktop computer.

General Behavior of the Model

Detailed quantitative predictions of the model were difficult to use in assessing its validity because of the lack of specific rate data and the lack of detailed quantitative measurements of the reaction. However, the general behavior of the model could be used to evaluate the validity of the overall scheme. As discussed in chapter III, the Si and SiN intensities increased faster than linear with pressure even when the N-atom density was taken into account. In figures 3-1 and 3-4 to 3-7, the first positive intensity increased roughly as the square of the pressure while the Si and SiN intensities increased even faster. Since the first positive intensity goes as the square of the N-atom density, figures 3-1 and 3-4 through 3-7 represent data where the N-atom **concentration** is approximately constant. To model these data, a series of calculations were made at four different pressures with both the N-atom and SiH₄ concentrations held constant. The rates chosen were mostly gas kinetic and are given below:

$k_1 = 2.7 \times 10^{-12}$	$k_2 = 5.9 \times 10^{-12}$	$k_3 = 1 \times 10^{-10}$
$k_4 = 1 \times 10^{-10}$	$k_5 = 6.6 \times 10^{-11}$	$k_6 = 3.3 \times 10^{-11}$
$k_7 = 1 \times 10^7$	$k_8 = 6.6 \times 10^{-32}$	$k_9 = 6.6 \times 10^{-11}$
$k_{10} = 3.3 \times 10^{-11}$	$k_{11} = 4.8 \times 10^6$	

Figure 5-3 shows the SiN(B²Σ) density as a function of the reaction time (time after the silane injection) for these conditions. The Si excited-state density followed a similar set of curves. As shown in the figure, the SiH₄ density was set to 0.1% of the total density while the N-atom density was set to 0.2% of the total density. Since the intensity of the emission is

CALCULATED TIME DEPENDENCE OF SiN EXCITED STATE DENSITY AS A FUNCTION OF PRESSURE (CONSTANT SiH₄ AND N-ATOM CONCENTRATION)

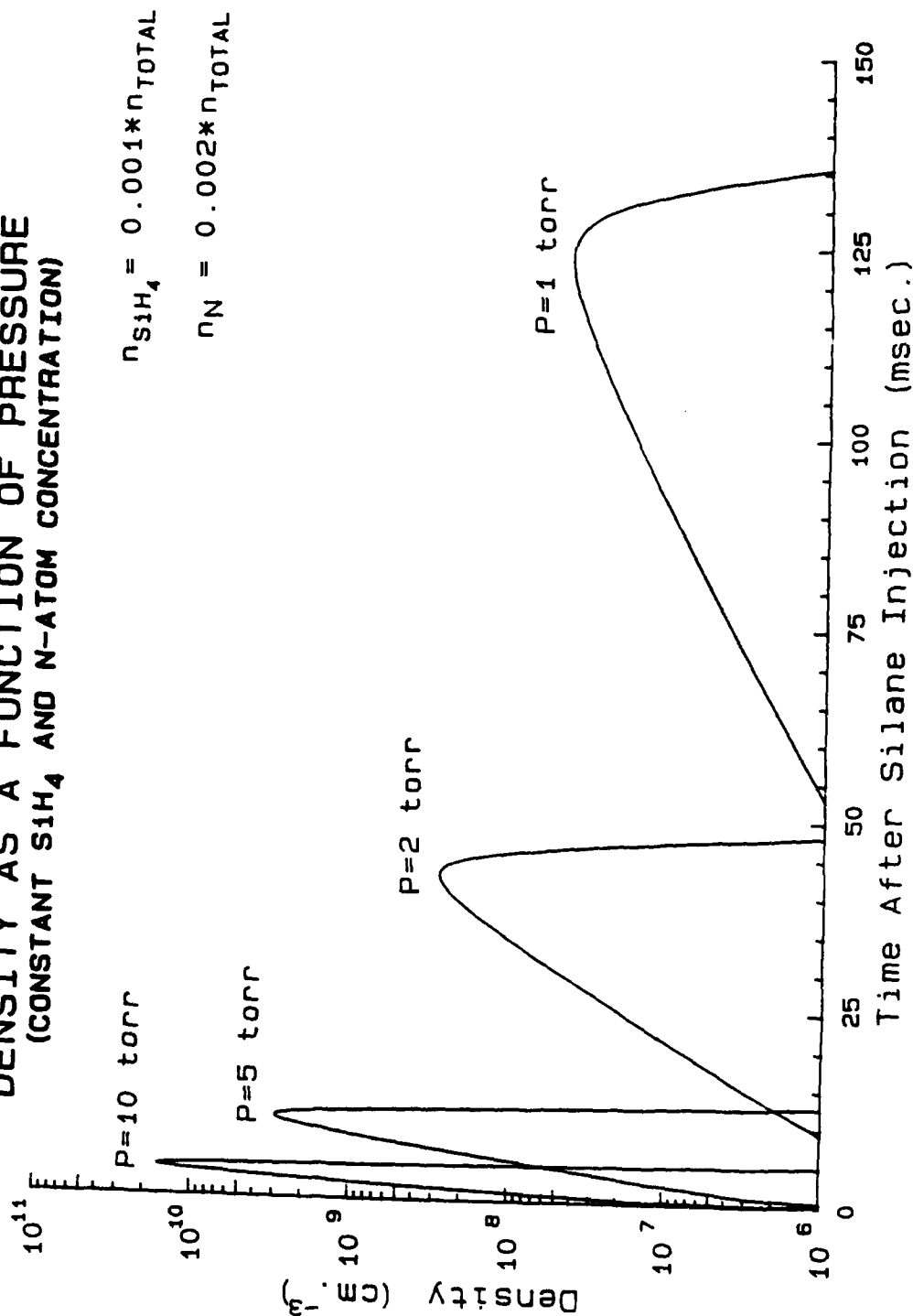


Figure 5-3: Calculated Time Dependence of SiN Excited State Density as a Function of Pressure

proportional to the excited state density, these curves are proportional to the chemiluminescence intensity. In figure 5-3, the ratio of the peak density at 10 torr to that at 1 torr is 351 while the calculated first positive intensity increases by a factor of 100. This is similar to the increases observed in the emission spectra. In addition to faster-than-linear increase in the SiN^* emission predicted by the model, the model also predicts a longer time for the occurrence of the peak emission and the spreading in time of the chemiluminescence. Both of these effects were observed in the reaction flame. The exact position in time of the peak and the ratio of the peak intensities at different pressures is a function of the specific rates put into the model, but the general behavior remains the same. It was also observed that the peak intensity could be made to move back and forth in the reaction zone by varying the SiH_4 flow (and to a lesser extent the discharge current). This is also predicted by the model as shown in figure 5-4. In this case, both the pressure and N-atom density were held constant while the SiH_4 density was varied. As can be seen in figure 5-4, as the SiH_4 density is decreased the peak in the emission occurs at later times. A similar (but less sensitive) effect is also observed for varying the N-atom density. Since the occurrence of the emission at a later time corresponds to the chemiluminescence occurring farther downstream of the injection port, this agrees with the observed movement of the flame in the experiments. As before, the specific location of the peak depends on the rates chosen in the model, but the general behavior remains the same.

The overall design of the model insures that the SiH_4 dissociated will be proportional to the N-atom density if a "titration" experiment is performed as described in chapter III. On the other hand, the resulting proportionality constant depends on the rates put into the model. To better understand this, consider the four reactions R-5, R-6, R-9, and R-10. Reactions R-5 and R-9 each result in the loss of an N-atom but produce a vibrationally excited N_2 molecule which can dissociate an SiH_4 molecule by reaction R-1. On the other hand, reactions R-6 and R-10 also result in the loss of an N-atom, but in this case no SiH_4 dissociation results. Thus it can be argued that more SiH_4 will be dissociated per N-atom if the ratio $(k_5+k_9)/(k_6+k_{10})$ is increased. This is, in fact, observed in the model, but the functional dependence of the SiH_4 dissociation is much more complex than the previous expression would lead one to believe.

CALCULATED TIME DEPENDENCE OF SiN EXCITED STATE DENSITY AS A FUNCTION OF SiH₄ DENSITY

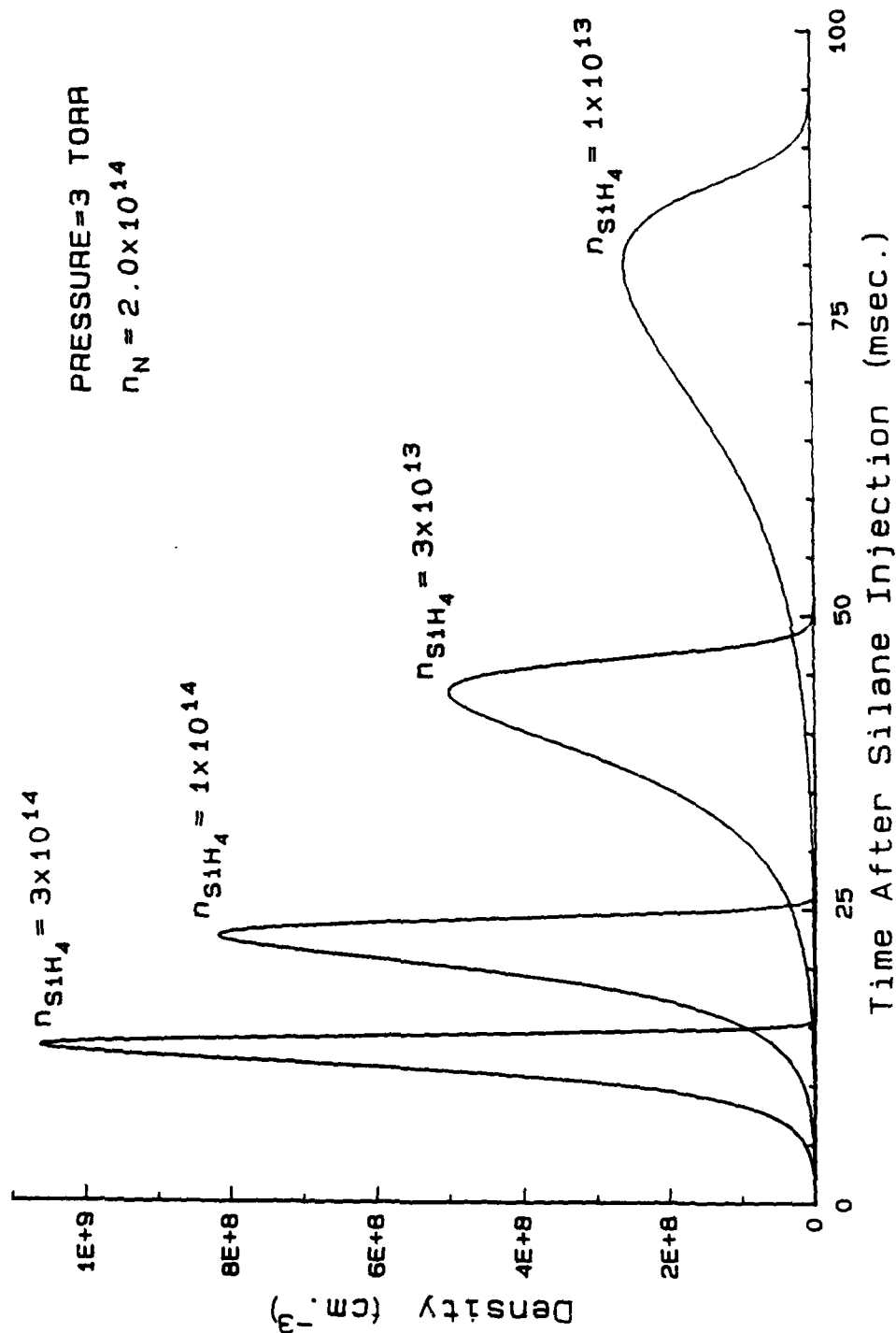


Figure 5-4: Calculated Time Dependence of SiN Excited State Density as a Function of SiH₄ Density

Comparison with the Data of Reference 30

Since the time dependence of the various species in the model are strongly affected by the magnitudes of the rates used, time dependent measurements of the reactive species could further validate the reaction model. As discussed earlier, and as shown in figure 4-2, Horie, et al. (reference 30) have made measurements of the time dependence of the SiH_4 , the N-atom, and (in one case) the H_2 density in the reactor at approximately 3 torr. Since these measurements could not be made in this experiment (Horie, et al. used a mass spectrometer), it was decided to try and model their results. To allow comparison of the model results with their data, the data points from figure 4-2 were digitized using an HP plotter. Since the data in figure 4b of reference 30 were the only group to contain H_2 data, this group was chosen for modelling. To arrive at the rates needed to model their data, a least-squares approach was attempted. Because of the 2:1 correspondence between H_2 and SiH_4 in the model, only the N-atom data and the SiH_4 data were included in the fitting effort. The approach followed the Marquardt algorithm as given by Bevington³⁶, but in this case the method did not work well. It was found very early on in the fitting that the iterative method of Marquardt often "over shot" a particular rate by an amount large enough to drive the rate negative. This condition played havoc with the integrator and, of course, gave unreal results. To suppress these excursions, the iterations were "damped" so that a rate could only be increased or decreased by a factor of ± 0.8 (times the rate) during an iteration. Another problem, which was never solved, appeared to have its origins in the shape of the chi-squared hypersurface³⁶. Many times the algorithm would begin searching for the chi-squared minimum along a path that pushed one particular rate to a very large value (much higher than gas kinetic). An attempt was made to solve this problem by "capping" the rates to some value less than gas kinetic, but even this method sometimes failed to yield a minimum in chi-squared. The worst problem of all was that the chi-squared minimum found by the procedure was a strong function of the starting values used for the iteration of the rates. Even with only 8 "unknown" rates, this made finding a true minimum very difficult. Exacerbating this problem even further was the fact that the calculations were by nature very slow. A typical "adjustment" of the rates might require 10 hours of desktop computer time, only to find the procedure had failed to find a minimum. As difficult as this procedure was, it was still more manageable than random shuffling of the rates to fit the data. In the end, a combination of "cut and try" and

least-squares was used to fit rates in the model to the data of Horie et al.

Figure 5-5 shows the results of this rate adjusting exercise along with data from reference 30 as digitized from their figure 4b. The continuous curves are calculations from the model, and the symbols are the data of reference 30. The "best fit" rates are given below:

$k_1=1.74 \times 10^{-12}$	$k_2=5.9 \times 10^{-12}$	$k_3=1 \times 10^{-10}$
$k_4=1 \times 10^{-10}$	$k_5=7.8 \times 10^{-11}$	$k_6=2.2 \times 10^{-11}$
$k_7=1 \times 10^7$	$k_8=5.25 \times 10^{-31}$	$k_9=8.0 \times 10^{-11}$
$k_{10}=2.0 \times 10^{-11}$	$k_{11}=4.8 \times 10^6$	

It must be stressed, however, that the above rates may not yield an absolute minimum in chi-squared, but represent the rates which yielded the smallest chi-squared observed during the work. Since no uncertainties were given in reference 30, the actual value of chi-squared could not be calculated, however for fitting purposes the data points were all assigned equal weights. One of the problems in trying to model these data is that Horie et al. used a gas mixture of N_2 and He in their discharge, but they do not state what the mixture was for the data given in figure 4-2. The model, of course, assumes the gas mixture entering the discharge is pure N_2 . The effects of He quenching of the vibrationally excited N_2 and perhaps SiH_4 dissociation (or ionization) produced by collisions with He metastables would need to be included in the model if one were to try to accurately model the data of reference 30. The vibrational distribution used as input to the model might also be considerably different if a large amount of He were used. In addition to these factors, the measurements themselves are very difficult. One of the difficulties which Horie et al. do not address is the problem of the introduction of the SiH_4 into the afterglow. As can be seen from figure 5-4, the reaction rate is a strong function of the SiH_4 density; therefore, if the SiH_4 is introduced through a small tube (introduced at a point) the higher density of the SiH_4 at the point of introduction will tend to "speed up" the reaction beyond what one might expect if the SiH_4 were more evenly distributed upon its introduction. Considering all of these problems, the fit is reasonable.

If one now takes this rate set and tries to fit either the data from figure 4-2(a) or 4-2(c), the fit is very poor. Since the gas mixture used in reference 30 was not known, this lack of consistency could be explained by assuming that any of the reactions involving N_2 would be changed by the introduction of He into the gas mixture. Since these are basically reac-

COMPARISON OF MODEL RESULTS WITH MEASUREMENTS OF REFERENCE 30 (Fig. 4b)

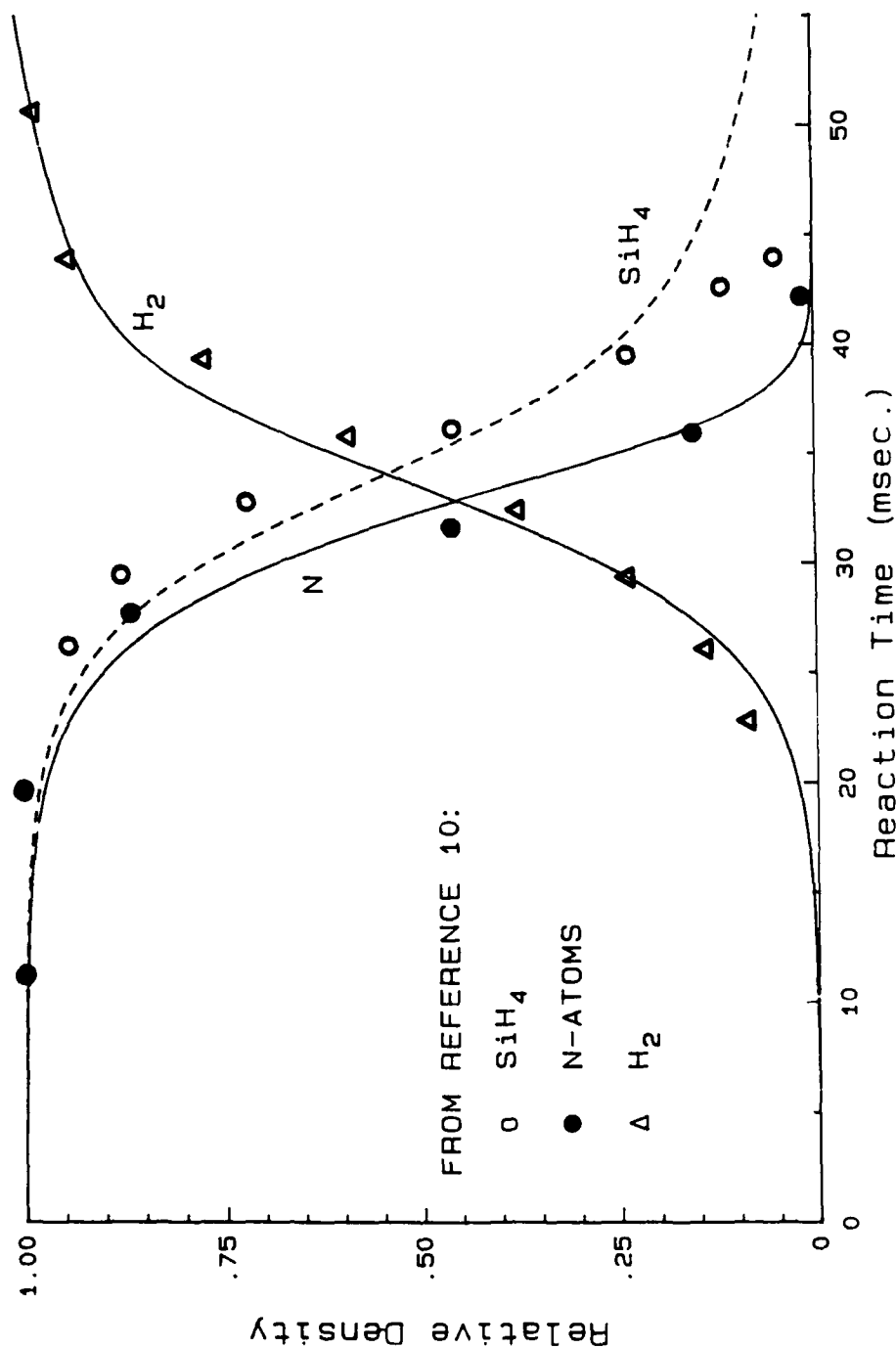


Figure 5-5: Comparison of Model Results with Measurements of Reference 30

tions R-1 and R-8, if the data from reference 30 could be fit by only adjusting these two rates, then the model would at least remain consistent. This procedure proved possible and the "best fit" rates for the other two data sets are given below:

Figure 4-2(a):	$k_1=3.07 \times 10^{-12}$	$k_8=2.32 \times 10^{-31}$
Figure 4-2(c):	$k_1=5.34 \times 10^{-12}$	$k_8=4.05 \times 10^{-31}$

One point that arises from the fitting procedure is that both k_1 and k_8 , derived from the fit, are somewhat larger than was expected. In all cases, k_8 exceeds the rate calculated from the Thompson theory and k_1 exceeds the 10^{-3} times gas kinetic rate for the v-to-E process. While it is difficult to assess the true rates from the rates arrived at using the unknown He-N₂ gas mixture, at least the rates calculated above do not exceed the basic gas kinetic rate. Both the general behavior of the model and the reasonable fit to the data of reference 30 give credibility to the model but in no way "prove" the model is the correct one.

Behavior of the Vibrational Distribution

During the reaction, the N₂ vibrational distribution changes significantly. The vibrational pumping supplied by reactions R-5 and R-9 is fast enough to overcome any v-T losses for the levels v=20 and v=13, and subsequent v-v exchange results in all the vibrational levels, up to the 48 considered, being excited. Figure 5-6 shows the N₂(X¹Σ) vibrational distribution at different times under the same conditions as in figure 5-5. Initially, only levels 13 and 20 are pumped but as the reaction proceeds, and v-v exchange occurs, all of the levels become significantly populated. The behavior of the vibrational levels above v=9 is especially important because these levels are available for dissociating SiH₄ in the reaction. Figure 5-7 shows the time dependence of this group of levels during the reaction. The reason the group "hangs up" after the reaction is complete is due to the small v-T rates in N₂. Certainly if diffusion were included in the model, these levels would be relaxed by diffusion to the walls of the tube. The peak fractional population above v=9 occurs at t=37.2 ms and reaches a value of 7.6×10^{-4} . This number is more than three orders of magnitude above the fractional population at t=0.

CALCULATED TIME DEPENDENCE OF FRACTIONAL VIBRATIONAL POPULATIONS IN N₂ (REACTION TIMES ARE IN MILLISECONDS)

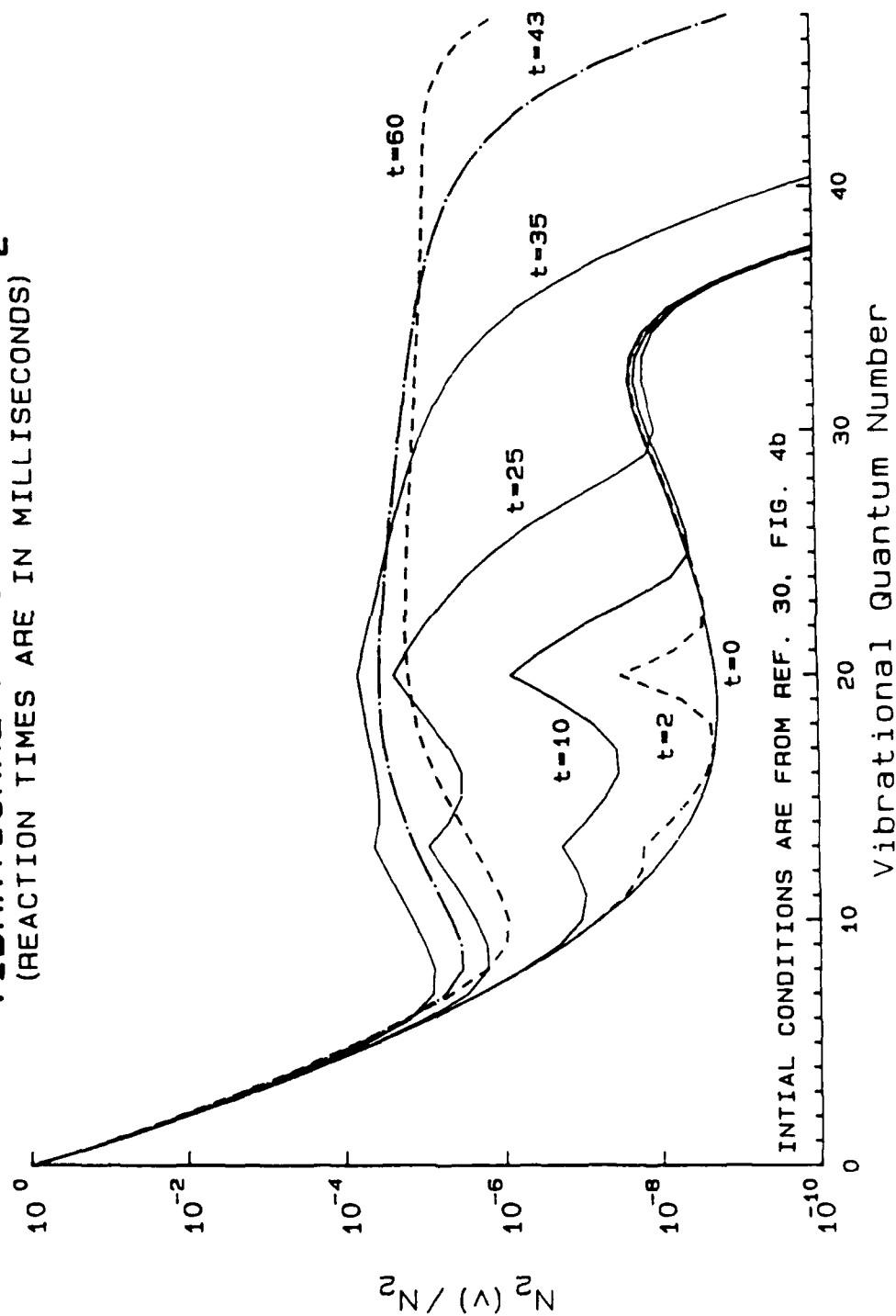


Figure 5-6: Calculated Time Dependence of Fractional Vibrational Populations in Nitrogen

FRACTIONAL VIBRATIONAL POPULATION AVAILABLE FOR SiH_4 DISSOCIATION DURING THE REACTION

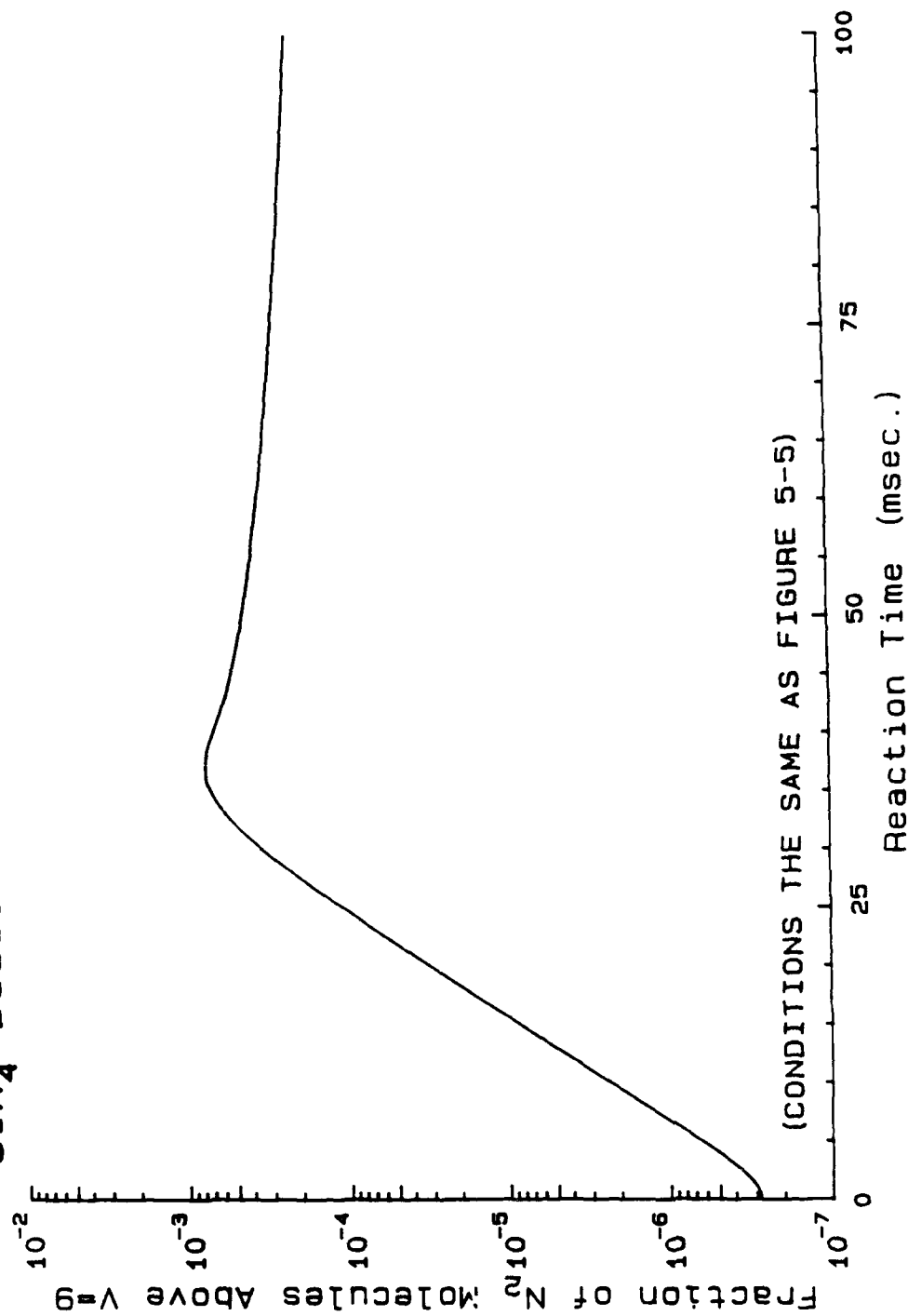


Figure 5-7: Calculated Time Dependence of Fractional Vibrational Population Available for SiH_4 Dissociation

Final Products, Higher Nitrides

The final products in the reaction are SiN, SiN₂, H₂, SiH₂ and SiH₄ (if complete dissociation does not occur). At lower pressures very little SiN₂ is formed. It is doubtful that in a real reactor SiH₂ remains for very long in the gas phase. It may be dissociated by collisions with vibrationally excited N₂ (as SiH₄ is) or it may diffuse to the walls and stick. Dewhurst and Cooper²⁹ analyzed the white powder which coated the tube walls and found it to contain mostly higher nitrides of silicon of the form Si_xN_y. The question of whether the powder is formed in the gas phase and "deposits" on the walls or whether the powder is actually formed on the walls is an interesting one. During the course of this investigation an attempt was made to observe particulates in the gas phase by directing a HeNe laser down the reaction vessel and looking for scattered light. No scattering could be observed, but the sensitivity of this method is unknown. At the higher pressures in the experiment, it might be possible for three-body reactions to occur among some of the nitrides to form higher nitrides such as



or



but it is doubtful that complex nitrides such as Si₃N₄ are actually formed in the gas phase during such short reaction times. Reactions between some of the simpler nitrides, such as SiN, and SiH₄ may also occur in the gas phase resulting in some hydrogenated nitride. A species of this type may have been the cause of the broadband absorption seen in the FT-IR experiment. Because of the low densities of the products and the low pressures in the experiment the most likely place for formation of more complex nitrides of silicon must certainly be the walls of the tube. It is therefore suggested that any higher nitrides produced in the reaction are produced on the reactor tube walls and not in the gas phase.

Chapter VI

Summary, Conclusions, and Recommendations

Visible and ultraviolet spectra of the chemiluminescence from the reaction of silane with active nitrogen have been obtained over the wavelength range 230-850 nm and a pressure range of 0.5 to 10 torr. The spectra at higher pressures are dominated by emission from Si and SiN and at low pressure by an unidentified broad-band emitter. The measurements indicate that both the Si and SiN emission intensities increase with pressure more rapidly than the first positive intensity of the N_2 afterglow. The measurements also show that the vibrational levels of the upper electronic state of SiN are populated to the same extent as those observed in the reactions of both $SiCl_4$ and $SiBr_4$ with active nitrogen. From the general behavior of the chemiluminescence, it is clear that the reaction involves some kind of chain reaction, and that direct reaction of SiH_4 with N-atoms can be ruled out. Silane dissociation, resulting from the reaction with active nitrogen, has been measured downstream of the reaction zone and correlated with the relative N-atom density. In spite of the evidence ruling out direct reaction of SiH_4 with N-atoms, these measurements show that for small amounts of SiH_4 the dissociation is proportional to the N-atom density in the afterglow. To explain this apparent paradox, a reaction model has been developed which can describe the general behavior of the Si and SiN chemiluminescence and the silane dissociation observed in the reaction. The rate-equation model involves only neutral species and uses as initial conditions the characteristics of a "typical" nitrogen afterglow. A key reaction in the model is the dissociation of SiH_4 by vibrationally excited, ground electronic state N_2 . This proposed reaction involves a transfer of vibrational energy to a dissociating electronic state of SiH_4 . While reactions of this type have been observed in other systems, no direct evidence of SiH_4 dissociation by vibrationally excited N_2 has ever been seen. The choice of this reaction as the driver of SiH_4 dissociation was arrived at by eliminating other possible reaction channels which could dissociate SiH_4 at the rates observed in time dependent measurements³⁰ and without perturbing the observed N_2 afterglow emission. Dissociation of silane by vibration-to-vibration (v-v)

exchange with $N_2(v)$ must also be considered as a possible mechanism, but no modelling of this scheme was attempted. If v-v pumping of SiH_4 is a significant driver of dissociation, the pumping must be enhanced during the reaction since the observed dissociation increases dramatically during the reaction. This implies the density of $N_2(v)$ levels responsible for pumping SiH_4 must also increase dramatically during the reaction. Because of rapid v-v up-pumping in N_2 , the densities of the higher lying vibrational levels are greatly altered by any mechanism of vibrational excitation; therefore, a further implication is that if v-v pumping of SiH_4 occurs it must come from the higher lying levels of $N_2(v)$. The vibrationally excited N_2 is produced by exothermic reactions of two nitrides of silicon with atomic nitrogen. The model demonstrates that the vibrational pumping available from these reactions is sufficient to drive the SiH_4 dissociation at the rates observed. In addition, the model gives the SiH_4 dissociation proportional to the N-atom density in the afterglow. The model includes a complete description of the exchange and loss of N_2 vibrational quanta and therefore allows accurate modelling of the time dependence of the SiH_4 dissociation. The model results have been compared with time dependent mass spectroscopy measurements of SiH_4 dissociation made by Horie, et al.³⁰ in a similar experiment, and the model can reasonably predict their observed results for a given set of conditions. The model could not describe all of the data of reference 30 under all conditions because the experiments in reference 30 were performed with a gas mixture of N_2 and He and no He was included in the model. Specifically, the effect of He on the vibrational levels of N_2 and SiH_4 dissociation induced by He metastables were not included in the model. In general, atomic species such as helium are known to effectively relax molecular vibrational levels so it might be expected that significant concentrations of helium in the gas mixture would alter the behavior of the N_2 vibrational populations and therefore affect SiH_4 dissociation. Helium metastables should not directly perturb the amount of SiH_4 dissociation, since their density is probably on the order of 1 part in 10^6 of the He density, but the time dependence of the dissociation can be affected. It was found in the modelling that the time of occurrence of the peak in the chemiluminescence and the rapid drop in SiH_4 density can be dramatically affected by the initial rate of SiH_4 dissociation caused by various species in the afterglow. Thus the presence of He metastables could affect the time dependence of the SiH_4 dissociation while not affecting the total dissociated density. Horie, et al. did not state the specific gas mixture used in their experiments; therefore, it was impossible to include He in the modelled results. While there is no

guarantee that the model developed here is the only model that will describe the observed results, the model is plausible, does not violate any laws of physics, and is generally successful at describing the observed results.

Application of the model reaction scheme to commercial reactors producing silicon nitride (Si_3N_4) cannot be strictly made due to differences between those systems and the system studied here. Since most silicon nitride reactors do not operate in an afterglow mode as described in this work, but instead operate as a low pressure discharge, the reaction scheme under reactor conditions is expected to be more complex. On the other hand, this work was begun for the reason that very little SiH_4 dissociation occurred in a $\text{SiH}_4\text{-N}_2$ discharge due to electron impact, thus many of the reactions described here would be expected to still occur in a low pressure reactor. In addition, many commercial reactors use gas mixtures of silane and ammonia instead of silane and nitrogen, thus the reaction scheme in these systems should be considerably different. The implications of the model to the formation of Si_3N_4 are that the reactions in the model rapidly lead to the formation of atomic silicon and SiN . At higher pressures or for very long reaction times, SiN_2 is also formed at densities comparable to the dissociated silane density. These densities are typically a factor of between 2 and 5 less than the density of N-atoms in the afterglow which is typically less than 1% of the N_2 density. It is clear then that these silicon-bearing radicals (along with smaller quantities of SiH_2 and SiH_3) are at very low densities for the formation of higher nitrides by three-body processes in the gas phase. Since reactors for Si_3N_4 production usually operate at pressures below 1 torr, it is doubtful that the nitride is formed in the gas phase and "rains down" on the substrate surface. It is far more likely that the reactions leading to Si_3N_4 formation occur on the substrate surface and rely on the species generated by the gas phase reactions described in this work to act as the "starters" for the surface reactions. The apparent rapid reaction of N-atoms with SiH_2 (and perhaps SiH_3) means that even under discharge conditions and even in reactors utilizing NH_3 the simpler nitrides (especially SiN) will be formed and be available for surface reactions. The preference of most commercial producers for gas mixtures containing NH_3 and the low pressures involved may indicate that species such as SiN_2 , formed in reactions with N_2 at higher pressures, may be deleterious to good quality film production. The fact that surface reactions are important for the formation of the higher nitrides opens a much larger arena for affecting the final nitride product. Specifically, the preparations of the

walls of the reactor, materials involved, and even the geometry may alter the film quality or growth rate.

Recommendations for Further Work

As is often the case, this work has created almost as many questions as it has answered. Of importance in any future work is accurate measurement of the time dependence of any of the observed species and chemiluminescence. Good measurements of the time dependence of the chemiluminescence would be particularly useful for checking the validity of the model. Particular attention to good flow conditions in the afterglow and to the method of silane introduction are imperative to achieving good time resolved measurements. Better construction of the afterglow system could give more uniform gas flow and perhaps a "shower head" system, similar to those used in commercial reactors, could be used to introduce the silane. Mass spectroscopy of the reaction products might help shed some light on the higher nitrides which are formed at higher pressures as evidenced by the infrared absorption discussed in chapter III. While Horie, et al.³⁰ used mass spectroscopy in their work, it is not clear over what mass range they surveyed the reaction products. The question of SiH_4 dissociation by vibrationally excited N_2 is another area that might be further addressed in another experiment. Unfortunately, it is difficult to prepare vibrationally excited N_2 with significant populations of $v \geq 10$ in a manner that is **reproducible** and **measurable**. One possible experiment would be to heat N_2 to approximately 2500°K in an oven and introduce SiH_4 into the gas stream leaving the oven. The reaction would be slow, but a slow flow system with diagnostics downstream of the reaction could measure either the SiH_4 dissociation or perhaps a higher silane, such as Si_2H_6 , formed from the radicals produced. One final suggestion for further work would be to bring a technique such as laser induced fluorescence (LIF) to the diagnosis of species formed in the reaction. It would be particularly useful if the species SiN_2 , which has been proposed as one of the major species produced at higher pressures could be identified in the gas phase. Spectroscopy of SiN_2 is scarce, however an ultraviolet absorption system has been identified in the wavelength range 300-360 nm in matrix isolation at 4°K⁷⁵. The estimated densities of SiN_2 in these experiments range from $6.5 \times 10^{12} \text{ cm}^{-3}$ at 3 torr to $2 \times 10^{13} \text{ cm}^{-3}$ at 10 torr. A technique such as LIF should be capable of measuring densities of this order.

References

1. Spear, W. E. and LeComber, P. G., "Substitutional Doping of Amorphous Silicon," Solid State Commun., Vol. 17, P. 1193 (1975).
2. Sterling, H. F. and Swan, R. C. G., "Chemical Vapour Deposition Promoted by R.F. Discharge," Solid State Electronics, Vol. 8, No. 8, p. 653 (1965).
3. DeJoseph, Jr., C. A., Garscadden, A. and Pond, D. R., "Spectroscopic Measurements in Silane Reactor Plasmas," Proceedings of the International Conference on Lasers '82, (1982).
4. Wright, N. A. and Winkler, C. A., Active Nitrogen, Academic Press (1968).
5. Herzberg, G., Molecular Spectra and Molecular Structure II. Infrared and Raman Spectra of Polyatomic Molecules, Van Nostrand Reinhold Co. (1945).
6. Bernheim, R. A., Lampe, F. W., O'Keefe, J. F., and Qualey III, J. R., "Visible and Near IR Si-H Vibrational Overtones of SiH_4 ," J. Chem. Phys., Vol. 80, p. 5906 (1984).
7. Harada, Y., Murrell, J. N., and Sheena, H. H., "The Far Ultraviolet Spectra of Methylsilanes," Chem. Phys. Lett., Vol. 1, p. 595 (1968).
8. Gordon, M. S., "Excited States and Photochemistry of Saturated Molecules. IX. Vertical Excited States of Silane," J. Chem. Phys., Vol. 69, p. 4955 (1978).
9. DeJoseph, Jr., C. A., Haaland, P. D., and Garscadden, A., "On the Decomposition of Silane in Plasma Deposition Reactors," IEEE Transactions on Plasma Science, PS-14, No. 2, p. 165 (1986).
10. DeJoseph, Jr., C. A., and Garscadden, A., "Electron- and Excited State Neutral- Induced Dissociation of Silane," 16th Annual Meeting of the Division of Electron and Atomic Physics, abstract DB72 (May 1985).

11. Purnell, J. H., and Walsh, R., "The Pyrolysis of Monosilane," Proc. R. Soc. London, Series A, Vol. 293, p. 543 (1966).
12. Newman, C. G., O'Neal, H. E., Ring, M. A., Leska, F., and Shipley, N., "Kinetics and Mechanism of the Silane Dissociation," Intern. J. Chem. Kinetics, Vol. 11, p. 1167 (1979).
13. Coltrin, M. E., Kee, R. J., and Miller, J. A., "A Mathematical Model of Silicon Vapor Deposition - Further Refinements and the Effects of Thermal Diffusion," J. Electrochem. Soc., Vol. 133, p.1206 (1986).
14. Robertson, R., Hils, D., and Gallagher, A., "Silane Pyrolysis," Chem. Phys. Lett., Vol. 103, p. 397 (1984).
15. Haaland, P., "Ion Kinetics in Silane Plasmas," PhD Thesis, Dept. of Chemistry, Havard University (1988).
16. Chatham, H., Hils, D., Robertson, R., and Gallagher, A. C., "Reactions of He^+ , Ne^+ , and Ar^+ with CH_4 , C_2H_6 , SiH_4 , and Si_2H_6 ," J. Chem. Phys., Vol. 79, p.1301 (1983).
17. Turban, G., Catherine, Y., and Grolleau, B., "Ion and Radical Reactions in Silane Glow Discharge Deposition of a-Si:H Films," Plasma Chemistry and Plasma Processing, Vol. 2, p. 61 (1982).
18. Haller, I, "Ionic Species in a Silane Plasma," Appl. Phys. Lett., Vol. 37, p. 282 (1980).
19. Nolet, G. "Kinetics of Decomposition of Silane (Diluted in Argon) in a Low Pressure Glow Discharge," J. Electrochem. Soc., Vol. 122, p. 1030 (1975).
20. Perrin, J. and Aarts, J. F. M., "Dissociative Excitation of SiH_4 , SiD_4 , Si_2H_6 , and GeH_4 by (0-100 eV) Electron Impact; Comparison with Alkanes," Chemical Physics, Vol. 80, p. 351 (1983).
21. Perrin, J., Schmitt, J. P. M., DeRosny, G., Drevillon, B., Huc, J., and Lloret, A., "Dissociation Cross Sections of Silane and Dislane by Electron Impact," Chemical Physics, Vol. 73, p. 383 (1982).

22. Perkins, G. G. A., Austin, E. R., and Lampe, F. W., "The 147-nm Photolysis of Monosilane," J. Am. Chem. Soc., Vol. 101, p. 1109 (1979).
23. Kushner, M. J., "A Model for the Discharge Kinetics and Plasma Chemistry During Plasma Enhanced Vapor Deposition of Amorphous Silicon," J. Appl. Phys., Vol. 63, p. 2532 (1988).
24. Emeleus, H. J. and Stewart, K., "Effect of Light on the Ignition of Monosilane-Oxygen Mixtures," Trans. Faraday Soc., Vol. 32, p. 1577 (1936).
25. Perrin, J. and Allain, B., "Quenching of Excited Mercury Atoms (6^3P_1 and 6^3P_0) in Collisions with SiH_4 , SiD_4 , Si_2H_6 and GeH_4 ," Chem. Phys., Vol. 123, p. 295 (1988).
26. Moore, C. E., Atomic Energy Levels - Volume 1, National Bureau of Standards Circular 467 (1949).
27. Levine, R. D. and Bernstein R. B., Molecular Reaction Dynamics and Chemical Reactivity, Oxford University Press (1987).
28. Wright and Winkler, pp. vii-viii.
29. Dewhurst, H. A. and Cooper, G. D., "Reactions of Active Nitrogen with Silane and Methylsilanes," J. Am. Chem. Soc., Vol. 82, p. 4220 (1960).
30. Horie, O., Potzinger, P., and Rieman, B., "Chemionization and Chemiluminescence in the Reaction of SiH_4 with Active Nitrogen," Chem. Phys. Lett., Vol. 129, p. 231 (1986).
31. Piper, L. and Caledonia, G., "Rate Coefficients for Reactions of Nitrogen Metastables with Silane," The 39th Gaseous Electronics Conference, Monterey Calif. (1986).
32. See for example: Van Atta, C. M., Vacuum Science and Engineering, McGraw-Hill, Inc. (1965).
33. Schlossberg, H. R. and Kelly, P. L., "Infrared Spectroscopy Using Tunable Lasers," in Spectrometric Techniques - Volume II, edited by G. A. Vanasse, Academic Press, New York (1981).

34. See for example: Ludwig, C. B., Malkmus, W., Reardon, J.E. and Thompson, J. A. L., Handbook of Infrared Radiation From Combustion Gases, N.A.S.A. publication NASA SP-3080 (1973).
35. Johns, J. W. C. and Kreiner, W. A., "Measurements and Analysis of the ν_4 Band of Silane," J. Mol. Spectrosc., Vol.60, p. 400 (1976).
36. Bevington, P. R., Data Reduction and Error Analysis for the Physical Sciences, McGraw-Hill (1969).
37. Drayson, S. R., "Rapid Computation of the Voigt Profile," J. Quant. Spectrosc. Radiat. Transfer, Vol. 16, p. 611 (1976).
38. White, J. U., "Long Optical Paths of Large Aperture," J. Opt. Soc. Am., Vol. 32, p. 285 (1942).
39. Striganov, A. R. and Sventitskii, N. S., Tables of Spectral Lines of Neutral and Ionized Atoms, IFI/PLENUM, New York (1968).
40. Jevons, W., "Spectroscopic Investigations in the Connection with Active Modification of Nitrogen. III-Spectra Developed by the Tetrachlorides of Silicon and Titanium," Proc. R. Soc. A, Vol. 89, p. 187 (1913).
41. Bredohl, H., Dubois, I., Houbrechts, Y., and Singh, M., "The Emission Spectrum of SiN," Can. J. Phys., Vol. 54, p. 680 (1976).
42. Anketell, J. and Nicholls, R. W., "The Afterglow and Energy Transfer Mechanisms of Active Nitrogen," Rep. Prog. Phys., Vol. 33, p. 269 (1970).
43. Foster, S. C., "The $B^2\Sigma^+ \rightarrow A^2\Pi_i$ System of Silicon Nitride, SiN," J. Mol. Spectrosc., Vol. 106, p. 369 (1984).
44. Herzberg, G., Spectra of Diatomic Molecules, Van Nostrand Reinhold Company (1950).
45. Stevens, A. E. and Ferguson, H. I. S., "Photoelectric Intensity Measurements Upon the SiN ($B^2\Sigma^+-X^2\Sigma^+$) Spectrum," Can. J. Phys., Vol. 41, p. 240 (1963).

46. Schofield, K. and Broida, H. P., "Chemiluminescent Emission from the Reactions of Volatile Silicon Compounds and Active Nitrogen," Photochemistry and Photobiology, Vol. 4, p. 989 (1965).
47. Caledonia, G. E., Davis, S. J., Green, B. D., Piper, L. G., Rawlins, W. T., and Weyl, G. M., "Analysis of Metastable State Production and Energy Transfer," AFWAL-TR-86-2087, (Final report for contract F33615-85-C-2568, Air Force Wright Aeronautical Laboratories, Wright-Patterson AFB, Ohio, 1986).
48. Pierson, R. H., Fletcher, A. N., Gantz, E. S. C., "Catalog of Infrared Spectra for Qualitative Analysis of Gases," Analytical Chemistry, Vol. 28, p. 1218 (1956).
49. Ebsworth, E. A. V., Hall, J. R., Mackillop, M. J., McKean, D.C., Sheppard, N., Woodward, L. A., "Vibrational Spectra and Structure of Trisilylamine and Trisilylamine-d₉," Spectrochimica Acta, Vol. 13, p. 202 (1958).
50. Nyquist, R. A. and Kagel, R. O., Infrared Spectra of Inorganic Compounds, Academic Press (1971).
51. Stedman, D. H. and Setser, D. W., "Chemical Applications of Metastable Argon Atoms II. A Clean System for the Formation of N₂(A³Σ_u⁺)," Chem. Phys. Lett., Vol. 2, p. 542 (1968).
52. Chaney, R., Schadt, R., Anderson, R., and DeJoseph, Jr., C. A., "Infrared Measurements of Disilane Production from a D. C. Discharge in Silane," The 37th Gaseous Electronics Conference, Boulder, Colorado (1984).
53. Mitchner, M. and Kruger, Jr., C. H., Partially Ionized Gases, John Wiley and Sons (1973).
54. Ho, P., Coltrin, M. E., Binkley, J. S., and Melius, C. F., "A Theoretical Study of the Heats of Formation of SiH_n, SiCl_n, and SiH_nCl_m Compounds," J. Phys. Chem., Vol. 89, p. 4647 (1985).
55. Huber, K. P. and Herzberg, G., Constants of Diatomic Molecules, Van Nostrand Reinhold Company (1979).

56. Niki, H. and Mains, G. J., "The 3P_1 Mercury-Photosensitized Decomposition of Monosilane," J. Phys. Chem., Vol. 68, p. 304 (1964).
57. Dunnwald, H., Siegal, Urban, E., Rich, J. W., Homicz, G. F., and Williams, M. J., "Anharmonic Vibration-Vibration Pumping in Nitric Oxide by Resonant IR-Laser Irradiation," Chem. Phys., Vol. 94, p. 195 (1985).
58. DeLeon, R. L. and Rich, J. W., "Vibrational Energy Exchange Rates in Carbon Monoxide," Chem. Phys., Vol. 107, p. 283 (1986).
59. Farrenq, R., Rossetti, C., Guelachvili, G., and Urban, W., "Experimental Rovibrational Populations of CO Up to $v=40$ from Doppler-Limited Fourier Spectra of the Sequences $\Delta v=1, 2$, and 3 Emitted by a Laser Type Source," Chem. Phys., Vol. 92, p. 401 (1985).
60. Rich, J. W., and Bergman, R. C., " C_2 and CN Formation by Optical Pumping of CO/Ar and CO/N₂/Ar Mixtures at Room Temperature," Chem. Phys., Vol. 44, p. 53 (1979).
61. Starr, W. E., "Excitation of Electronic Levels of Sodium by Vibrationally Excited Nitrogen," J. Chem. Phys., Vol. 43, p. 73 (1965).
62. Harvey Michels, private communications.
63. Coltrin, M. E., Kee, R. J., and Miller, J. A., "A Mathematical Model of the Coupled Fluid Mechanics and Chemical Kinetics in a Chemical Vapor Deposition Reactor," J. Electrochem. Soc., Vol. 131, p. 425 (1984).
64. Boo, B. H. and Armentrout, P. B., "Reaction of Silicon Ion (2P) with Silane. Heats of Formation of SiH_n , SiH_n^+ ($n = 1,2,3$), and $Si_2H_n^+$ ($n = 0,1,2,3$). Remarkable Isotope Exchange Reaction Involving Four Hydrogen Shifts," J. Am. Chem. Soc., Vol. 109, p. 3549 (1987).
65. Slater, R. C., Hyman, H. A., Trainor, D., and Flusberg, A., "Research on Sources of Gas Phase Metastable Atoms and Molecules," Final Report for Contract F33615-79-C-2051, AFWAL-TR-82-2029, (1982).

66. Cerogora, G., Hochard, L., Touzeau, M., and Ferreira, C. M., "Population of $N_2(A^3\Sigma_u^+)$ Metastable States in a Pure Nitrogen Glow Discharge," J. Phys. B: At. Mol. Phys., Vol. 14, p. 2977 (1981).
67. Bailey, W. F., "Collision Induced Dissociation of Diatomic Molecules," Ph.D. Thesis, Air Force Institute of Technology (1978).
68. Capitelli, M. and Dilonardo, M., "Nonequilibrium Vibrational Populations of Diatomic Species in Electrical Discharges: Effects on the Dissociation Rates," Chem. Phys., Vol. 24, p. 417 (1977).
69. Schwartz, R. N., Slawsky, Z. I. and Herzfeld, K. F., "Calculation of Vibrational Relaxation Times in Gases," J. Chem. Phys., Vol. 20, p. 1591 (1952).
70. Bray, K. C. N., "Vibrational Relaxation of Anharmonic Oscillator Molecules: Relaxation Under Isothermal Conditions," J. Phys. B (Proc. Phys. Soc.), Vol. 1, p. 705 (1968).
71. Black, G., Wise, H., Schechter, S., and Sharpless R., "Deexcitation of Metastables at Plasma Boundaries," Final report for contract F33615-72-C-1613, ARL 73-0182 (1973).
72. Walkup, R., Avouris, Ph., Dreyfus, R. W., Jasinski, J. M. and Selwyn, G. S., "Laser-Induced Fluorescence Detection of Diatomic Products of Reactive Etching: SiN, SiO, and SiF," Mat. Res. Soc. Symp. Proc., Vol. 29, p. 269 (1984).
73. Gear, C. W., "The Automatic Integration of Stiff Ordinary Differential Equations," Communications in ACM, Vol. 14, p. 176 (1971).
74. See the discussion of stiff equations in: Press, W. H., Flannery, B. P., Teukolsky, S. A., and Vetterling, W. T., Numerical Recipes, Cambridge University Press (1986).
75. Lembke, R. R., Ferrante, R. F., and Weltner, Jr., W., "SiCO, SiN₂, and Si(CO)₂ Molecules: Electron Spin Resonance and Optical Spectra at 4 K," J. Am. Chem. Soc., Vol. 99, p. 416 (1977).

76. Kee, R. J., Rupley, F. M., and Miller, J. A., "The Chemkin Thermodynamic Data Base," Sandia National Laboratories Report, SAND87-8215 (1987).

77. Pete Haaland private communication.

Appendix A

Heat of Formation of SiN

The heat of formation of a diatomic molecule can be calculated if the dissociation energy of the molecule is known and the heats of formation of the dissociated products are known. If $H_f(AB)$ is the heat of formation of species AB then,

$$H_f(AB) = H_f(A) + H_f(B) - D_0(AB) \quad (\text{eq. A-1})$$

where $D_0(AB)$ is the dissociation energy of AB measured with respect to the zero point energy of the molecule. For SiN the dissociation energy has not been clearly established. Herzberg⁴⁴ gives the dissociation energy as $D_0=4.5$ eV from the work of Gaydon. However, in his later book,⁵⁵ Herzberg does not list a value for the dissociation energy. Bredohl, et al.⁴¹ used an extrapolation of their calculated ground electronic state potential which gave a value of $D_e=5.84$ eV. Since it has only been since the work of Foster in 1984⁴³ that the electronic energy of the $A^2\Pi$ has been accurately determined, another look at the dissociation energy was performed during this work. The extrapolation technique given in Herzberg⁴⁴ was used for each state for which Foster gave at least three terms describing the vibrational energy levels. The vibrational energy levels of each electronic state were calculated until the vibrational energy reached a peak value at some V_{max} . The value of the energy at this point was considered the dissociation energy D_e . For the $X^2\Sigma$ and $A^2\Pi$ states, the calculated energies were 5.84 and 5.37 eV, and for the $D^2\Pi$ state the calculated energy was 7.93 eV. Since the $D^2\Pi$ state dissociates into $\text{Si}(^3\text{P})+\text{N}(^2\text{D})$, its limit should lie 2.38 eV (the $\text{N}(^4\text{S})-\text{N}(^2\text{D})$ energy spacing²⁶) above the two lower states used in the calculation. Using this difference gives a third value for the $\text{Si}(^3\text{P})+\text{N}(^4\text{S})$ limit as 5.55 eV. Since the zero point energy is ≈ 0.07 eV, these extrapolated values give values for D_0 between 5.30 and 5.77 eV. On the other hand, extrapolation of the $B^2\Sigma$ state gave a value of $D_e=4.69$ eV. Since the B-state also dissociates into $\text{Si}(^3\text{P})+\text{N}(^2\text{D})$, this would give a value of the dissociation energy of the ground state as 4.69-2.38 or 2.31 eV. This is an extremely low value. One might argue that the B-state value is anomalous and should be thrown out, but in light of the uncertainty over the years in placing the $A^2\Pi$ state it is not clear that this would be wise.

Averaging the three "good" values gives a dissociation energy of $D_0=5.59\pm.24$ eV. Subtracting the zero point energy gives $D_0=5.52\pm.24$ eV. Since the extrapolation method is prone to give high values for the dissociation energy, and with the anomalous behavior of the B-state extrapolation, the value originally given by Herzberg will be used for the heat of formation calculation. Using the $H_f(@298^\circ\text{K})$ values for Si and N from appendix B,

$$H_f(\text{SiN}) = 107.7 + 112.9 - 4.5 \cdot 23.03 = 117 \text{ (Kcal/mole)}.$$

Considering the uncertainty in the dissociation energy, this value must be given an equal uncertainty. It is doubtful the true value exceeds this value by very much, but the true value could be very much smaller than the value given above. The heat of formation of the SiN $B^2\Sigma(V=5)$ state, discussed in chapter III, can be calculated from the molecular constants of Foster⁴³ and the above value for the heat of formation of the ground state. This gives

$$H_f[\text{SiN}(B^2\Sigma(V=5))] = 117 + 82.6 = 200 \text{ (Kcal/mole)}.$$

Appendix B

Heats of Formation Used In This Work

<u>Species</u>	<u>Heat of Formation</u>	<u>Reference(s)</u>
H	52.1	76
H ₂	0.0	76
HSiN	117	77
HNSi	49	77
N(⁴ S)	112.9	76
N(² D)	167.8	76,26
N(² P)	195.2	76,26
N ₂ (X ¹ Σ)	0.0	76
N ₂ (X ¹ Σ, V=10)	62.8	76,55
N ₂ (X ¹ Σ, V=17)	101.9	76,55
N ₂ (X ¹ Σ, V=20)	117.3	76,55
N ₂ (A ³ Σ)	142.1	76,55
NH	85.2	76
NH ₂	45.5	76
Si	107.7	54
SiH	91.7	54
SiH ₂	68.1	54
SiH ₃	47.8	54
SiH ₄	8.2	54
SiN(X ¹ Σ)	117	(appendix A)
SiN(B ² Σ, V=5)	200	(appendix A)

*Units are Kcal/mole at 296°K

Appendix C

The Function P(T) in Equation 5-10

For the function P(T) in equation 5-10, the following procedure was used. Capitelli⁶⁸ gives an expression for the time constant of the v=1 relaxation at one atmosphere as

$$\tau(T) = 5.7 \times 10^{-12} \cdot \text{Exp}(234.9T^{-1/3}) \quad (\text{eq. C-1})$$

where τ is in sec. and T is in °K. In terms of the VT rate, τ is given by

$$\tau(T) = \left[\rho_{N_2} (VT)_{1,0} \right]^{-1} \quad (\text{at } \rho_{N_2} = 1 \text{ atm}) \quad (\text{eq. C-2})$$

Using equations 5-10, 11, 12, and 14, P(T) was calculated in terms of $\tau(T)$. Two hundred values of P(T) were then calculated over the temperature range 150-1000°K and a rational function of the form,

$$P(T) = \frac{a+bT+cT^2}{d+eT+fT^2} \quad (\text{eq. C-3})$$

was least-squares fit to the calculated values. The values of the coefficients were found to be:

$a=1.140616$	$d=0.7228253$
$b=-0.002328813$	$e=-0.01295966$
$c=4.009294 \times 10^{-6}$	$f=5.635459 \times 10^{-5}$

Using this function, the τ rates could be calculated to within 1% of the values given by eq. C-1 over the temperature range 150-1500°K.